POLITECNICO DI TORINO

DIPARTIMENTO DI INGEGNERIA MECCANICA E AEROSPAZIALE

Corso di laurea in ingegneria aerospaziale

Progetto dei Sistemi Aerospaziali Integrati

A.A. 2016 - 2017

Preliminary design and system integration for a VTOL aircraft

Team Mini-Bee

Victor Miherea
Martin Samake
Francesco Viglione
Alessio Vitali

Table of contents

1. Introduction

1.1. Abstract

This work concerns the design of a Vertical Take-Off Landing (VTOL) aircraft with the purpose of transportation about 220 kg of payload. The technical details will be shown afterwards. Furthermore, the work was focused on the integration of the on-board systems on an existing configuration, developed by *PLACIS* (Supméca): Mini-Bee. Indeed, the distinctiveness of this work is that it was made in close cooperation with the students from Supméca and the choices made were dictated by previous configurations.

The project can be divided into two separated configurations, with both of them fulfilling the requirements:

- **Mini-Hornet**: developed only on preliminary design and can be considered as an alternative configuration of the Mini-Bee.
- **Mini-Bee**: the 'frozen' configuration was integrated with the main subsystems. The main work was made on this configuration

Figure 1.1.1: Mini-Hornet and Mini-Bee mockups
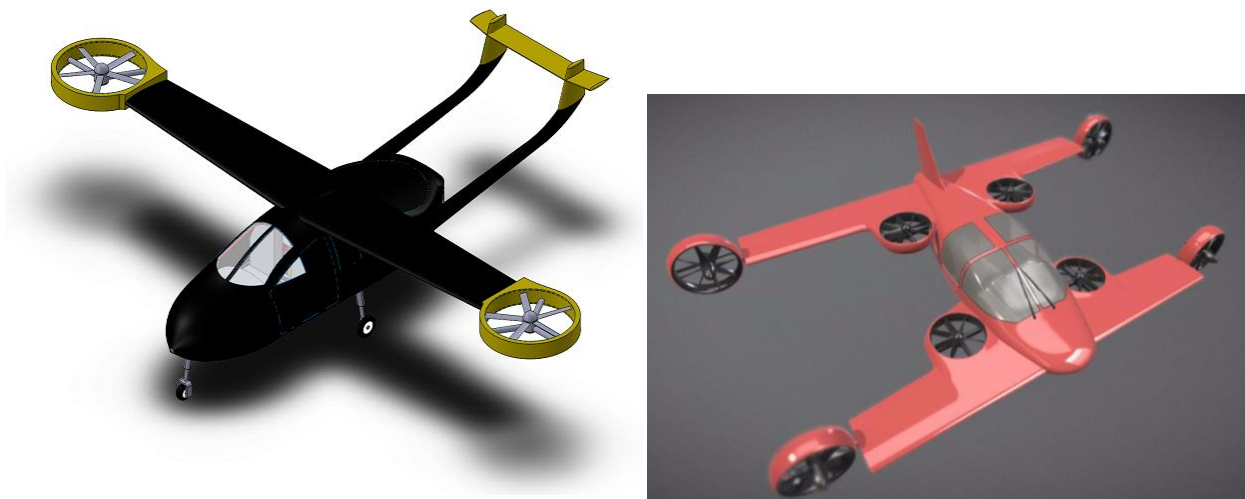
The preliminary design will be described as made for the Mini-Hornet. The mission profile was made for both of them, but, in general, they will coincide.

The systems integration was made partially for the Mini-Hornet, but was totally developed for the Mini-Bee configuration.

So, when we will refer to the systems we will consider the systems integrated on the Mini-Bee.
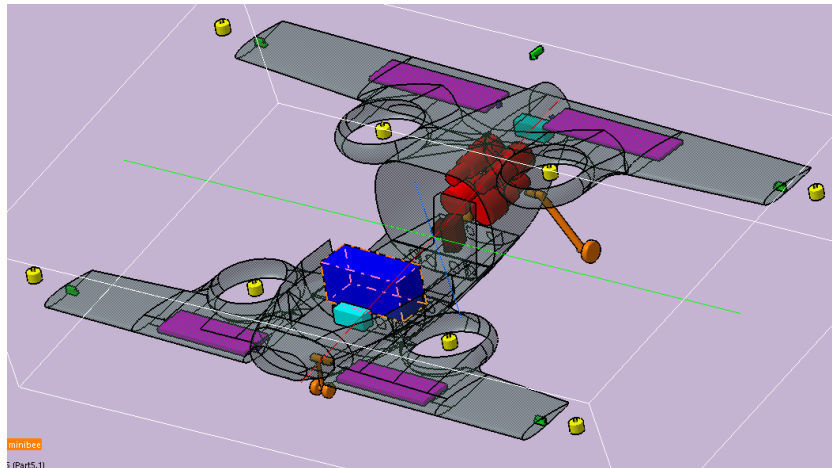
Figure 1.1.2: All Systems integrated on the Mini-Bee Configuration. It is also indicated the C.G. position of the systems.

The tools used are:
- Solidworks and CATIA for the CAD
- ASTRID for Preliminary Design, Mission Profile and Systems budget calculations
- X-Plane for flight simulation

1.2.   Theme description

The realization of this type of aircraft - VTOL aircraft for personal usage - is matter of time.

An indicator that this kind of travelling may be an important source of income can see, as example, the first service in the world for passenger transportation, that will start in July in Dubai: a taxi drone, Chinese model *eHang 184*, piloted by a command center that receives in input the destination coordination indicated by the client, will bring 120 kg of payload to the destination far 50 km.

It is only the beginning of this way to travel. The difference with a drone is that the aircraft designed in this project can carry more payload and can fly faster.

The another advantage is that although it may seem a kind of aircraft used in general aviation, it can take off and land without the need of a runway, as helicopters do. Disengaging from the runways the general aviation is brought to a new point of view of what travelling by air may be: a personal "*flying car*" for personal usage.

The ways in which this VTOL aircraft can be used are numerous. It goes from personal and business usage to rescue and exploration missions.

1.3.   Requirements

- Number of passengers/pilots: 2 (or 220 kg of payload)
- Maximum range: 600 km + 50 km (see Figure 3)
- Cruise Speed: 220 km/h (typical of general aviation aircrafts)
- Maximum Speed: 300 km/h
- Take-Off and Landing: Vertical
- Configuration: Tiltrotor
- Propulsion: Hybrid in series
- Structures: wide utilization of composite materials
- Systems architectures: all-electric
- Man/aircraft interface: simple and ergonomic

Figure 1.1.3: the maximum distance that can be reached if the departure is from Turin

The introduction presented to Placis is:

The purpose of this report is to describe and detail the method used in optimization of on-board systems for the Mini Bee project. To do that, we mixed personal skills with utilization of useful tools such as "Astrid", which is a program developed by PoliTo PhD students, in order to provide a single interface able to work through the sizing of whole aircraft on-board installations and, thus, to simplify our work.

We chose to develop a premium version of Mini Bee, which consists in having a retractable landing gear, a VIP equipment and a range of 600 km + 50 km. This aircraft is required to be a VTOL with a revolutionary hybrid power supply system and equipped with eight rotors, four of which are fixed (hover rotors) and working only during take-off and landing, while the remaining four are tiltable, providing thus, both thrust and control for maneuvers. Hover rotors are batteries powered, whereas the tiltable ones are powered by four electric fuel generators which are, basically, turbo charged axial engines, each integrated with an electric generator that actuates, in turn, a 55 kW electric engine. Other constraints for this project are:

- *Cruise speed: 220 km/h*
- *Maximum speed: 300 km/h*
- *Cruise altitude: 2500 m*
- *Maximum altitude: 4000 m*
- *Full-electric systems architecture*

2. Reference aircrafts

Because of the peculiarity of the project there are no existing similar aircrafts *in toto* that can be compared to.

Furthermore it was made a database of different aircrafts and then the statistical mean data were chosen and used as input for the preliminary estimation.

These aircrafts have in common the same payload requirements.

Some of the aircrafts we referred to are:

- Cessna Skycatcher, Diamond DA20, A.C. Super Decathlon, Aviat A-1C Husky for the cruise.
- Bell 206, MD500, R44 for the VTOL.

In the table below is indicated the database used:

For cruise:

Reference Aircrafts for cruise	MTOW (kg)	P (kW)	Max Range (km)	z_cr (m)	Vcr (km/h)	S (m2)	c (m)	AR	fuel cap (kg)
Cessna Skyhawk	1157	134,23	1185,28	4267,20	225,94	16,20	1,47	7,47	160,50
Cessna Skylane	1406	171,51	1694,58	5516,88	268,54	16,20	1,48	7,43	263,46
Piper Arrow	1247	149,14	1629,76	4937,76	253,72	15,14	1,40	7,70	218,04
Piper Archer LX	1157	134,23	966,74	4297,68	237,06	15,14	1,40	7,70	145,36
AA-2 Patriot	1089	134,23	1135,28	3962,40	231,50				181,70
Beechcraft A23A Musketeer	1089	123,04	1251,95	4572,00	188,90	13,60	1,36	7,32	181,70
Cessna 150	726	82,03	777,84	4267,20	151,86	15,00	1,48	6,81	78,74
Spencer S-12-D	1406	193,88	1126,02	4572,00	216,68				181,70
Rockwell Commander 114A GT	1202	193,88	1307,51	5029,20	290,76	14,00	1,40	7,11	205,93
Thurston TA16 Seafire	1451	186,43	1609,39	5486,40	250,02	17,00	1,51	7,49	272,55
Average	1193	150,26	1268,43	4690,87	231,50	15,29	1,44	7,38	188,97

For hover:

Reference Aircrafts for VTOL	MTOW (kg)	P (kW)	A (m2)	D (m)	T/A (kg/m^2)
R22	621	98,00	46,20	7,67	13,44
R44	1089	183,00	80,12	10,10	13,59
Bell 206	1451	310,00	81,1	10,16	17,89
MD500	1157	207,00	54,6	8,34	21,19
EC120	1715	376,00	46,20	7,67	37,12

We gathered the data of the helicopters in order to make some considerations about the power required for the hover but later on, during the process, we realized that the disk loading factor T/A of our aircraft is much larger than the one of the reference vehicles, which are light weight helicopters due to the fact that they have a small payload mass, and are closer to the values that can be find in tilt rotors or in other

helicopters that, anyway, have different payload requirements than ours. For this reason the required power for hover will be estimated applying the Actuator Disk Theory.

Below it is indicated the main categories of considered aircrafts and representative aircrafts for each category.

- **Cessna 172 Skyhawk**. This aircraft was used as reference for the general characteristics and performance. This one, in particular, was used for the performance estimations during cruise.

- Gross weight: 2,450 lb (1,111 kg)
- Cruise speed: 122 kn (140 mph; 226 km/h)
- Service ceiling: 13,500 ft (4,100 m)
- Fuel capacity: 56 US gallons (212 litres)
- Avionics : Garmin G 1000
- Never exceed speed : 163 kn (188 mph; 302 km/h)

Figure 2.1: Cessna 172 Skyhawk and some its characteristics

- **Bell 47**. The need to consider the vertical Take-Off and Landing leads us to consider the configuration of a helicopter. However, for the power calculation used during Take Off and Landing, there were used different considerations, as can be seen later. The helicopters are used to have a rotor diameter too big for the configuration desired in this design.

Figure 2.2: Bell 47 J

- **Agusta Westland Project Zero**. This unmanned demonstrator was considered as a model for the all-electric tilt-rotor aircraft, indeed it shows the capabilities of electric propulsion in aviation, and for the usage of the state-of-art technologies and materials.

Figure 2.3: Project Zero by Agusta Westland. « Half Plane, half helicopter » aircraft

- **Agusta Westland 609**. Maybe the most known VTOL Tiltrotor aircraft. This configuration inspired in part the Mini-Hornet Configuration. The AW 609 is aimed at the civil aviation market and has clearly different characteristics and performances from ours, but how it works is very similar to the Mini-Bee configuration. So, AW 609 will be one of the principal references during this project.

Figure 2.4: Agusta Westland 609

- **Mini-Bee and other innovative projects.** As the project of the Mini-Bee is in progress, it has to be considered this aspect. So, the study is partially restricted to the latest version of the Mini-Bee. In the end, because of the innovative type of the aircraft, it is necessary to compare with other new projects.

Figure 2.5: Mini Bee (2016)

Figure 2.6: EHANG 184. This Drone will b operate as taxi in July 2017, in Dubai

As said before, the choices of reference aircrafts are limited to the scarcity of similar aircraft at all.

3. Preliminary Design

3.1.1. Layout definition guidelines

At this point we know the requirements we must apply to our aircraft and we choose a set of reference vehicles according to those requirements, so we can define a layout from scratch. Since the requirements are non-conventional, it follows that also the layout is non-conventional and we have many degrees of freedom. For this reason, we may apply some other restrictions in order to optimize the decisional process:

- We should prefer a layout that is as compact as possible so that the aircraft is operable in a large variety of spots such as building roofs, small hangars etc. This means that the rotors area, that significantly affects the floor area covered by the aircraft, should be kept as small as possible. It implies that a multiple rotor solution is preferable since increasing the number of rotors while keeping a constant total rotor surface allows a higher compactness, although it reduces the total efficiency of the rotors.

- The layout should allow a relatively low power budget in order to reduce fuel consumption. This requirement conflicts with the previous one since the power required for the hover condition has the following relation with the disk area:

$$P \propto \frac{1}{\sqrt{A}}$$

In a first approximation, this is true also for a multiple rotor configuration where A equals the total area covered by all the rotors. Power wise, the best solution for hover is to utilize a large rotor, as helicopters do. This means that we have to find a compromise with these first two restrictions.

- The final layout should be as simple and essential as possible. Our aircraft is required to perform vertical take-off and landing but also a high-performance cruise comparable with the one made by general aviation airplanes. The best solution for the hover phase would be to have a single large rotor that provides the traction necessary to balance the take-off weight (helicopter), while the best solution for the horizontal flight cruise phase would be to have a propeller that produces the necessary thrust to compensate the aerodynamic drag and a fixed lifting surface for the lift generation. If we want to design an aircraft from our requirements we have to merge these two aspects in an aircraft that possibly is not as performing as a helicopter during hover and not as performing as a general aviation aircraft during cruise but that can satisfactorily carry out both operations.

  In order to satisfy this requirement, we can decide to have a layout with one or more hover rotors and one or more propellers, as in the case of the Eurocopter X-3 compound helicopter, or to adopt a tilt-rotor configuration, as in the case of the Leonardo AW609. These two examples represent a different approach to solve the presented problem. The compound helicopter is conceptually closer to a standard helicopter but the intrinsic speed limit of this kind of aircraft is surpassed with additional propellers for the high-speed cruise, an angular speed of the main rotor that is reduced at high-speeds in order to avoid the

dissymmetry of lift and small lifting surface that compensate the reduction of rotor traction as a consequence of the rotor speed reduction. The tilt-rotor is closer to an aircraft by means of resemblance and cruise performance: the relatively small rotor disks give to the tilt-rotor poor hover performances compared to the one of a normal helicopter but, once tilted, they can be efficiently used as a propeller in horizontal flight mode where the aircraft relies only on the lift provided by the fixed wing so it allows to also overcome the cruise altitude limit of rotary wings aircrafts.

Figure 3.1: Eurocopter X3 compound helicopter

Figure 3.2: Leonardo AW609 tilt-rotor

Since our aircraft has to hover just during take-off and landing, has to be able to fly at an altitude that allows it to easily cross the Alps and to fly at a maximum speed of 300 km/h, the tilt-rotor configuration is the best choice. Anyhow we still can consider the option of having additional hover rotors that support the hover phases.

- During hover phases the centre of gravity of the vehicle and the centre of traction must coincide. Hence in the layout definition the rotors have to be located symmetrically with the respect of a likely centre of gravity during a design phase where it is unknown.

- The market target of the final product is mainly consisting of high-end consumer looking for an innovative and exclusive product. This means that the aesthetic factor has to be considered early on in the design process.

Summing up the additional considerations we derive some guidelines applicable to the layout definition in order to obtain a layout of the aircraft.

3.1.2. Chosen layout

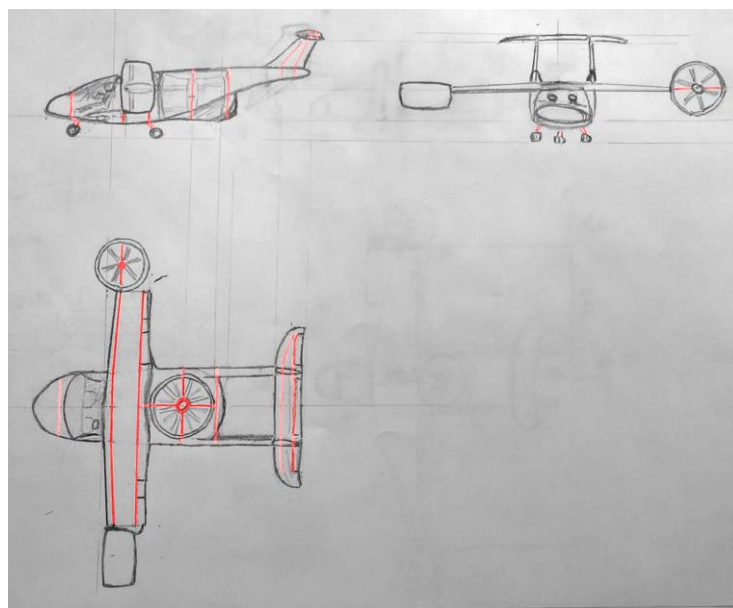At last we choose the following layout:

Figure 3.3: preliminary design layout

This layout is characterized by:

- Our aircraft is required to have a series hybrid propulsion system. So, we have to generate power with a thermal engine and then transform it into electric power through a generator. Every rotor will be powered through an electrical motor mounted in the rotor hub. We decide to limit the vertical flight just to the take-off and landing phases so that we can size the thermal generator for the horizontal flight phase and then use a high energy density battery pack to absorb the required power peaks during the vertical flight.
- 2 ducted tilting rotors at the tips of the wing. Ducted rotors are heavier than non-ducted rotors but they also offer the following benefits:

  - o Increased aerodynamic efficiency of the rotor due to reduced blade tip losses;
  - o Lateral noise reduction;
  - o Safer ground operations;
  - o Protection from blade strike;
  - o Protection in case of blade detaching;
  - o The duct acts as an air intake expanding pre-expanding the incoming flow and as a nozzle for the outflow.

- 2 coaxial counter-rotating ducted rotors merged in the rear of the fuselage. Coaxial counter-rotating rotors placed at a proper distance one from another (approximately between 1/10 and 2/10 of the rotor radius) have a greater efficiency and allow a smaller disk area by a factor of ~ $1/\sqrt{2}$ to ~ 1/1.14 than a single rotor providing the same thrust. Furthermore, the reaction moments of the two rotors cancel out each other. The main disadvantage of this solution is the greater lateral noise produced but this can be reduced by utilizing a non-constant spacing of the blades or noise insulation materials in the part of the fuselage surrounding the hover rotors duct.

- High wing configuration. This choice is bounded by the presence of the tilt rotors at the tip of the wings. We want to design the aircraft in such a way that it can land horizontally in case of emergency so the tilt rotors must have a certain ground clearance also in their horizontal flight position. In this way, we can also place the cockpit and the engine and cargo bay below the wing without affecting the accessibility for pilot, passengers or maintenance personnel. Since the maximum Mach for the aircraft is about 0.24 at 300 km/h there is no need to adopt a sweep angle. In order to reduce the flectional loads on the wing root we decide to apply a taper ratio to the wing.

- Double tail boom with high horizontal empennage. This choice is consequential to the placing of the hover rotors at the rear end of the fuselage. Adopting double boom, we keep a structural continuity between the fuselage and the tail. The horizontal empennage is placed in an elevate position so that it can receive a clean air flow since we adopt a high wing configuration.

- Mobile control surfaces on the wing for roll control and lift augmentation, two rudders on the two vertical empennages, mobile surfaces on the horizontal empennage for pitch control. The aerodynamic control surfaces are intended to be used during the horizontal flight mode, when they receive enough dynamic pressure for a proper functioning.

- We use a tricycle landing gear. The main gear is positioned just behind the hypothetical centre of gravity and is attached to the fuselage in correspondence with a fuselage main rib since it has to bear the weight of the vehicle. The front gear is placed below the front of the cockpit and also attached to the fuselage main rib situated between the cockpit and the nose of the aircraft.

- The cockpit layout has to comfortably accommodate the pilot and a passenger. Given the market segment we intend to put this aircraft in, the cockpit has to resemble, in terms of dimensions and habitability, the interior of a luxury sports car. So, with this in mind, we sketched the cockpit dimensions. We also

    intend to place a small boot big enough to carry two golf bags just behind the cockpit.

- The fuel generator and the electric generator are located in the bay below the wing box, between the cockpit and the hover rotors.
- The front part of the cockpit has a glass cockpit with an integrated avionic system. The bay inside the nose of the aircraft contains components of the avionic system and the battery pack.

3.2. Preliminary design calculations

For the preliminary design calculation and the estimation of the weight and the main dimensions of the aircraft we use the Aircraft Conceptual design module of the software ASTRID. Astrid requires some input data that are going to be evaluate by comparison with the reference aircrafts and by "handmade" calculations. The procedures will be described in this section. ASTRID does not support the preliminary design of VTOL vehicles so we decided to use it for the sizing of the as if it was a conventional aircraft. In this way, we can size the vehicle for the climb and the cruise phase and accordingly the thermal engine. In parallel, we calculate the power required for the hover phase during take-off and landing so that we can subsequently size the batteries necessary to compensate the extra demand of power.

3.2.1. Installed power estimation

To evaluate an initial value of the installed power of our aircraft we gathered a small database of some two-seater single engine piston prop general aviation aircrafts with the same payload requirements. As aforementioned, the thermal engine used as a generator should be able to provide all the power necessary to the aircraft during the horizontal flight phases, so we are confident that by extracting the average power from the vehicles in the database we can get a good result.

Table 3.1: installed power estimation from reference aircrafts

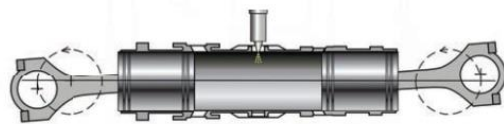| Reference aircrafts for cruise	P (hp)	P (kW)
Cessna Skyhawk	180	134.23
Cessna Skylane	230	171.51
Piper Arrow	200	149.14
Piper Archer LX	180	134.23
AA-2 Patriot	180	134.23
Beechcraft A23A Musketeer	165	123.04
Cessna 150	110	82.03
Spencer S-12-D	260	193.88
Rockwell Commander 114A GT	260	193.88
Thurston TA16 Seafire	250	186.43
Average Power	202 hp	150 kW

For this power rating and this category of aircrafts piston engines are usually preferred since they offer the best specific fuel consumption. Still, we can choose

between gasoline and diesel fuelled piston engines: the first are lighter, offering a higher power to weight ratio while the latter have a lower fuel consumption. In both cases, especially in the case of a diesel engine, the specific fuel consumption can be considered approximately constant varying the throttle, while this is not true for a turboprop engine. Initially we were inclined to choose a gasoline engine such as a Lycoming or a Continental but then we found a developing diesel engine from the manufacturer Gemini that aims to increase the power to weight ratio by adopting a two-opposed-piston-per-cylinder-design, maintaining the typical low specific fuel consumption of the diesel engines.
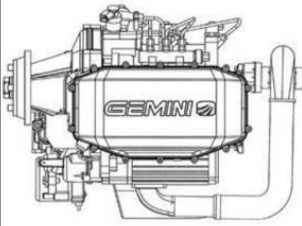

With the introduction of the all-new Gemini uniflow diesel engine, Superior Air Parts continues its history as a leader in making sport and general aviation engines greener, more attainable, more efficient and more affordable for pilots around the world.

Gemini is the first diesel engine developed from the ground up for the next-generation of experimental and light sport aircraft. Its unique uniflow, two-opposed-pistons-per-cylinder design offers a number of advantages, including:

Gemini's unique Uniflow twin-piston design.

• *Highly efficient two-stroke operation*
• *Lighter weight with higher torque at lower RPM**
• *Mechanically simpler design with fewer moving parts*
• *Green operations with much lower emissions*
• *Up to 20% lower fuel burn than avgas piston engines**
• *Runs on Jet A, diesel or bio-diesel fuels*
• *Retrofittable with many current piston engine designs*
• *Modular design simplifies model growth*

200 SERIES®

180-200 HP / 134-149 KW
3 Cyl, 6 Pistons
.386 BSFC

ENGINE DIMENSIONS
28.74" W x 16.34" H x 28.54" L
72.99 cm W x 41.50 cm H x 72.49 cm L

WEIGHT
276 pounds
125 kg

Figure 3.4: extract from the brochure of the Gemini 200 diesel engine

We choose the Gemini 200 model which provides the power we require with an engine weight of 125 kg and a SFC of $0.386\frac{lb}{hp\cdot h}$.

3.2.2. Electric power generation and rotors electric motors

The power generated by the diesel engine has to be transformed into electric power. We should find a generator with a high efficiency and a high power to mass ratio. The same has to be done for the rotor engines. The chosen solution was found in the work done by Siemens in developing electric propulsion components with high power densities for aviation. The motor/generator produced with this technology has a power density of $\sim 5\, kW/kg$, efficiency of about 95% and is scalable for a wide range of powers.
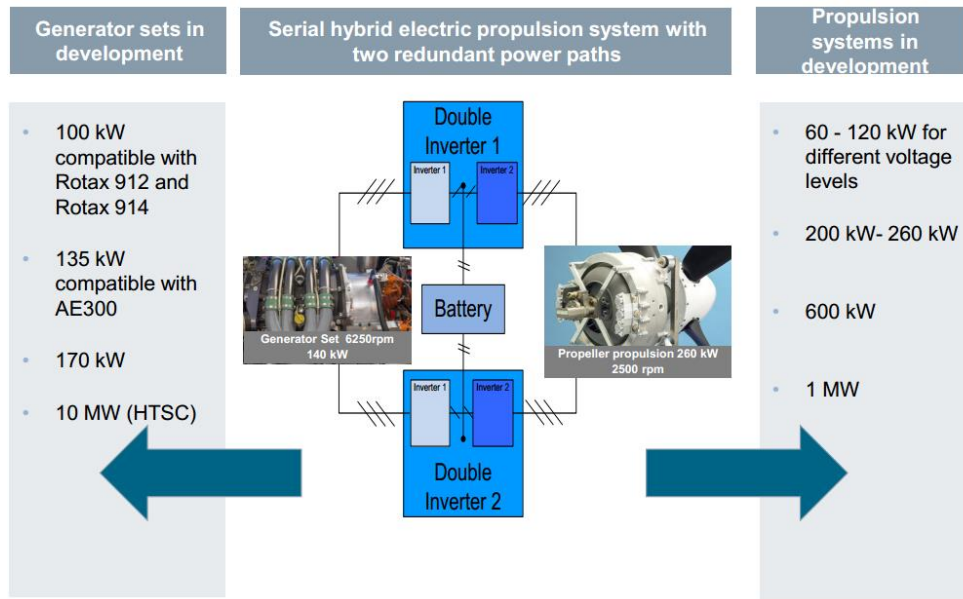
Figure 3.5: power ranges of the Siemens electric propulsion components

Since the technology is scalable, we assume to adopt an electric generator with a power output that is:

$$P_{gen\ out} = P_{thermal\ out} \cdot \eta_{gen} = 200 \cdot 0.95\ hp = 190\ hp = 142\ kW$$

That leads to:

$$m_{gen} = \frac{142\ kW}{5\ \frac{kW}{kg}} = 28.34\ kg$$

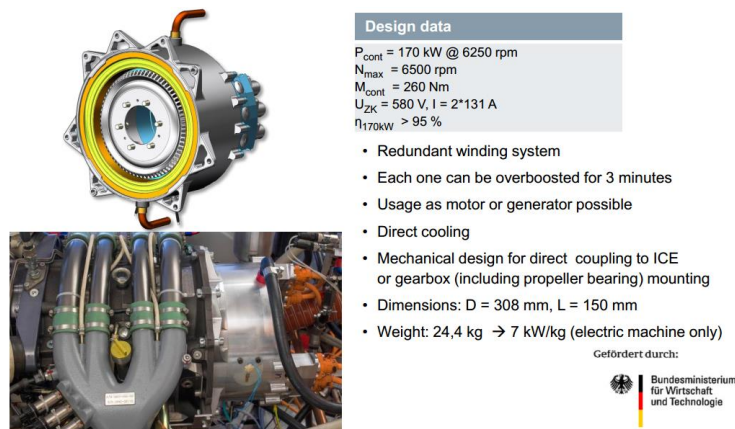The data of our electric generator are similar to the lab tested generator in the following figure:

Figure 3.6: lab tested 170kW Siemens generator

This technology has already flown on the DA36 E-Star 2 hybrid motor glider with the propeller driven by a 65 kW version motor:
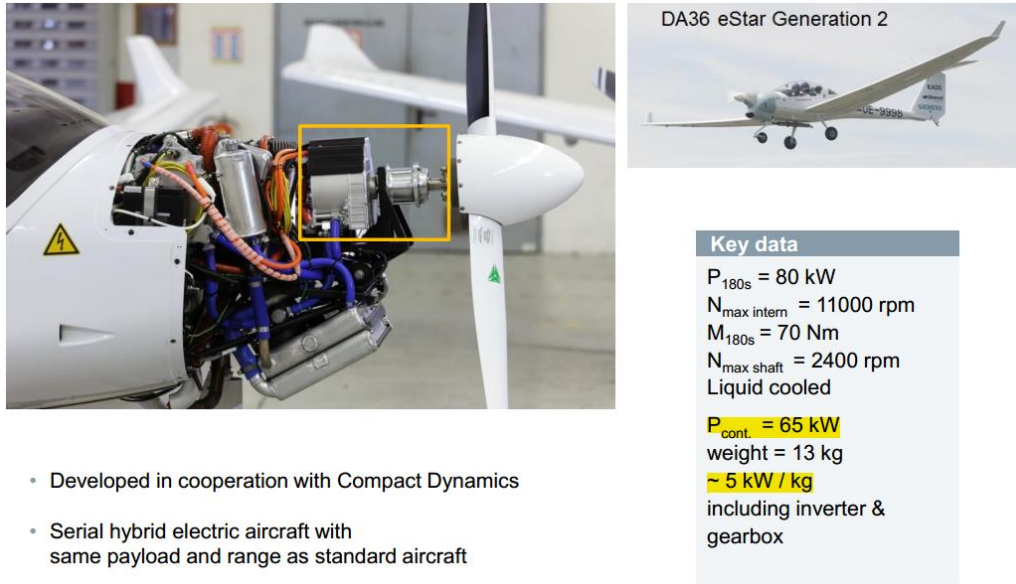
DA36 eStar Generation 2

Key data

P_{180s} = 80 kW
$N_{max\ intern}$ = 11000 rpm
M_{180s} = 70 Nm
$N_{max\ shaft}$ = 2400 rpm
Liquid cooled

$P_{cont.}$ = 65 kW
weight = 13 kg
~ 5 kW / kg
including inverter &
gearbox

- Developed in cooperation with Compact Dynamics
- Serial hybrid electric aircraft with same payload and range as standard aircraft

Figure 3.7: DA36 E-Star 2 application of the Siemens motor and chosen motor for the rotors of the designed aircraft

Since the version of the Siemens motor mounted on the eStar fits the available power per rotor of our aircraft, we decide to pair it with the rotors of our aircraft.

$$P_{available\ per\ rotor} = \frac{142\ kW}{2} = 71\ kW$$

The generator and the motors can all be over boosted for 3 minutes, while producing a +23% of the nominal power.

3.2.3. Hover: disk area estimation

The rotor motors have been chosen so now we know the power required for hover which is given by the power consumption of all the four rotors active at the same time:

$$P_{hover} = 65 \cdot 4\ kW = 260\ kW$$

The disk area necessary to hover with the available power can be derived through the following equation derived from the Actuator Disk Theory:

$$P = \frac{T^{1.5}}{\sqrt{2\rho A}}$$

Where T is the necessary traction, given by $MTOW \cdot g$ and ρ is the air density. The radius of the disk is given by:

$$r = \frac{T^{1.5}}{P\sqrt{2\rho\pi}}$$

The radius of one tilt rotor disk is given by:

$$r_{tilt} = \frac{(0.25 \cdot MTOW \cdot g)^{1.5}}{P_{rotor} \cdot \sqrt{2\rho\pi}}$$

since all the rotors give all the same amount of traction the traction of the single rotor is given by 25% of the MTOW weight.

The disk area of the coaxial counter rotating rotors is larger since the two superposed rotors have a smaller disk area by a factor reduction factor $RF = 1/\sqrt{2}$ to than a single rotor providing the same thrust. So it is possible to modify the previous equations as follows:

$$2 \cdot P = \frac{(2 \cdot T)^{1.5}}{\sqrt{2\rho \left(\frac{A}{RF}\right)}}$$

Leading to:

$$r_{hover} = \frac{(0.5 \cdot MTOW \cdot g)^{1.5}}{2 \cdot P_{rotor} \cdot \sqrt{2\rho\pi}} \sqrt{RF}$$

In order to evaluate an initial value for the rotor disks area and radius we consider a $MTOW = 1200 \, kg$ derived from the reverence aircraft database:

Table 3.2: MTOW of the reference general aviation aircrafts

Reference aircrafts for cruise	MTOW (kg)
Cessna Skyhawk	1157
Cessna Skylane	1406
Piper Arrow	1247
Piper Archer LX	1157
AA-2 Patriot	1089
Beechcraft A23A Musketeer	1089
Cessna 150	726
Spencer S-12-D	1406
Rockwell Commander 114A GT	1202
Thurston TA16 Seafire	1451
Average	1193

The results for the disk area of the rotors are the following:

MTOW = 1200 kg	Disk area [m^2]	Disk radius [m]
Tilt rotors	2.49	0.89
Hover rotors	3.46	1.05

The total area occupied by the disk rotors is:

$$A_{tot} = 2 \cdot A_{tilt} + A_{hover} = 8.44 \, m^2$$

considering that the two hover rotors are superimposed.

These results will be updated at the end of the preliminary design when the MTOW will be evaluated and given as an input by ASTRID.

3.2.4. Battery pack sizing

In order to size the battery pack we have to calculate the power boost needed and evaluate a discharge duration. We decide to use Li-ion batteries with the following characteristics:

<div align="center">

Li-ion batteries

Energy/weight D_{Li-ion}	160	Wh/kg
Power/weight	1.8	kW/kg
Energy/volume	270	Wh/L
Efficiency η_{Li-ion}	0.9	
Depth of Discharge	0.94	

</div>

We suppose that the take-off and landing may have each a maximum of $60\ s$ in hover or transition from hover to horizontal and we want to size the battery pack so that it can guarantee a total of $t_{discharge} = 120\ s$ of power boost with one charge. Besides, we want to size the battery pack considering not only the nominal power required by the rotors, but the over boosted power of $80\ kW$: this means that the total boost power is given by:

$$P_{boost} = (80 \cdot 2)_{hover\ rotors} + (15 \cdot 2)_{boost\ tilt\ rotors} = 190\ kW$$

In the over boosted condition the efficiency of the rotors drops from 95% down to ~ 70%, with this loss in efficiency being not linear as the power increases. Actually, also the thermal engine can generate a boost of power in case of need so, in order to be not too conservative, we consider an over boost efficiency of $\eta_{boost} = 0.8$. We get the following results:

$$m_{batteries} = \frac{P_{boost} \cdot t_{discharge}}{D_{Li-ion} \cdot DOD \cdot \eta_{boost} \cdot \eta_{Li-ion}} = 58.49\ kg$$

3.2.5. ASTRID Aircraft Conceptual Design inputs

Now we can provide ASTRID with the input data necessary to elaborate the calculations for the preliminary design sizing. As mentioned earlier, ASTRID does not support VTOL aircrafts, so we have to use it as if our vehicle is a conventional pistonprop airplane. In order to consider the presence of the electric generator and the electric motors and their efficiencies, we put a fictitious *Electric Payload* in ASTRID with a mass given by the sum of the generator, the batteries and the electric motors:

$$m_{EP} = m_{gen} + m_{batt} + 4 \cdot m_{mot} = 138.82\ kg$$

And we adjust the efficiency of the propeller using a global efficiency that considers also the energy loss during the energy transformation process:

$$\eta_{EP} = \eta_{prop} \cdot \eta_{gen} \cdot \eta_{mot} = 0.8 \cdot 0.95 \cdot 0.95 = 0.722$$

Now we can proceed with the ASTRID inputs.

3.2.5.1. Preliminary data

Aircraft type:	Single engine propeller driven airplane	
Aircraft engine:	Pistonprop	☐ Hybrid aircraft
Number of engines:	1	
Select FAR:	Far23 (Mtow < 5800 kg)	
T(with AB)/T(without AB):		
Number of persons on board:	2	
Weight for person (including hand luggage) [kg]:	110	
Dropped payload [kg]:	0	
Carried Payload [kg]:	138.8	
Maximum Mach:	0,24	
Take off field distance [m]:	?	480
Landing field distance [m]:	?	500
Cl_max:	?	1,9
Cl_max_TO:		2,5
Cl_max_LND:		2,5
Cl during cruise (mean):		0,77
Airfield altitude [m]:		0
Aspect ratio (A):	?	7
Fuselage length [m]:	?	5
Cruise altitude [m]:		4000
Percentage of throttle during cruise [%]		90
Altitude TC [m] (for no turbocharged engines set this value to 0 meters):		0
Thrust/weight ratio in combat:		

Figure 3.8: Preliminary Data input screen

- In this input window it is possible to notice the *Electric Payload* that represents the electric generation and propulsion system.
- We also set a take-off and a landing field distance since we want our aircraft to perform an horizontal landing in case of emergency and a horizontal take of if wanted. The $C_{L_{MAX}}$ coefficients given are representative since the contribution given by hover rotors and tilt rotors can be huge. For example, if the aircraft is approaching for a horizontal landing, with tilt rotors and hover rotors contributing for the 50% to the total lift of the aircraft, the stall speed increases by a factor $\sqrt{2}$:

$$V_{S(T=50\% L)} = \sqrt{\frac{0.50 \cdot W/S}{\frac{1}{2}\rho C_{L_{MAX}}}} = \sqrt{2} \cdot V_S$$

So it is as if the $C_{L_{MAX}}$ was doubled.

- The aspect ratio given in input is calculated from the general aviation database.
- The fuselage length is derived by adding and rounding the hover rotor diameter, a rough value of the wing root chord, the cockpit length and a value of about 75 cm for the nose.

3.2.5.2. Fuel weight – LND&TO – Turns

Fuel weight

Cd_0:		0,0333
Delta Cd_0 due to external elements (bombs, external tanks):	?	0
Wetted area (estimated) [m^2]:		56,79
Oswald factor (e_clean):	?	0,8
Skin friction coefficient C_f:	?	0,004
Propeller efficiency (cruise) [ex. 0,7-0,8]:		0,722
Thrust or Power required at operational altitude for further climb [kg] or [kW]:		0,00
Electric power required by electric users [kW]:		10

Cruise segments:

Cruise segments:	Single-segment cruise	+ – Rename	
Mission type:		Best Range	
Percentage of payload dropped at the beginning of the segment [%]:			
Range [km]:	700	Endurance [h]:	4
Cruise speed (average) [km/h]:			224,96
SFC (cruise) [lb/Hp/h] or [lb/lbf/h]:	0,39	SFC (with afterburner) [lb/lbf/h]:	?
Combat time [minutes]:			
E during cruise:			11,48
Fuel weight in cruise (phase) [kg]:	47,73	Fuel weight in combat (phase) [kg]:	0,00

Fuel weight (cruise) [kg]:	47,73	Fuel weight (combat) [kg]:	0,00
Fuel weight for take off and climb[kg]:			0,00
Fuel weight for secondary power and reserves:	5 % ?		2,39 kg
Total fuel weight [kg]:			50,12

Figure 3.9: fuel weight input window: cruise

- Here it is possible to notice the value of the propeller efficiency adjusted considering the electric efficiency.
- As for the requirements, the aircraft must be able to cover a range of 600 km plus 50 km of reserve. Since the aircraft has a series electric propulsion system, the fuel generator should work at its nominal power rate for most of the time, in order to increase the efficiency. For this reason we decided to input a total range of 700 km: in this way we attribute no fuel consumption to the other phases such as climb and have a fuel margin that can absorb possible variation of the power output of the fuel generator.

Figure 3.10: fuel weight input window: landing, take off and climb

3.2.5.3.   Wing Geometry

Figure 3.11: Wing geometry input parameters

- The input for the wing geometry are the same mentioned in the layout definition.

WING GEOMETRY
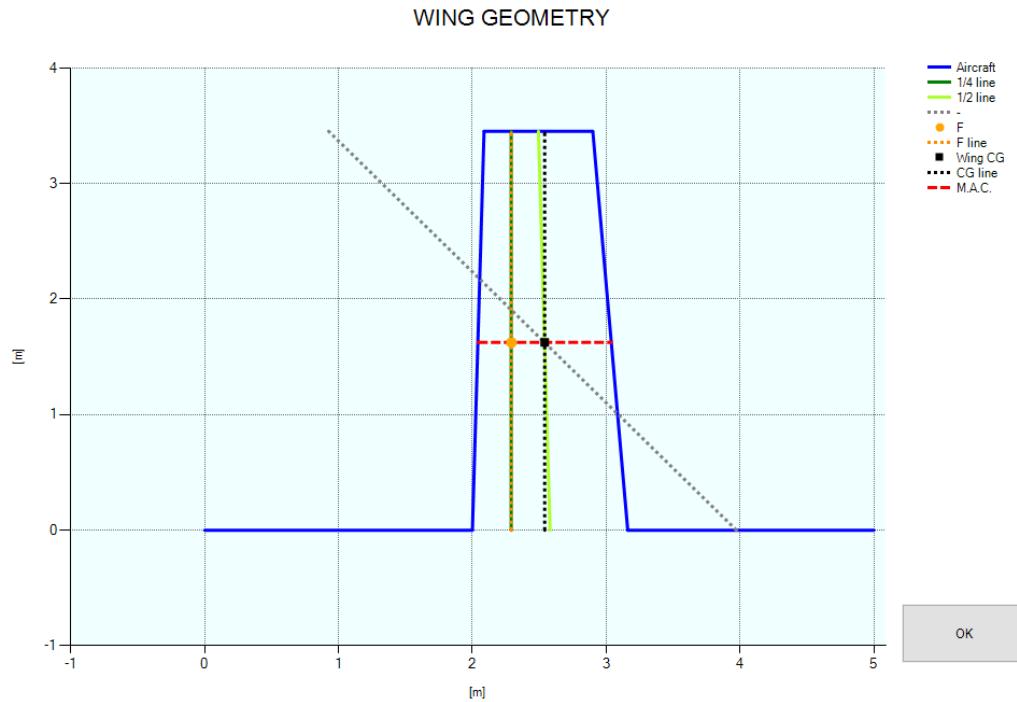

Figure 3.12: wing geometry sketch from Astrid

3.2.5.4.   Thrust/Power

Maximum thrust - pistonprop and turboprop

Minimum take off speed [m/s]:		29,07
Take off speed [m/s]:		34,88
Maximum propeller efficiency [ex. 0,7-0,8]:		0,722
Power per engine [kw] or [hp]:	111,94	150,12
Selected engine power [hp]:		200
(T/W)_max or (P/W)_max:		0,12

Figure 3.13:Power input window

- The first input the equivalent efficiency of the propeller, which is in fact the efficiency of the components between the fuel generator shaft to the propeller. Then ASTRID requires the power of the selected engine. The screenshot of the inputs has been taken after the calculation was done so the final maximum power required for the horizontal flight mode is already visible. It is expressed as a power to weight ratio and it is equal to $(P/W)_{MAX} = 0.12 \frac{kW}{kg}$.

3.2.5.5.   Weight estimation

Empty weight [kg]:	491,09
Fuel weight [kg]:	50,12
Payload weight (passengers+dropped+carried) [kg]:	358,80
Take off weight [kg]:	900,01

Figure 3.14: ASTRID output of the weights estimations

26

- In the last input window ASTRID requires to insert a series of complexity coefficients that are used to evaluate the weight of the various components and subsystems of the aircraft. Then it also requires other inputs that are used for the weights estimation, such as the maximum load factor, set at 3.8 as for CS-23, and the selected engine weight.

3.2.6. ASTRID results

3.2.6.1.   Weights Breakdown

We now rearrange the results provided by ASTRID according to all the consideration made early on in this chapter. We obtain the following results:

Table 3.3: aircraft weights result after the preliminary design

	PoliTo Hornet (preliminary)	
	m [kg]	% MTOW
Payload/crew	220	24.44
Structure	177.49	19.72
Wing	44.18	4.91
Tail	13.25	1.47
Fuselage	93.08	10.34
Landing Gear	26.98	3.00
Systems	452.42	50.27
FCS	35.97	4.00
Electric + Prop. systems	344.51	38.28
Fuel System	13.49	1.50
ECS	4.5	0.50
Avionic System	53.95	5.99
Empty Weight	629.91	69.99
Fuel Weight	50.12	5.57
Payload Weight	220	24.44
MTOW	900	100.00
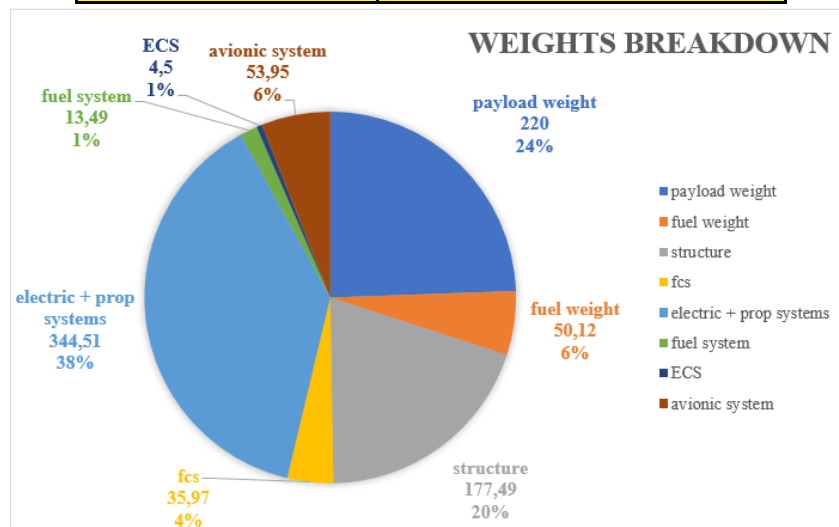
Figure 3.1: weights breakdown of the aircraft after the preliminary design

The "Structure" weights consider the sum of the wing, tail, fuselage and landing gear weight. The landing gear weight is evaluated by ASTRID following a statistical procedure and includes the weight of the landing gear actuators. The "Systems" weight includes all the weight of the aircraft subsystems (except from the landing gear actuators) that are going to be sized in detail for the Mini-Bee in the following chapters. In particular, the weight of the Electric and Propulsion systems are put all together and include:
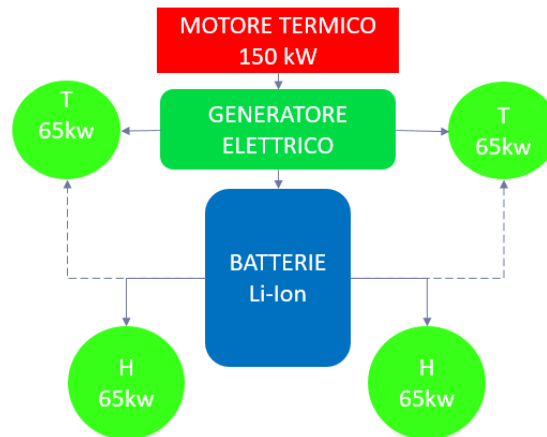
Figure 3.2: scheme of the Electric + Propulsion system

The weights subdivision for the Electric + Propulsion system is presented in the following table:

Table 3.4: weights of the electric + propulsion system

	m [kg]
Electric + Prop. systems	344.51
Fuel generator Gemini 200	*125*
Siemens electric generator	*28.34*
Battery pack	*58.49*
Electric motors	*65*
Propellers + installation	*67.68*
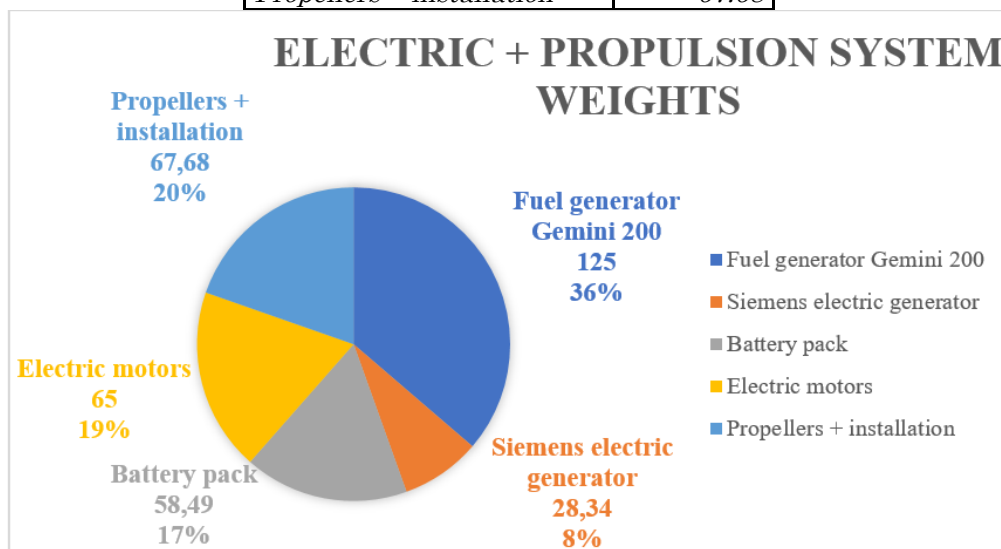
Figura 3.3: weights breakdown of the electric + propulsion systems

3.2.6.2. Matching Chart
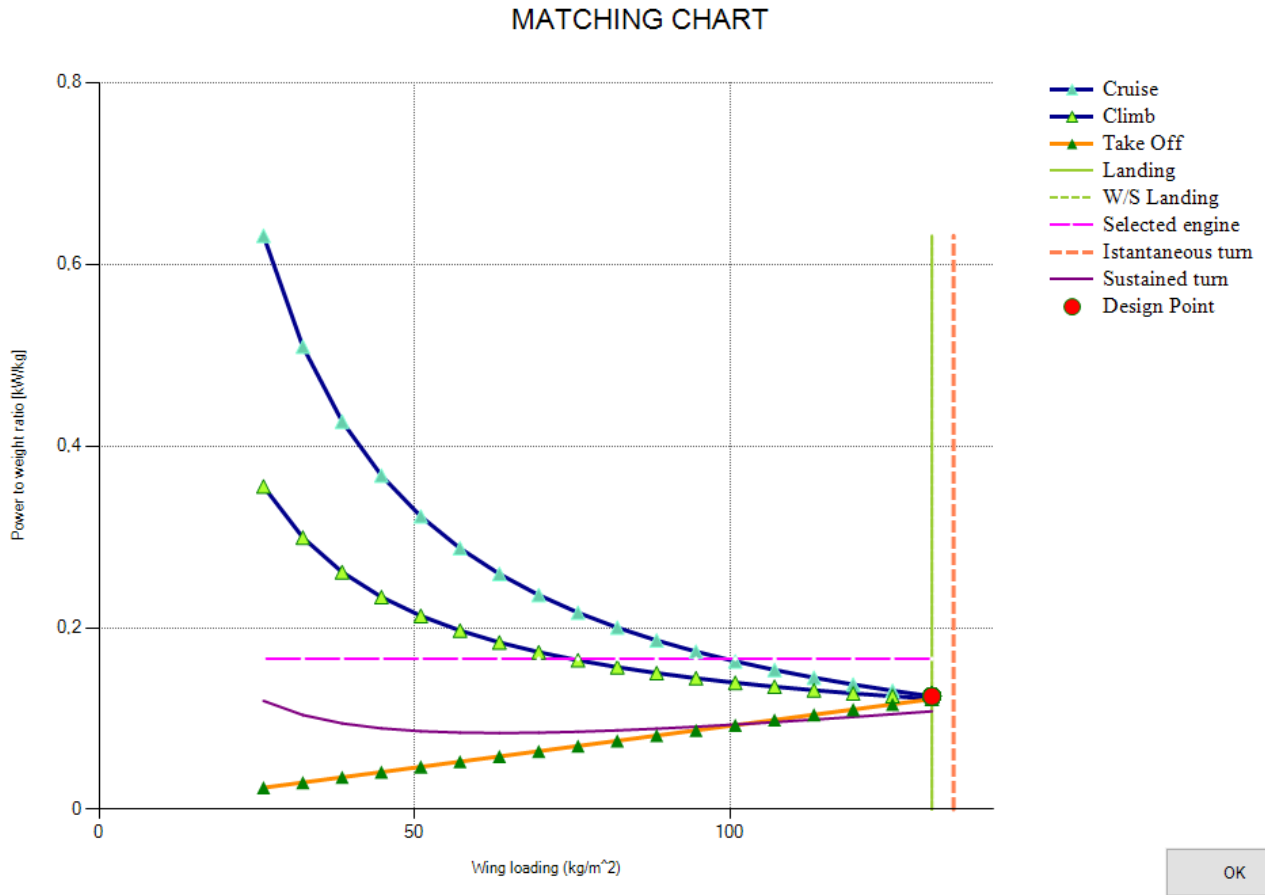
Figura 3.4: Matching Chart for the aircraft after the preliminary design

The matching chart of our aircraft, a power to weight ratio vs wing loading plot, shows that the preliminary design of our aircraft is optimized for the cruise, the climb, the take-off, the landing and the sustained turn. The instantaneous turn curve is not considered in the sizing of our aircraft since it is a maneuver generally required to fighter aircrafts. The pink dashed line represents the installed power on the aircraft, which means the available power from the generator, considering all the electric efficiencies. Since this curve is above the design point, it means that the aircraft has enough power to face the horizontal flight phases and also a margin of extra generated power that can be used to recharge the batteries during cruise.

3.2.7. Battery recharge time estimation

Another output of the preliminary design made with ASTRID is the maximum power needed during horizontal flight that is required to the fuel generator. Knowing that value and the nominal power of the fuel generator we can estimate the time needed to recharge the batteries at the beginning of the cruise phase.

The maximum power consumption required during the horizontal flight phases is calculated by ASTRID and expressed as:

$$(P/W)_{MAX} = 0.12 \frac{kW}{kg}$$

Considering the evaluated maximum take-off weight, we can calculate the power required to the fuel generator:

$$P_{prop} = (P/W)_{MAX} \cdot MTOW = 108 \; kW$$

The nominal power of the fuel generator is $P_{gen} = 149 \; kW$. The available power for battery recharge calculated at the fuel generator shaft is given by:

$$P_{available} = P_{gen} - P_{prop} = 41 \; kW$$

During the sizing of the battery pack we assumed that the discharge phase has a duration of $t_{discharge} = 120 \; s$ where we have to feed the rotors with a total of $190 \; kW$. Considering all the efficiencies of the power chain between the rotors and the batteries we get the following power outflow during the discharge:

$$P_{discharge} = \frac{(190)_{rotor \; power}}{(0.8)_{motor \; boost \; efficiency} \cdot (0.9)_{battery \; efficiency}} = 264 \; kW$$

Considering the available power from the fuel generator, the power inflow that arrives to the battery during the recharge phase considering all the efficiencies is:

$$P_{recharge} = (41)_{available \; power} \cdot (0.95)_{el.generator \; efficiency} \cdot (0.9)_{battery \; efficiency} = 35 \; kW$$

Assuming the same energy flow during charge and discharge phases, the time required to recharge a fully discharge battery pack is given by the following equation:

$$t_{recharge} = t_{discharge} \cdot \frac{P_{recharge}}{P_{discharge}} = 905 \; s = 15 \; min$$

3.2.8. Hover: disk area calculation after the preliminary design

Now that we have a new value of the maximum take-off weight we can adjust the estimation of the rotor disks area and radius. In order to be conservative for this purpose we consider a required total required thrust equal to:

$$T = (MTOW + 50 \; kg) \cdot g = 950 \; kg \cdot g$$

We obtain the following results:

MTOW = 1200 kg	Disk area [m^2]	Disk radius [m]
Tilt rotors	1.21	0.62
Hover rotors	1.72	0.74

The total area occupied by the rotors now is significantly reduced as a result of the reduction of the MTOW. Now we have $A_{tot} = 4.12 \; m^2$, meaning that there has been a reduction of over 50% of the required disk area.

3.3. Preliminary design summary

In the table below all the results of the preliminary design are summarized:

Dimensions	
Wing surface	6,81 m
Wing span	6,91 m
Width	8,27 m
Aspect Ratio	7
Mean Chord	0,99
Taper Ratio	0,7
Length	8 m
Tilt-rotors diameter	1,24 m
Hover Rotors diameter	1,48 m
Weights	
Payload	220 kg
Structure	177,49
Systems	452,42 kg
Fuel	50,12 kg
MTOW	**900 kg**
Performance	
SFC (cruise)	0,386 lb/Hp/h
Cruise speed	220 km/h
Max speed	300 km/h
Range	600 km (+ 50 km)

4. CAD mock-up

In this chapter are reported the CAD model of the aircraft component and of the complete mock-up.

4.1.   Wing

We realize the wing with the following characteristics.

Table 4.1: Wing Characteristics

Airfoil profile	NACA 2410
Wingspan	6.96 m
Root chord	1.17 m
Tip chord	0.82 m
Taper ratio	0.7

The structure of the wing sees two wing spars and nineteen ribs. The ribs are not equally distributed along the wing but they are more nearby in the central section of the wing in order increase the structural strength. With a higher-level structural analysis, probably we will see that some ribs are not necessary. In addition, the front wing spar could give structural problems due to the sweep angle that introduce a flexional-torsional coupling in the structure stress.

At the tips of the wing we put the 5-blades tilt rotors. In the future project-iterations, the shape of the tilt rotors should be reviewed in order to reduce the drag coefficient.
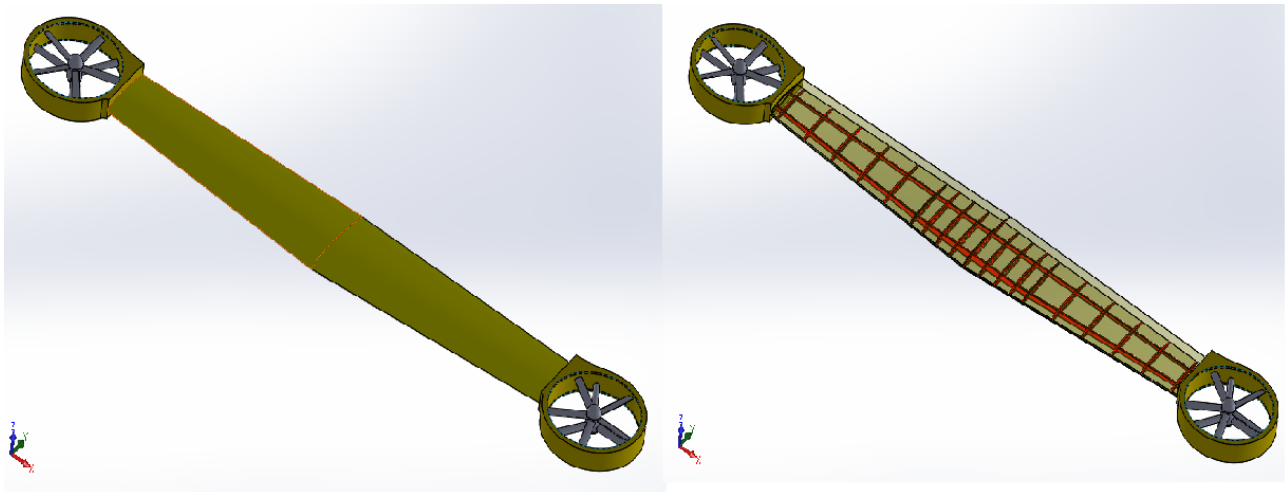
Figure 4.1: Wing on CAD, note the inside structure

4.2.   Fuselage

The fuselage was thought to be more similar as possible to a car shell. With this purpose, we take inspiration both from a sport car and from the Mini-Bee fuselage.

The structure of the fuselage sees six stingers and six formers. The first and the last three formers are thicker than the other ones due to their position: on this formers are joined the wing and the landing gear so their structure must be more resistant. In order to guarantee the structural continuity, the position of the third formers will

probably be modified in the future iteration, avoiding structural brake in correspondence of the door. We also realize the door for the luggage van.

The rear part of the fuselage is integrated with the duct for the five-blades counter-rotating rotor so we realize the siege.
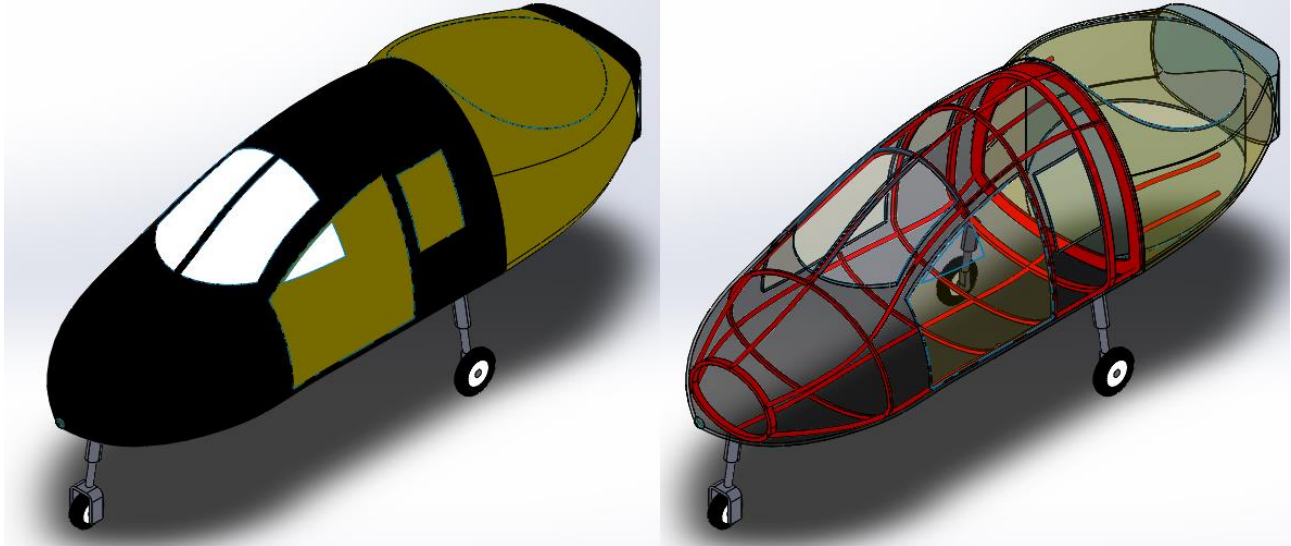
Figure 4.2: Fuselage on CAD, note the inside structure.

4.3. Tail

Due to the presence of the counter-rotating rotor, we cannot use a classical solution with one central tail, so we use two side tail body. At the end of the tail bodies are integrated the rudders and the equilibrator. In this way, we obtained a structural continuity where the tail is connected with the fuselage end with the rear control surface. We also realize the structure of the tail with two spar and seven ribs. The rudders have two wing spar and three ribs and the equilibrator has two spars and six spars. Also in this case the number and position of the structural elements should be reviewed with a higher-level structural analysis.
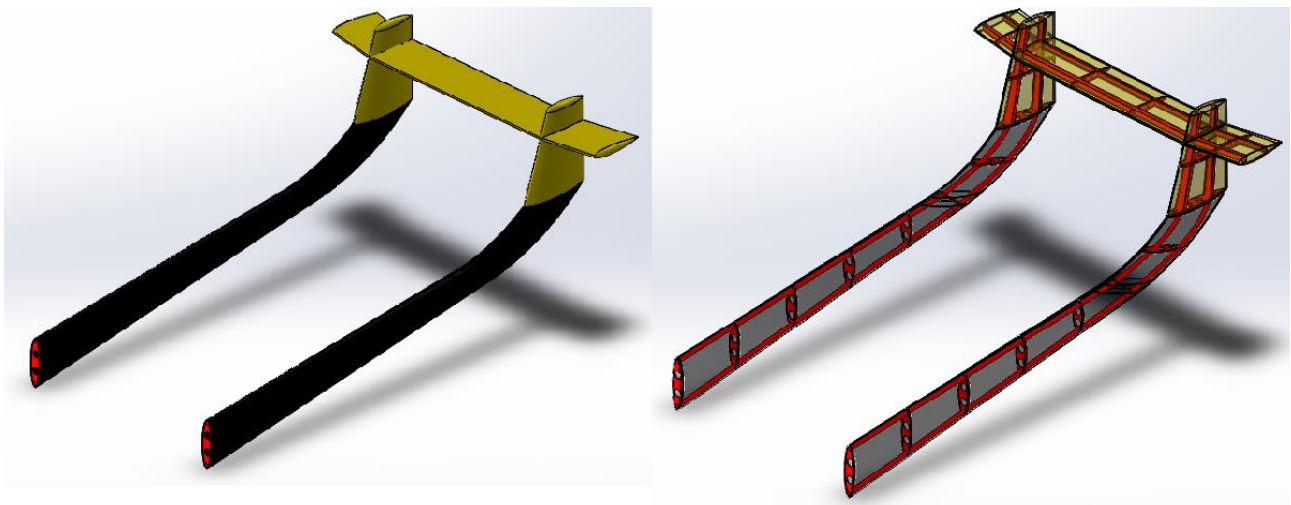
Figure 4.3: Tail on CAD, note the inside structure.

4.4.   Cabin and service bay

We realize a preliminary mock-up of the cabin, which include the seats and the cockpit. Then we realize the front bay where will be allocated the batteries and the rear bay with the thermal engine, the electric generator and the luggage van.
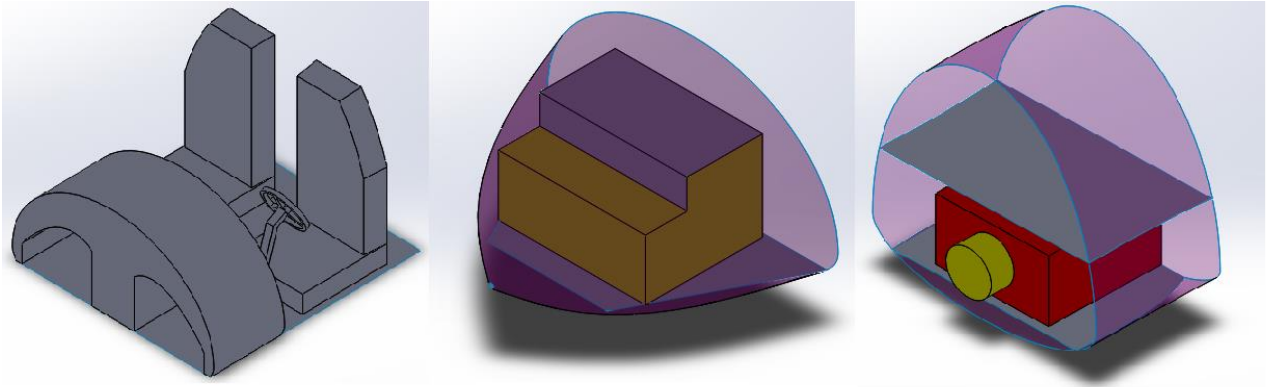
Figure 4.4: Cabin and Service bay on CAD

In the wing, fuselage and tail mock-up, the characteristic of the structural elements, such as dimensions, position, number or shape, are approximate. With the future studies, they could change in order to reduce the structure weight maintaining the structural strength.

4.5.   Final mockup

After the assembly of the elements of the aircraft, we obtained the following mock-up.
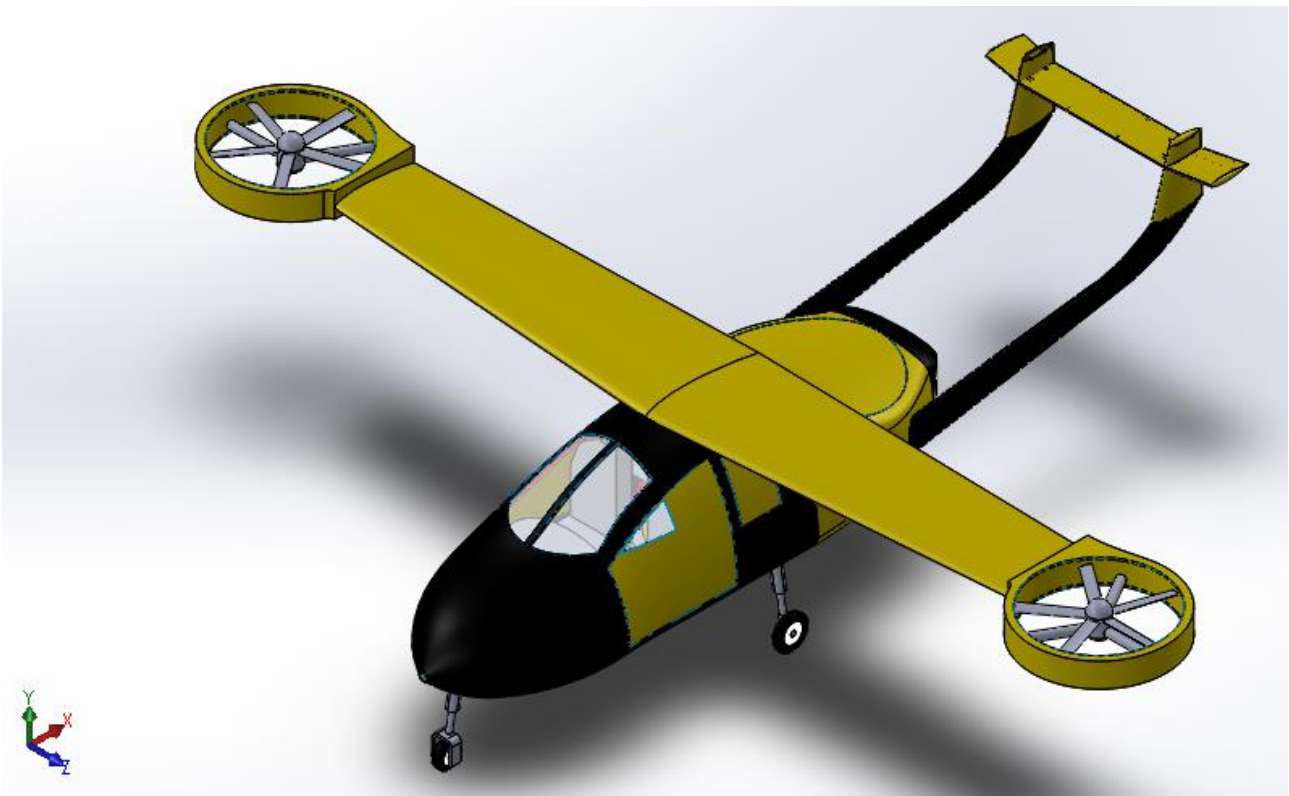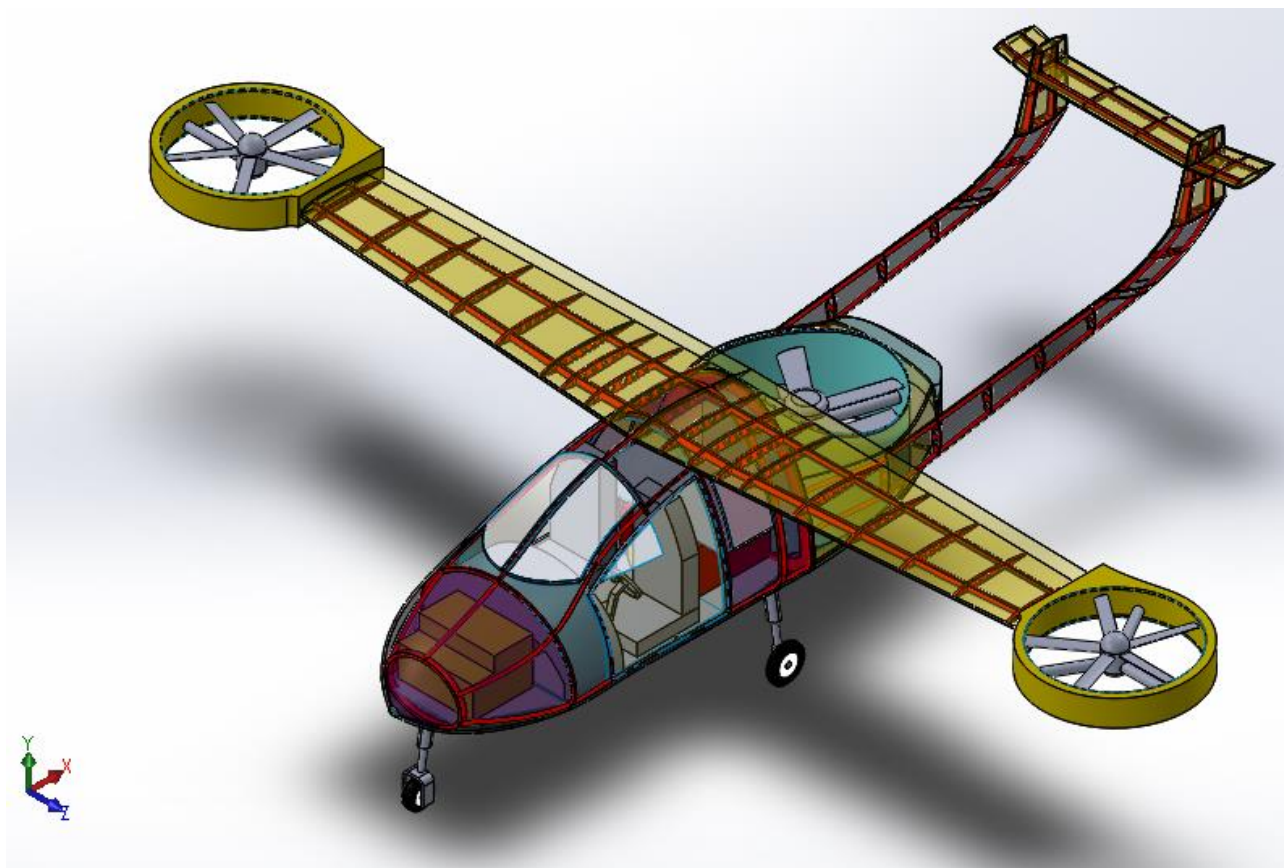
Figure 4.5: Final mock-up on CAD
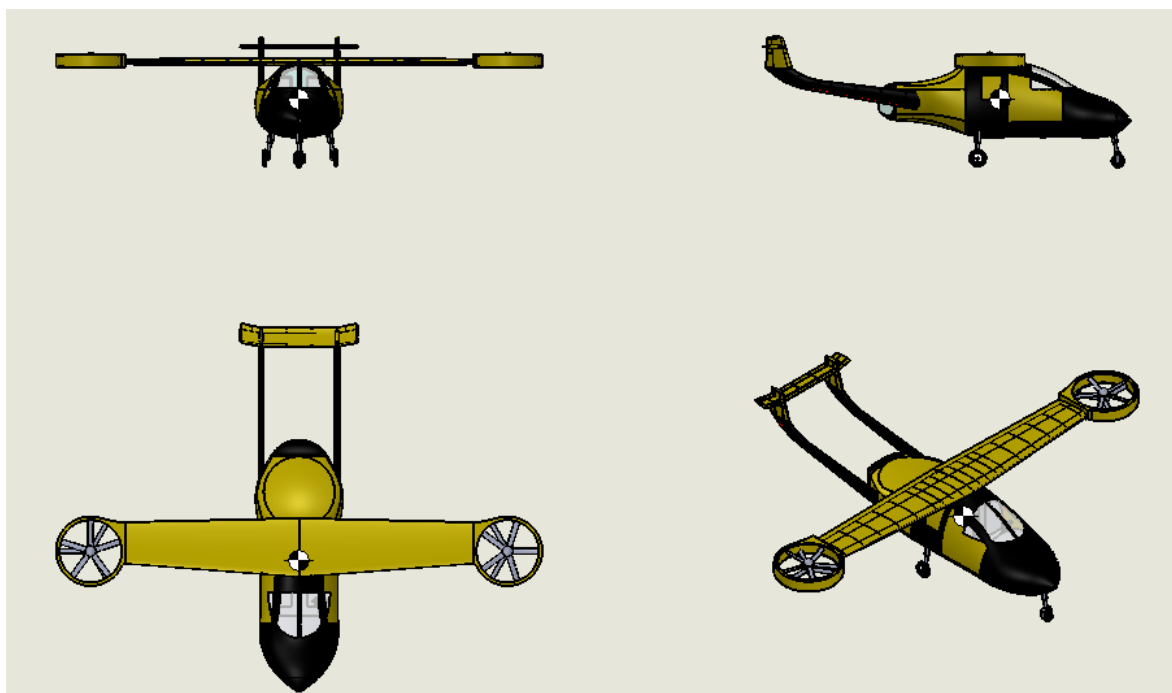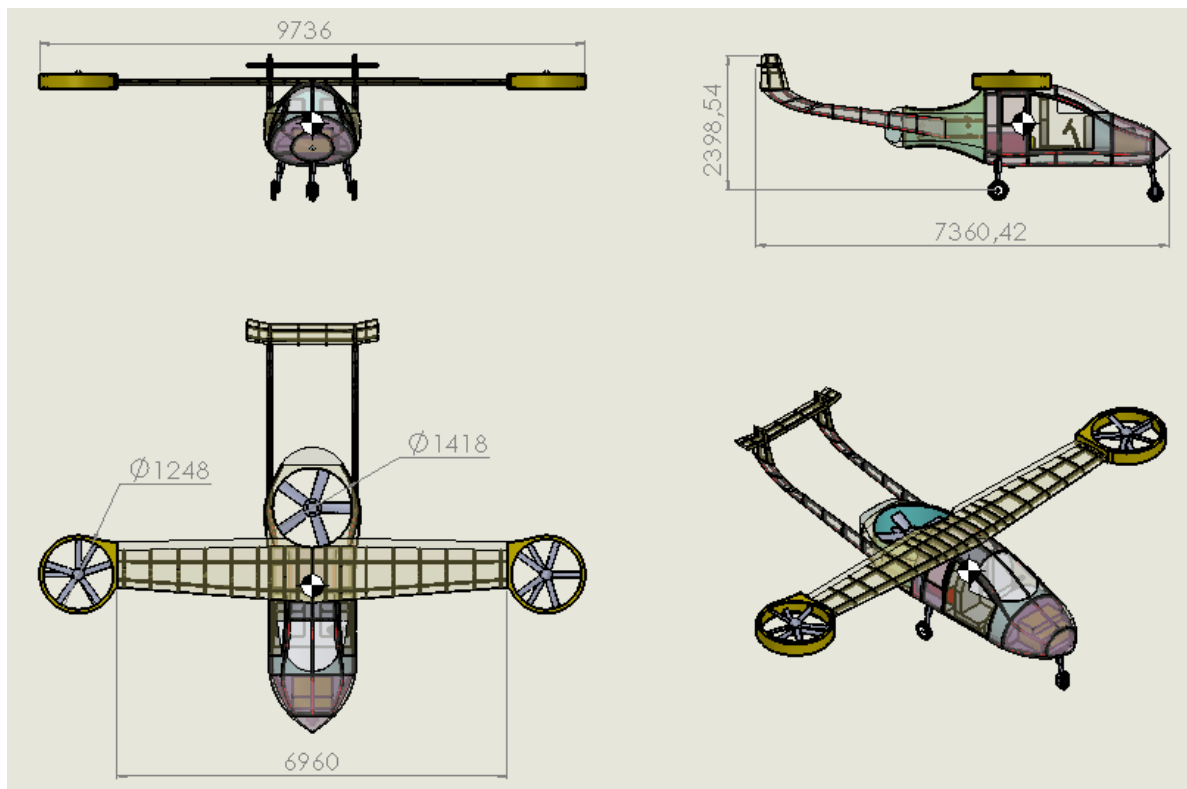
Figure 4.5: Different views of the Mini-Hornet on CAD and its quotes.

5. Mission profile and aircraft geometry

The software, as input of the system analysis, require to define the mission profile. For our mission we supposed to have a 600 km trip from Turin to Paris across the Alps. After the vertical take-off and the transition from vertical to horizontal flight where the aircraft uses the extra power of the batteries, we climb to the cruise altitude of 2500 m. For the first 10 minutes of the cruise, the batteries are recharged. Then, we climb to an altitude of 4000m in order to cross the Alps so the aircraft descents to the original cruise altitude. At the end of the main cruise phase, we descent and prepare for the vertical landing, but we abort the landing at the last minute and decided to fly for others 50km looking for other landing spot.
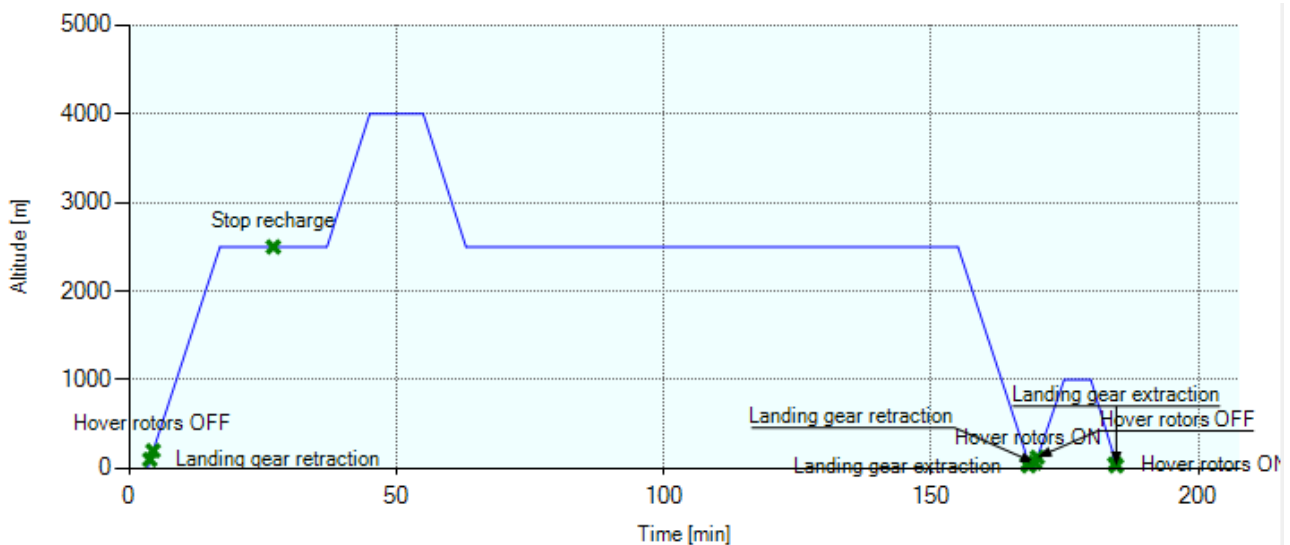
Figure 5.1 - Mission profile

The following step is to provide to Astrid the input data of the preliminary Mini-Bee design. The result are the following:
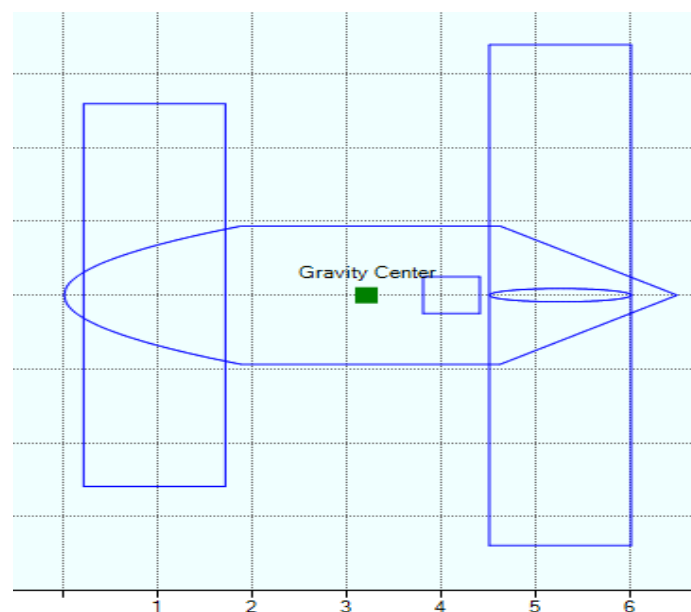
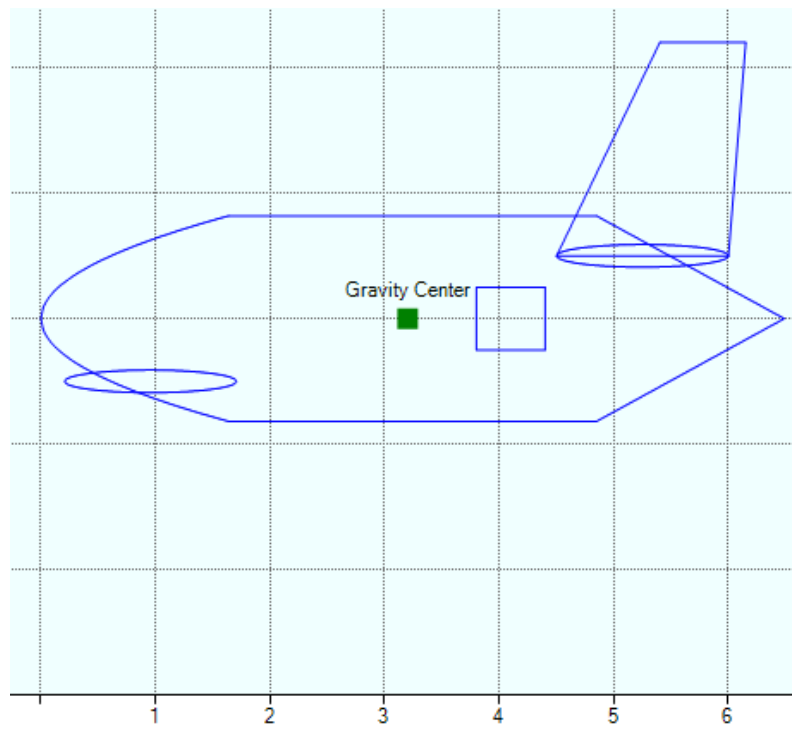
Figure 5.2 : ASTRID geometry input, top view

Figure 5.3 : ASTRID geometry input, side view

6. Avionic System

The Avionic System is one of the most important and complex subsystem of the Mini-Bee Plane because of the necessity to give to the pilot an ergonomic guidance and a maximum reliability of the autopilots installed on-board. These requirements are indeed one of the most restricting: the ability of the plane to compute the mission without many pilot's operations.
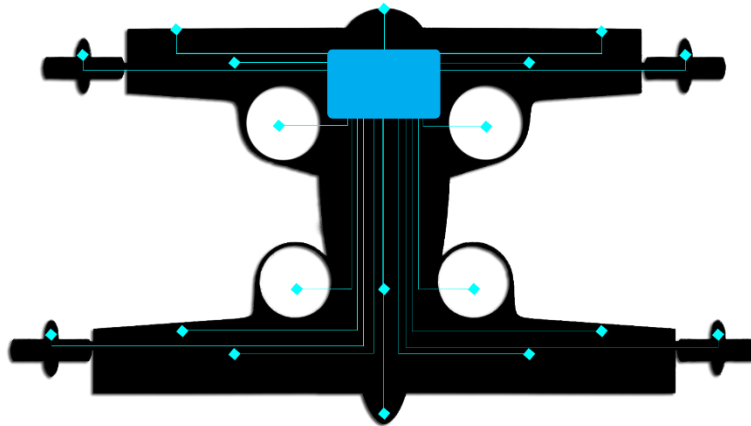

Figure 6.1 : Scheme of the Avionic System. The blue dots indicate the sensors used to process all the data

In all our systems study we focused on the integration of these subsystems. In this case, we chose an Avionic System that describes better this philosophy: the **Garmin G 1000**. It includes a series of sensors which are used to measure the outside and inside physical quantities. At this integrated avionic system was added some more components that link to another important subsystem: the Flight Control System.

6.1. Avionic System components

6.1.1. Garmin G 1000

This integrated Avionic System includes:

- PFD/MFD – Primary Flight Display/Multi-Function Display: on these displays are indicated all information critical to flight, included all air data, navigation data and weather information. It is also possible to visualize the information about aircraft subsystems health.
- COM/NAV functions: the COMmunication functions include audio control unit, automatic management receiver, intercommunication system (AMRIS), Datalink subsystem and SATCOM subsystem; for the NAVigation functions, we have an Air Navigation System, an Air Data Inertial Reference System (ADIRS) which is linked to the PFD or MFD, a Flight Management System (FMS), and a Global Positioning Navigation System (GPS).

- Autopilot (FCS via rotors and rudder): due to the Navigation subsystems, the Flight Control Computer and the attitude and heading reference system (AHRS) it is possible to aviate and navigate the plane automatically with complete fly-by-wire electric actuators.
- HUMS (Health and usage monitoring system): all the subsystems are continuously monitored and all the data are saved to permit, during the maintenance or checking, to evaluate a potential hazard or malfunctions.
- TCAS (Traffic Alert and Collision Avoidance System): this subsystem is closely related to the navigation subsystems.
- Weather Radar

6.1.2. Head-Up-Display *SAAB Aviguide*

This HUD is linked with the flight guidance computers with the purpose to give the possibility to the pilot to aviate and navigate the plane with head up and eyes out for increased safety and control with faster decisions and situational awareness.

The *Saab AviGuide™* HUD System offers the following:

- A fully integrated solution: Optics, Image Generation
- A full-feature system: Symbology & Video
- A certified system solution: Supplemental or Primary Flight Display
- A true NVG compatible solution: Both optically and physically
- A defined growth path for future functions: Hardware & software modularity

6.1.3. Flight Control Computer

In particular, the FCC chosen are **Athena 311** from **Rockwell-Collins**, in number of three plus one more for the redundancy.

Figure 6.1: Athena 311 Flight Control Computer

This FCC is designed with a full range of autopilot and mission management functions, which include autonomous landing and route navigation, both crucial

for the Mini-Bee. Thus, the stability and performance robustness is guaranteed throughout the flight envelope.

6.2. Complete avionic configuration

The weight of this subsystem is indicated below:

Table 6.1: the mass, power and volume budget of the Avionic System

	Mass [kg]	Power [W]	Volume [m^3]	Number installed	Number of redundancies
G 1000	28.29	345	0,09407	1	0
Aviguide SAAB	14	120	0,011	1	0
FCC Athena 311	2.5	18	0,001969	3	1
TOTAL	49.79	501	0,110977		

This Avionic System of the *Mini-Bee* can be divided into four macro-subsystems:

- Flight Data Computer and Data Paths
- Engine Indication System
- Com/Nav System
- Autopilot

In the figures below all the dashed rectangles are included in Garmin G1000 Avionic Integrated System.

6.2.1. Flight Data Computer and Data Paths
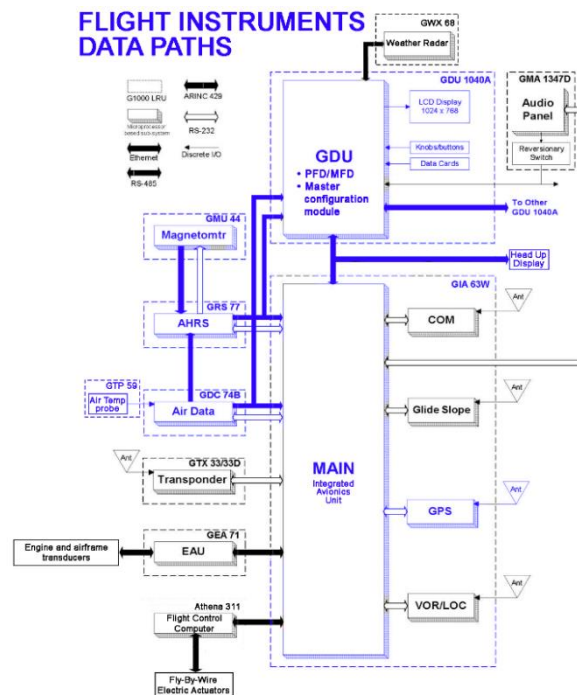
*Figure 6.2: Flight Instruments like sensors and Data
Paths made by a series of data buses and dedicated units*

The data received from the air and from the flight and subsystem sensors are processed into the dedicated computers, then the info are sent to the main computer, called Integrated Avionics Unit. All this information of the Avionics unit are sent, in the end, on one hand, to the Garmin Display Unit and HUD which shows to the pilot all necessary information and, on the other hand, to the Flight Control Computer, ready to be used by the autopilot.

Let see an example in the figure below, in which was zoomed one of the data paths integrated on G1000:
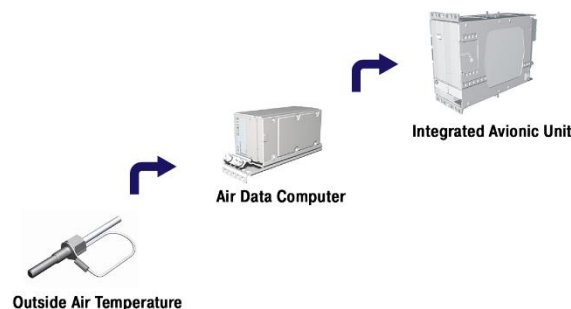
*Figure 6.3: An example of a data path, from the
sensor to the Integrated Avionic Unit*

The Garmin OAT probe provides outside air temperature measurements, which are processed by the Garmin ADC. At this point, the ADC gives air data calculations to the Integrated Avionics and the PFD's.

The integrated avionics interface unit communicates with external avionics over many different interfaces. In the standard configuration, all interfaces are digital, and provides full functionality when integrated with other Garmin avionics equipment, as well as many other avionics equipment with digital interfaces.

6.2.2. Engine Indication System
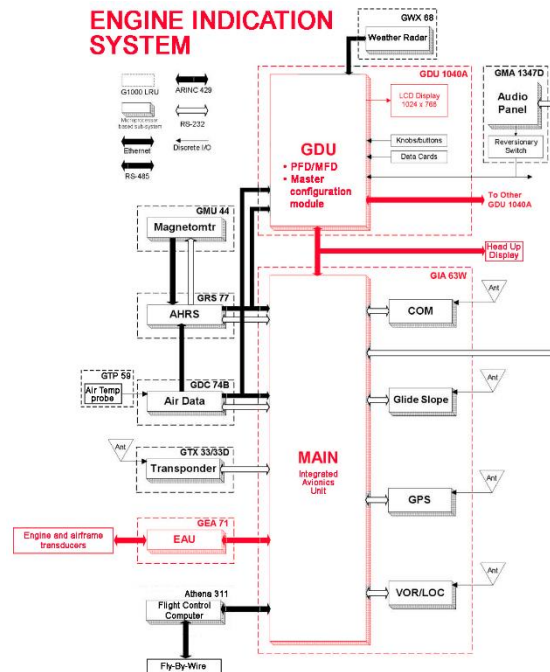
Figure 6.4: Engine Indication Unit processes airframe and engine data

The Engine Airframe Unit is a microprocessor-based LRU (Line Replaceable Unit) that receives and processes signals from the engine and airframe sensors, which may include engine temperatures, oil temperature and pressure, fuel measurement, airframe discrete inputs and other airframe inputs. At this point, the data are sent to the Main Avionics Integrated Unit and to the Garmin Unit Display.
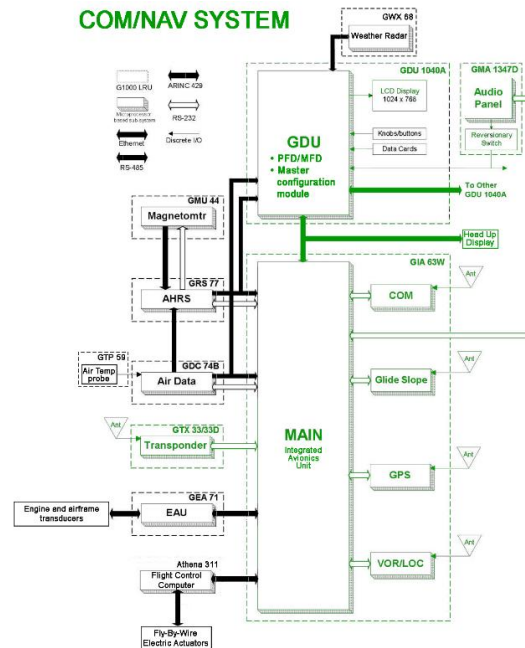
6.2.3. Com/Nav System

Figure 6.5: Communication and Navigation
Subsystem

The COM/NAV System is more complex. The sensors in this case are a series of antennas that are linked to dedicated computers or subsystems. For greater clarity let see the figure below:
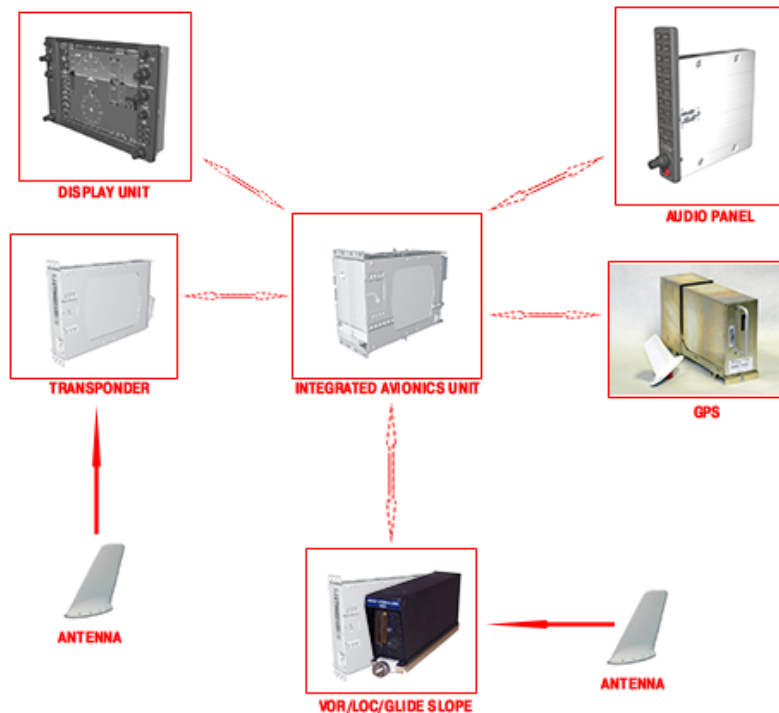

Figure 6.6: The apparats present on G 1000 dedicated for the
Communication and Navigation

The Display Unit and the Audio Panel are the interface between the pilot and the integrated avionics unit. The Audio Panel integrates NAV/COM digital audio, intercom system and marker beacon controls. The transponder is a mode-S providing modes A, C, and S. The GPS is a remote-mounted unit containing a GPS/WAAS (Wide Area Augmentation System) Receiver and a Universal Access Transceiver (UAT).
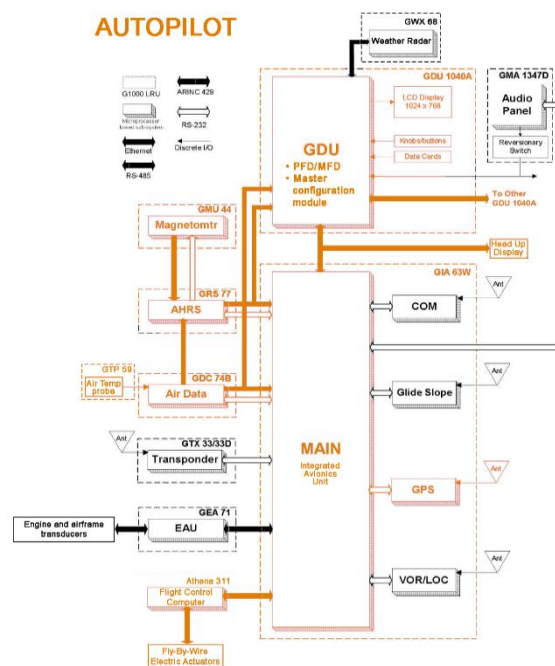
Figure 6.7: Autopilot is an interaction between G 1000 and
the Flight Control Computer

6.2.4. Autopilot

At this point the integrated avionic system (G 1000) is not sufficient to control the flight automatically. So a Flight Control Computer (FCC) is added. The FCC chosen is an *Athena 311* from *Rockwell-Collins.* Although the G 1000 provides an attitude and heading reference system (AHRS) that can be combined with the Air Data Computers and the Engine Airframe Unit, so there is provided additional information ready to be used by FCC. Once the information is processed by the FCC, the fly-by-wire electric actuators are driven.

It is worth to stress the necessity of an Autopilot sub-system that minimizes the pilot intervention, as the typical target of this aircraft is not made by a professional pilot.

6.2.5. Avionic System location and Load Diagram

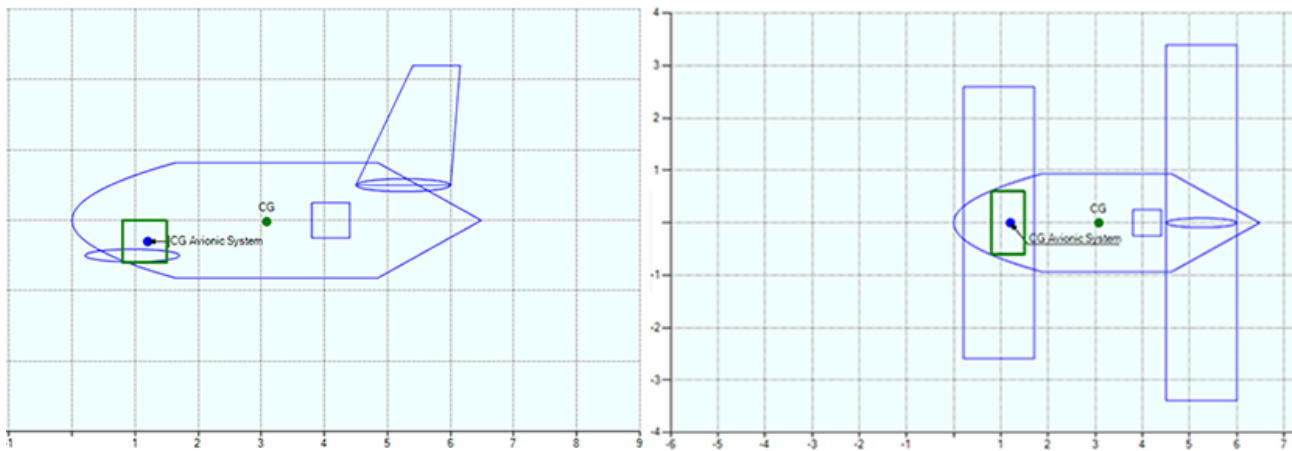The figure below shows a schematic position of the avionic system center of gravity.

Figure 6.8: Avionic system location, side and top view

The Position of the C.G. and the moments of inertia of the avionic system are indicated in the table below:

Table 6.2: The Position of C.G. of the Avionic Subsystem and its moments of inertia

Avionic System Gravity Center	
$X[m]$	1,20
$Y[m]$	0,00
$Z[m]$	-0,30
Moment of Inertia	
$I_x[kg\ m^2]$	3,983
$I_y[kg\ m^2]$	180,994
$I_z[kg\ m^2]$	177,011

The load diagram indicates the absorbed power during all the mission phases.
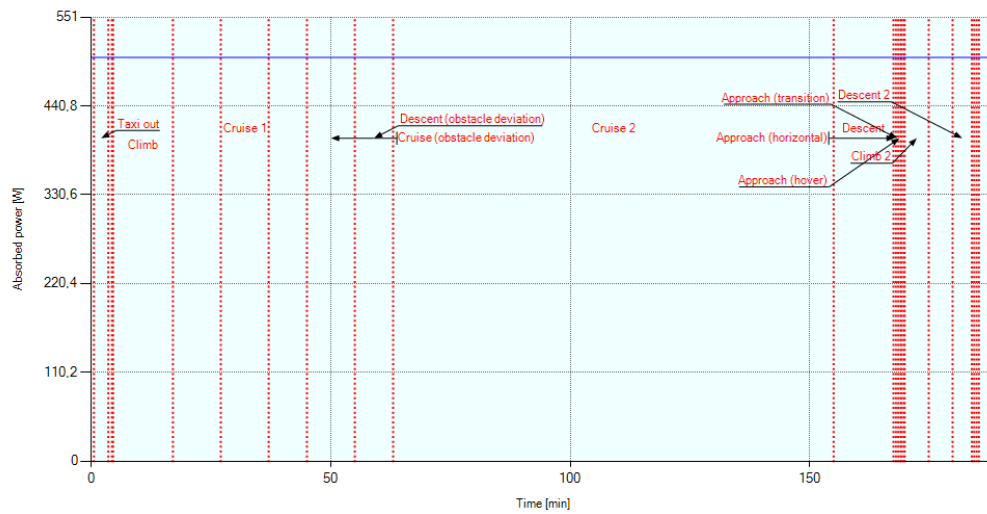
Figure 6.9: Avionic power budget

We can notice that the Avionic System, because of its importance, is activated throughout all the mission. The power load is constant because it is calculated considering the nominal power required by its components. Actually, the integrated avionic system is made of many different sub-units, such as the LRUs of the G1000, that are not all active at the same time. Though, the nominal values used are a good approximation for a first estimation of the power budget.

In the end let see the absorbed power by each main subsystem.

Figure 6.10: In position 1 and 2 we have the Athena 311 FCC.
In position 4 is indicated the power used by G1000, and in
position number 5 is indicated the dedicated HUD from
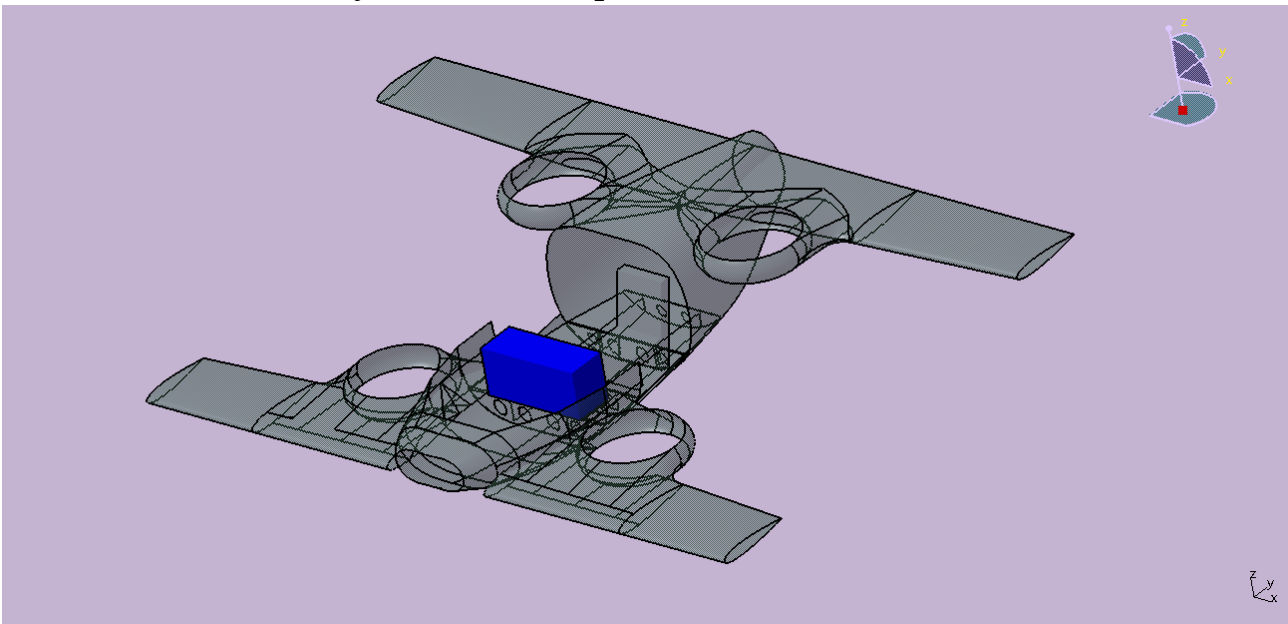
6.3.   Avionic System mock-up

Figure 6.11: Avionic system mock-up

7. Flight Control System

7.1. Architecture

The Mini-Bee has a non-conventional architecture thus also the flight control system is different from the one we can find on a typical aircraft. The only mobile aerodynamic sufrace is the rudder of the vertical empenage while there are none on the two wings. In both vertical and horizontal flight mode the flight control of the Mini-Bee is performed exploiting the thrust and the reaction moments provided by the eight rotors. Furthermore the four external rotors tilt during the transition phases between vertical and horizontal flight with a 90° stroke. Is apparent that an advanced autopilot and control system are required in order to allow a proper controllability to the pilot, anyway the design of those systems are beyond the scope of this project.

Since the Mini-Bee has an all-electric architecture the most obvious choiche is to apply a fly-by-wire scheme to the flight control system. The main advandages of this configuration are the reduced weight and an enhanced ease of redundancy of the electric cables compared to the hydraulical or mechanical lines. Besides, an all electric interface increases both maintainability and reliability. Input signals to the flight control systems are provided by the flight control computer and distributed to each rotor engine, to the rudder and to the rotor tilting actuators which are all powered by the electrical system. The purpose of this section is to size the actuators.
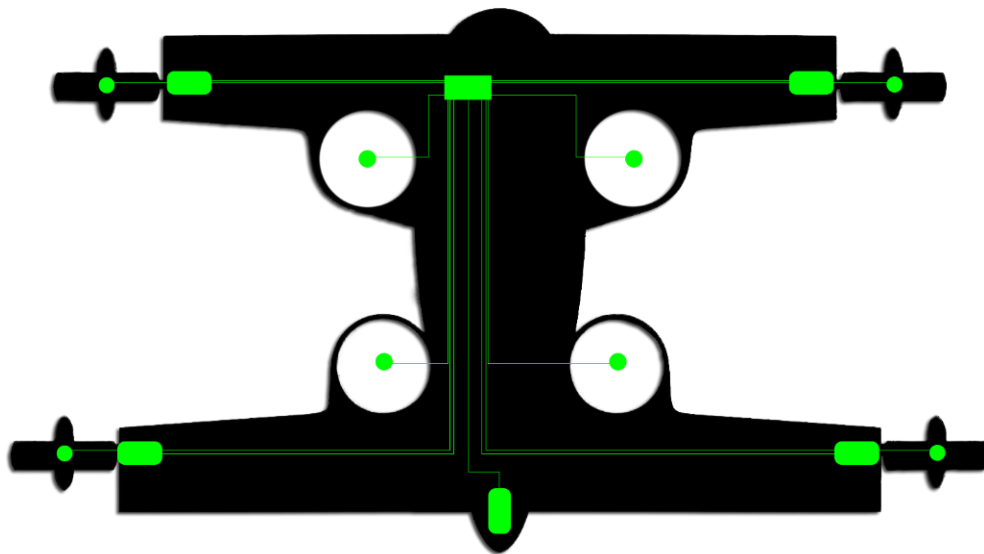

Figure 7.1: Draft of the Flight Control System of the Mini-Bee

7.2.   Actuators sizing

The used approach is to evaluate the stall moment required and the zero-load speed of the actuator, based on the mobile surface linked to the actuator, then it is possible to choose an off-the-shelf actuator with the proper specifications.

Every actuator is characterized by a force versus velocity chart (moment vs angular speed for rotary actuators) which reports the stall force F_0 (or stall moment M_0) that is the maximum load the actuator can bear at zero speed without retroceding and the maximum actuation speed with no loads applied on the actuator V_v (or ω_v). These two parameters are found at the intersection of the characteristic curve with the axis of the force vs velocity chart. This characteristic curve delimits the operating range of the actuator and the nominal power of the actuator can be estimated considering a force equal to $\frac{2}{3}F_0$ and a speed of $\frac{V_v}{\sqrt{3}} = \frac{V_v}{1.73}$:

$$P = F \cdot V = \frac{2}{3}F_0 \frac{V_v}{\sqrt{3}}\frac{1}{\eta} \qquad (linear\ actuator)$$

$$P = F \cdot V = \frac{2}{3}M_0 \frac{\omega_v}{\sqrt{3}}\frac{1}{\eta} \qquad (rotary\ actuator)$$
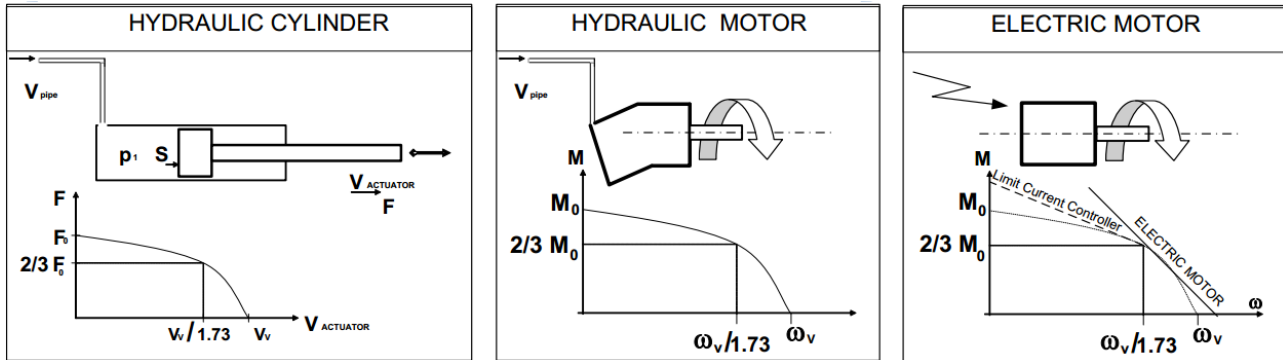
where η is the motor efficiency.

Figure 7.2: Characteristic curve for hydraulic and electric actuators.

Electric actuators are always driven by an electric motor which is rotary so the power diagram is a moment vs angular velocity chart. However, it is possible to have electric linear actuation by coupling an electric motor with a screw drive system or with an integrated hydraulic circuit (Electro-Hydrostatic Actuator). In the latter case the hydraulic circuit is fully integrated in the actuator that is considered an electric component from the architectural and maintenance point of view. The moment vs angular velocity chart of the electric motor is slightly different from the ones typical of hydraulic actuators but it is possible to size electric actuators applying the relations previously shown with a slight error.

7.2.1.   Rudder

7.2.1.1.   Stall moment

The first step is to evaluate the stall moment of the rudder. This is done by providing Astrid with the following input data:

Rudder stall moment evaluation: Astrid input data

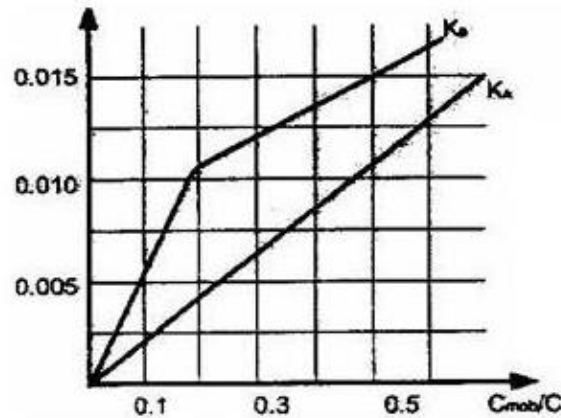|	
Mobile surface area	$A = 0.15\ m^2$
Vert. emp. mean chord	$\bar{c}_v = 1.275\ m$
Rudder mean chord	$\bar{c}_r = 0.26 m$
Max deflection angle	$\delta_{max} = 35°$
Max incidence angle	$\alpha_{max} = 5°$
Reference speed (70% V_{cruise})	$V = 150\ km/h$
No loads actuation time	$t_{0\ load} = 0.5\ s$
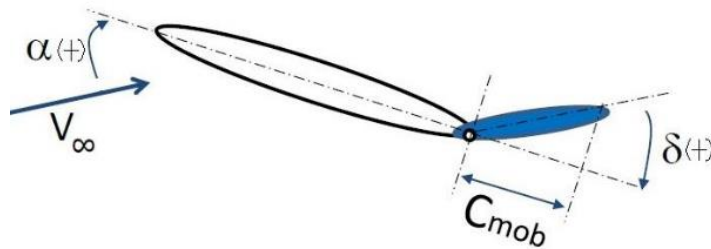
Figure 7.3: Input measures scheme
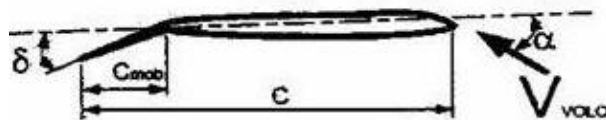

$$C_\mu = K_A\, \alpha^o + K_B\, \delta^o$$

Figure 7.4: Stall moment coefficient estimation

From the graph in the above figure, due to the flight conditions and due to the mobile surface dimensions, Astrid evaluates the hinge moment coefficient applying the following relation:

$$C_\mu = K_A \cdot \alpha + K_B \cdot \delta = 0.407$$

The stall moment of the rudder is then:

$$M_{0\ rudder} = 16.88\ Nm$$

7.2.1.2. Actuator sizing

Since the stall moment is known, we can size the actuator. We decide to use a linear EHA so we have to choose an arm b for the rudder.
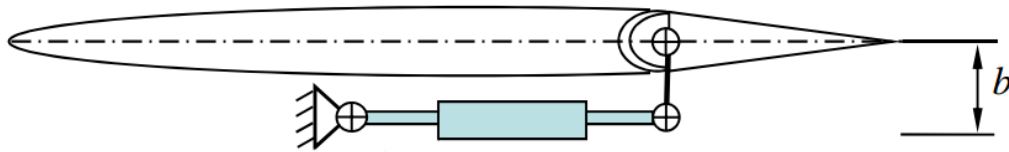

Figure 7.5: Linear actuator attached to a mobile surface.

Astrid suggests to select an arm equal to half the chord of the mobile surface:

$$b = \frac{\bar{c}_r}{2} = 0.13\ m$$

Then it sizes the stall force required for the actuator using the following relationship:

$$F_{0\ actuator} = \frac{M_{0\ rudder}}{b} = 129.85\ N \qquad (actuator\ stall\ force)$$

Given the stall force it is possible to look for some actuators available in the market that can bear the required stall force and that have a stroke and an actuation speed such that it is possible to satisfy the requirement of no load actuation time. The required stroke is given by the following relation:

$$stroke = b \cdot 2 \sin\left(\frac{\delta}{2}\right) = 0.2162\ m$$

While the zero-load speed of the actuator is given by:

$$V_{v\ actuator} = \frac{stroke}{2\ t_{0\ load}} = 0.2162\ \frac{m}{s}$$

7.2.1.3. Chosen actuator

The chosen actuator has the following characteristics:

<u>Rudder electric linear actuator</u>

CEF Industries 8618M80

Nominal power	13 W
Mass	0.45 kg
Nominal force	667 N
Stall force	1290 N
Linear speed	9.4 mm/s
Stroke	0.086 m
Voltage	270 VDC

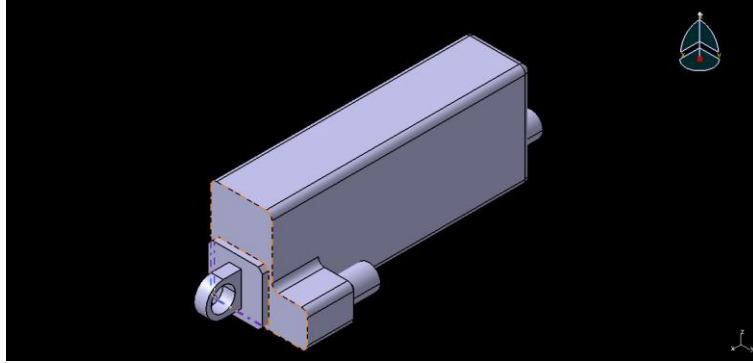| Dimensions (mm)	20×41×206
Active	1
Redundancy	1

Figure 7.6 CEF Industries 8618M80

The stall force of the chosen actuator is significantly higher than the one we need but its linear actuation speed allows us to move the surface with the required $t_{0\,rudder} = 0.5\,s$. According to the catalogue the actuator is built for a voltage of 28 VDC. We decided to power the actuators through the 270 VDC bus and for this reason we reduced the weight of the original actuator by 20% since the dimensions and thus the weight of an electric motor decrease with the increase of the voltage. Now that the actuator is chosen we adjusted the value of b as a function of the new stroke and put it as an input of the actuator sizing in Astrid:

$$b = \frac{stroke}{2\sin\left(\frac{\delta}{2}\right)} = 0.1430\,m$$

Then we obtain the nominal power required by the actuator to operate the rudder:

$$P_{rudder} = 9.94\,W$$

7.2.2. Tilting actuators
7.2.2.1.   Stall moment
In order to size the tilting actuators of the external rotors we used a similar procedure to the one applied for the rudder but this time we had to produce an estimation of the stall moment and give it as an input to Astrid. Since the hinge of the tilt rotor nacelle, the thrust axis and the center of mass of the tilt rotor can be considered as lying on the hinge axis, the main contribution to the stall moment is given by the gyroscopic couple due to the angular velocity ω of the rotor. The gyroscopic moment G is a transient effect and is proportional to the actuation speed of the tilt rotor about the hinge axis $\dot{\theta}$:

$$G = J_r \omega \dot{\theta}$$

where J_r is the moment of the inertia of the rotor disk and is given by the following equation:

$$J_r = \frac{mr^2}{2}$$

with m and r being respectively the mass and the radius of the rotor disk.

We evaluated a rough estimation of the weight of the rotor disk assuming a composite material with density $\rho = 1800\ kg/m^3$, 8 blades with mean chord $\bar{c} = 0.1\ m$, mean thickness $\bar{h} = 0.012\ m$. In this way, we obtain:

$$m = 8 \cdot \rho \overline{ch} r = 8.64\ kg$$

To estimate the stall moment G we need to find the maximum angular speed ω of the rotor disk. To define ω we assume that it is such that we don't have a critical local speed at the blade tip. We can calculate the allowed ω for two cases: the hover condition and the horizontal flight at maximum speed.

In the hover phase the total speed seen by the tip of the blade is given by the sum of the tangential speed of the tip V_{tip} and the induced speed of the external flow u that can be evaluated using the Actuator Disk Theory:

$$u = \frac{P}{T}$$

where P is the power of the rotor and T the thrust. The maximum ω_{max} allowed can be find using the following equation:

$$a = \sqrt{u^2 + (\omega_{max} \cdot r)^2}$$

$$\gamma R^* Tem = u^2 + (\omega_{max} \cdot r)^2$$

$$\omega_{max\,hover} = \frac{\sqrt{\gamma R^* Tem - \left(\frac{P}{T}\right)^2}}{r} = 680\,\frac{rad}{s} = 6494\ rpm$$

We assumed to fly at sea level with a temperature $Tem = 288\ K$.

The same calculation can be done for a flight condition at maximum speed $V_{max} = 300\ km/h$ and an altitude of $4000\ m$. In this case, we use the same equations applied earlier but the flow speed incident to the rotor is obtained by summing the induced speed u and the external flow speed:

$$V = u + V_{max}$$

The result is then:

$$\omega_{max\,V_{max}} = \frac{\sqrt{\gamma R^* Tem - \left(\frac{P}{T} + V_{max}\right)^2}}{r} = 627\,\frac{rad}{s} = 5987\ rpm$$

In this case the allowed rotor speed is lower since the flow speed at the rotor tip is higher.

There are still some considerations to do before defining a value for the angular speed of the rotor. The rotors of the Mini-Bee are characterized by a high value of the disk loading T/A. The Mini-Bee has a disk loading of about $190\ kg/m^2$ which is higher than the one of the Bell V22 Osprey with a disk loading of $130\ kg/m^2$ and far beyond the

typical value for a light-medium weight helicopter (less than $20\ kg/m^2$). Rotors with a high disk loading are characterized by a higher solidity and higher twist of the blades, the Actuator Disk Theory becomes less accurate and cannot describe the evolution of the flow around the airfoil of the rotor blades. For this reason, we decided to assume as ω the maximum value allowed at max speed significantly reduced by about the 25%:

$$\omega = 5987 \cdot 0.75\ rpm \cong 4500\ rpm$$

The last parameter to define is the actuation speed of the tilt rotor. We decided to set an actuation time from the hover to the horizontal flight position and vice versa of 3 seconds, so we obtain $\dot\theta =\ 30\frac{deg}{s}$.

Now we can finally evaluate a rough value of the gyroscopic moment of the tilt rotor to use as the stall moment of the tilt rotor actuator:

$$G = \frac{mr^2}{2}\omega\dot\theta =\ 236.87\ Nm \cong 240\ Nm$$

We can now provide the input data to Astrid:

<div align="center">

Tilt rotor actuator sizing: Astrid input data

Stall moment known	$G = 240\ Nm$
Max deflection angle	$\delta_{max} = 90°$
No loads actuation time	$t_{0\ load} = 1.2\ s$

</div>

7.2.2.2. Chosen actuator
The chosen actuator has the following characteristics:

<div align="center">

Tilt rotor electric rotary actuator

MOOG 965	
Nominal power	$152\ W$
Mass	$3.88\ kg$
Nominal moment	$248.6\ Nm$
Stall moment	$282.5\ Nm$
Nominal speed	$35\ deg/s$
Zero-load speed	$87\ deg/s$
Stroke	$90\ deg$
Voltage	$270\ VDC$
Dimensions (mm)	$89\times180\times226$
Active	4
Redundancy	8

</div>

Also in this case, we reduced the weight of the actuator by 20% per the fact that we power it with 270 VDC.
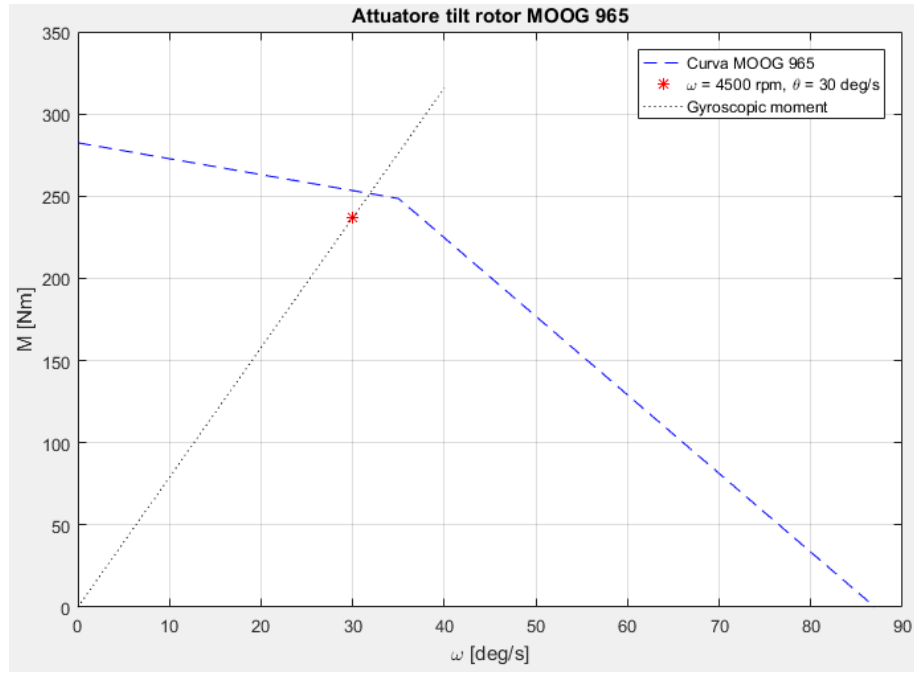
Figure 7.7: Moment vs angular velocity chart of the MOOG 965

The above figure shows the moment vs angular velocity chart of the chosen tilt rotor actuator, with the red point showing the load point at the rotor angular velocity ω estimated in the previous section and an actuation speed of $30 \, deg/s$. Since the gyroscopic moment is proportional to the actuation speed $\dot{\theta}$, by increasing the actuation speed the moment opposing to the actuator motion increases. This means that the set of working points on the chart are not just the one in the area delimitated by the characteristic curve (blue dashed line) but also lay on the gyroscopic moment curve (black dotted line). It is possible to tilt the rotor at the zero-load angular speed of $87 \, rad/s$ only when the rotor is not moving and the gyroscopic moment is none. For this reason, the value of the zero-loads actuation time $t_{0 \, load} = 1.2s$ given as an input in Astrid has not a real physical value and has been chosen with the purpose of having an output power budget equal to the nominal power of the Moog 965 actuator.

7.2.3. Rotor collective pitch actuation

We assumed the rotor disks to have a fixed blade pitch as it is typical for multi rotor applications. A variable pitch increases the efficiency and the performance of the rotor in terms of thrust response but also increases the mechanical complexity of the system and affects the power budget of the flight control system by adding a pitch control actuator. Furthermore, a fixed blade pitch rotor controls the variation of thrust by varying the rotation speed of the rotor requires a variation of the kinetic energy that is supplied by the electric motor. This leads to constraints on the flight envelopes of multirotor helicopters. In particular, the response time of the rotor is limited by the rotational moment of inertia of the motor-rotor pair so this is a more evident problem on heavier multirotor helicopters that require larger rotors. By introducing a variable collective pitch rotor the thrust can be regulated by varying the pitch of the blades

while keeping a constant rotor speed avoiding the transient load due to the variation of the rotor kinetic energy.

Considering a possible future evaluation of a trade-off analysis of a fixed pitch rotor against a variable collective pitch rotor we decided to report here the technical specifications of two actuators designed to control the pitch of the rotor blades for an unmanned aerial vehicle and accordingly we can suppose they are sized to satisfy the typical actuation speed and loads for that job.

Figure 7.8: Description of the rotor pitch actuators from the Moog brochure

Rotor collective pitch linear actuators

MOOG 801/973

Nominal power	33 / 59 W
Mass	2.86 kg
Nominal force	823 / 1557 N
Stall force	1290 N
Linear speed	40.1 / 38.1 mm/s
Stroke	0.1214 / 0.1143 m
Voltage	28 VDC
Dimensions (mm)	83×90×264 / 284

Considering a collective pitch control with uniform variation of the pitch for all the blades of the rotor we can consider to use one actuator for each rotor that controls all the blades. During hover and transition phases all the 8 rotors are working while during cruise just the four external tilt rotors need the collective pitch control which is continuous through the whole flight. So we obtain the following additional power loads:

Table 4.1: Number of actuators used in the two main flight configurations and the power used (including the redundancies)

MOOG 801/973	n. of Active Rotors	Required Power [W]
horizontal flight	4	132 / 236
vertical/transition	8	264 / 472

7.3. Astrid results for the Flight Control System

7.3.1. Power Budget
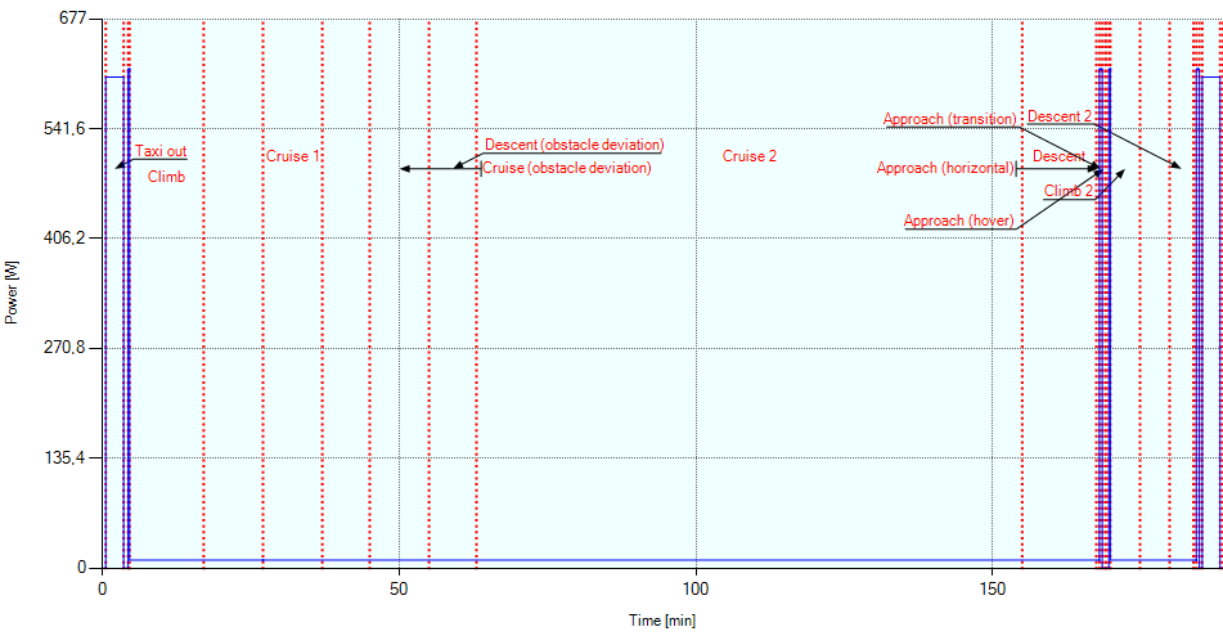
Flight Control System - Power Budget

Figure 7.9: Flight Control System, power budget

In the power budget of the flight control system shown in the figure above, the phases of transition between vertical and horizontal flight stand out showing a peak of the power absorbed by the flight control system, with $605\,W$ mostly required by the actuators of the tilt rotors that require about $150\,W$ each. Moreover during horizontal flight the only actuator running is the one that governess the rudder.

7.3.2. Mass and Volume Budget

Surface	Category	Total weight [kg]
Rudder	Electric	0,72
Tiltrotor ant sx	Electric	7,76
Tiltrotor ant dx	Electric	7,76
Tiltrotor post sx	Electric	7,76
Tiltrotor post dx	Electric	7,76

Total actuation system weight [Kg]
31,76

$$Total\ Volume = \ 0.0293318\ m^3$$
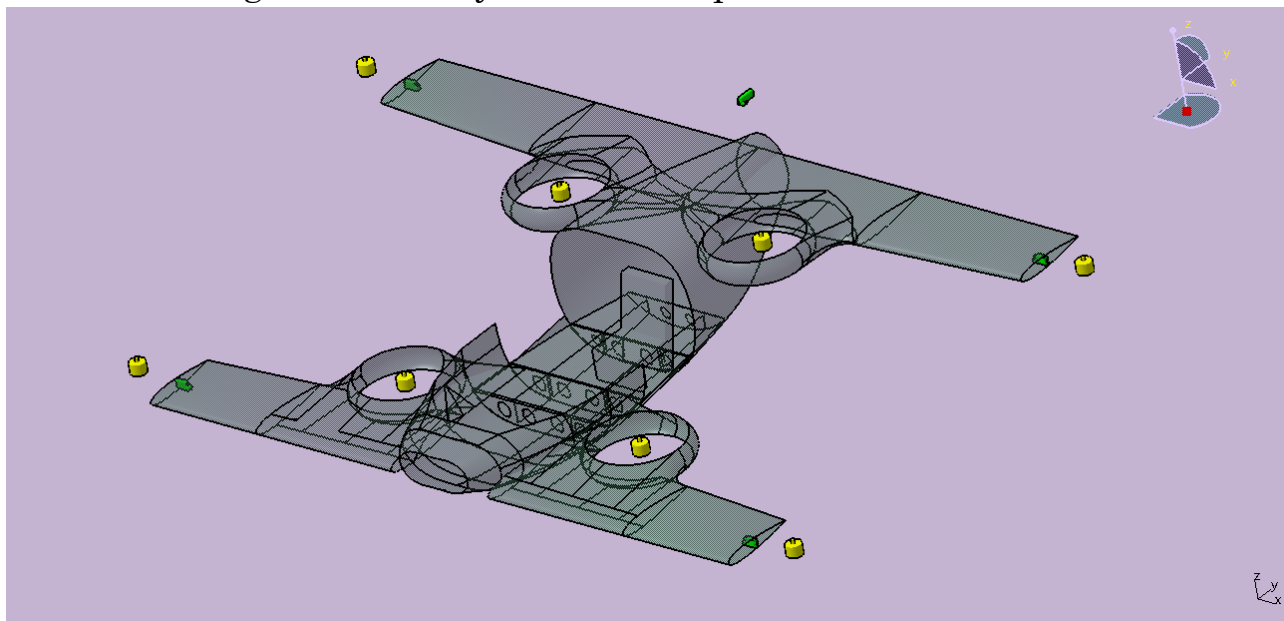
58

7.4.   Flight Control System mock up

Figure 7.10: Flight Control System on the Mini-Bee CAD

The installation of the Flight Control System on the Mini-Bee is strictly reliant on the position of the mobile surfaces and parts of the aircraft but most of the weight of the system is due to the tilt rotor actuators which are close to the tilt rotor so their center of gravity is close to the thrust center of the external rotors and then also close to the center of gravity of the whole aircraft.

8. Landing Gear
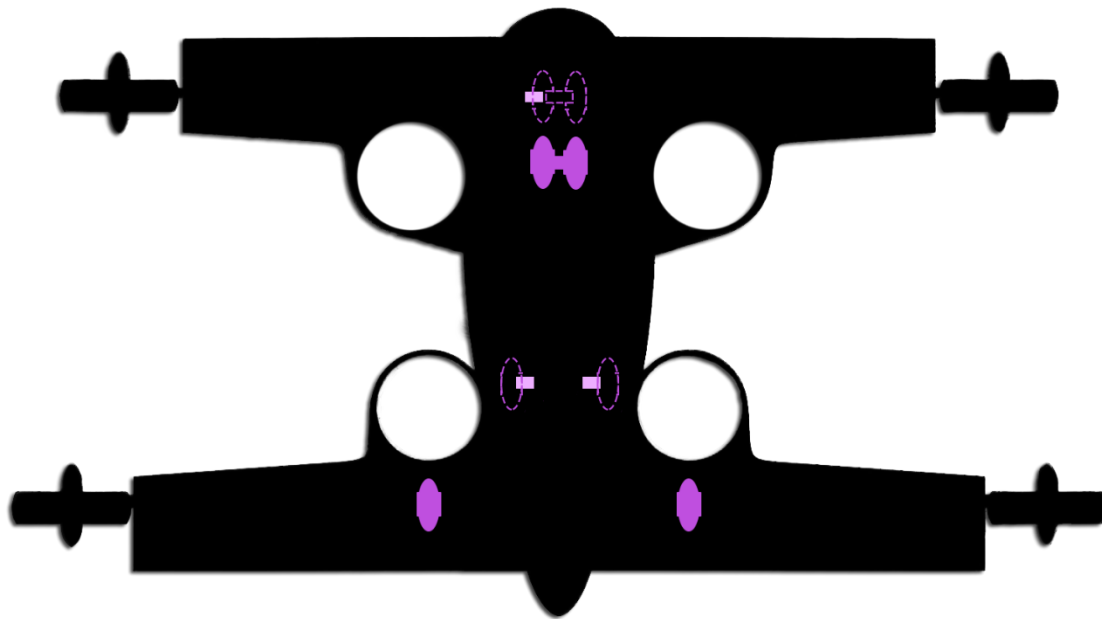
Figure 8.1: Schematic view of landing gear, where dashed lines represent the retracted position and the full ones the extracted position.

Installed Landing Gear has a tricycle configuration and is made up by a thinner forward single structure equipped with two wheels in order to guarantee a major stability during taxi turning maneuvers, and by a more solid double structure for the main gear. This is justified by the fact that the aircraft center of gravity is definitively closer to main gear structures and, of course for static stability matters, it's included between those and the forward one.

As we can see in the figure above, in order to avoid problems during taxi maneuvers, the main gear is extracted towards fuselage sides, for guaranteeing a larger laying base particularly during turns, and both structures are extractable in a way that, in case of actuation failure, the gear is able to extract in a "free fall" way.

As first approximation, we assumed the landing gear system weight equal to 4% of MTOW, obtaining the value of 48 kg; furthermore, we assigned 60% of this value to the structure (legs and wheels) and the remaining to actuators, thus obtaining respectively 28.8 kg and 19.2 kg. Finally, we allocated 70% of structure weight to the main gear and the 30% to the forward one, or rather 20.16 kg (m_m) and 8.64 kg (m_f).

8.1.Retraction actuator sizing

Starting from this mass value, we calculated the stall torque the actuator needs to provide in order to extract and retract the gear legs, as follow:

$$T_{s,f} = F_f \times b_f = 42.4 \, Nm$$

for forward structure, where $b_f = 0.5$ m is the distance between structure center of gravity and the leg hinge and $F_f = m_f \times g = 84.76 \, N$. Same for main gear produces:

$$T_{s,m} = F_m \times b_m = 79 \, Nm$$

with $b_m = 0.8 \, m$, and $F_m = m_m \times g = 98.88 \, N$.
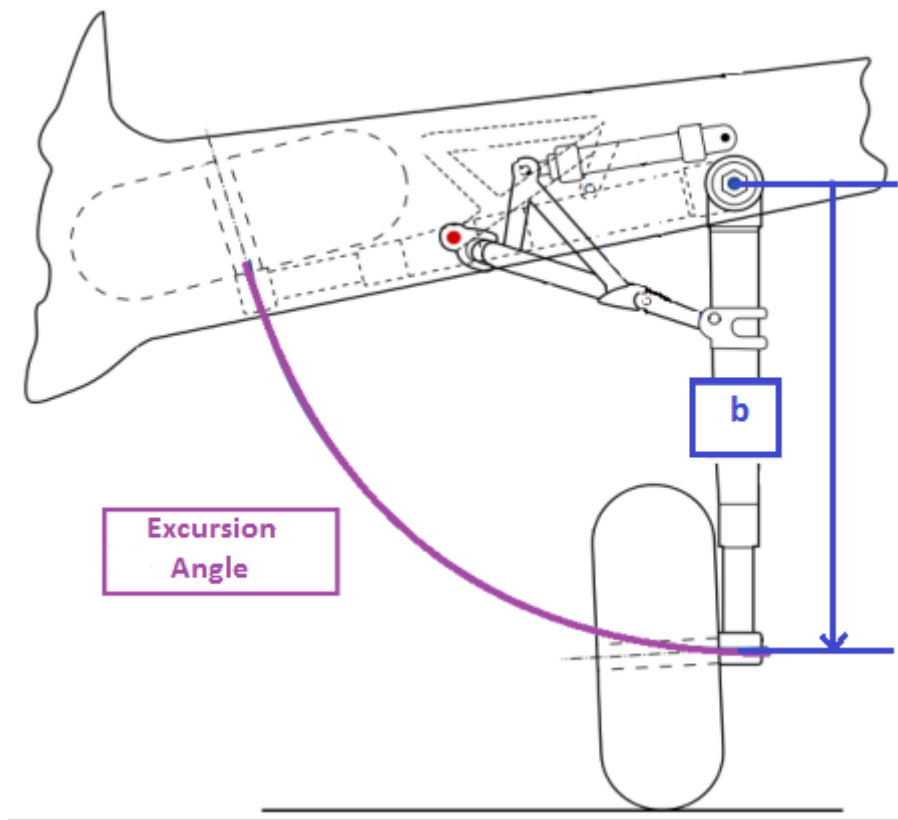
Figure 8.2: It's shown the leg center of gravity can be placed, as a good approximation, in the wheel center. We need excursion angle, in order to calculate the actuation speed required for achieving desired actuation time.

We have a forward excursion angle of about 100°, and setting required actuation time $t_a = 3 \, s$, the relative actuation speed is $v_{a,f} = 0.58 \, rad/s$, while the main gear required speed, is $v_{a,m} = 0.52 \, rad/s$. It is possible to calculate now, the actuator required power given by:

$$W_f = \frac{\left[\frac{2}{3} T_{s,f} \times \frac{v_{a,f}}{\sqrt{3}}\right]}{0.8} = 11.8 \, W$$

and

$$W_m = 2 \times \frac{\left[\frac{2}{3}\, T_{s,m} \times \frac{v_{a,m}}{\sqrt{3}}\right]}{0.8} = 40\ W$$

Furthermore, Astrid gave us the actuators amperage $I_f = 0.04\ A$, $I_m = 0.07\ A$, and masses $m_{retraction,f} = 0.76\ kg$, $m_{retraction,m} = 0.81\ kg$.

Since our architecture is all electric, we chose to install Electro-Hydrostatic Actuators (EHA) with desired characteristics, that basically are electric powered actuators (each activated by an electric motor) with an integrated hydraulic circuit providing the necessary power for actuation.

Figure 8.3: A MOOG electro-hydrostatic actuator.

The supply voltage is settled to 270 V DC, because of our engines integrated generators.

8.2. Steering actuator sizing[1]

This mock-up provides for just forward gear steering. We start from calculating the percentage of MTOW the leg has to bear, as follow:

$$W_p = MTOW \times g \times \frac{M}{F} = 5562.8\ N$$

where $M = 2\ m$, and $F = 4.26\ m$ as showed below:

---

[1] For sizing this actuator, we assumed in Astrid, the forward struct had just one wheel with a bigger diameter (0,3 m), while the real configuration has 2 wheels with a 0.2 m diameter.
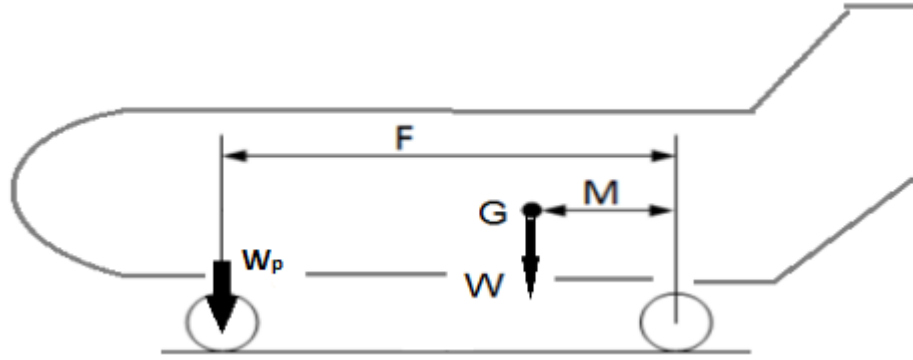
Figure 8.4 F is the distance between the forward and main gears, and M the one between the main structure and aircraft center of gravity.

We can find, this way, the steering torque:

$$T_{steering} = f \times W_p \times a = 289 \; Nm$$

where $f = 0.8$ is the friction coefficient between tires and runway and $a = \sqrt{R^2 - R_{def}^2} = 0.0654 \; m$, with $R = 0.15 \; m$ wheel radius and $R_{def} = 0.13 \; m$ radius of deformed tire as shown below:
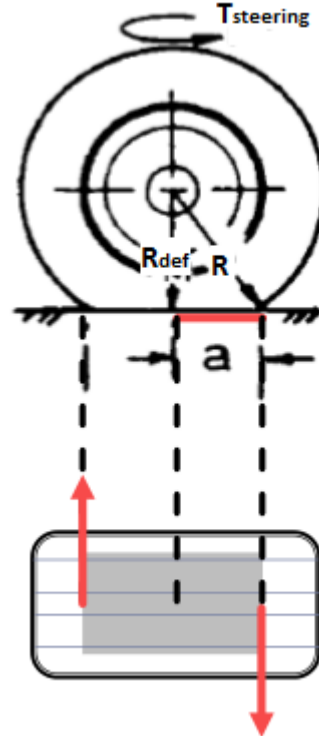

Figure 8.5: definition of "a" and contact surface extension.

By setting the desired steering speed $v_{steering} = \pi/6$ rad/s, the actuation power results:

$$W_{steering} = \frac{T_{steering} \times v_{steering}}{\eta_a} = 175.4\,W$$

with $\eta_a = 0.863$ steering actuator efficiency. We chose again an EHA powered @ 270 DC, with a power as just obtained, $I_{steering} = 0.65\,A$, and a mass $m_{a,s} = 1.16$ kg.

8.3. Braking Actuators Sizing[2]

Since the aircraft is a VTOL, we decided to size braking actuators just in need of emergency brake during taxi phases, as well they could be used in case of horizontal landing because of failure, jointly with tiltable rotors reverse thrust.

We settled a stopping length $L_s = 40m$ when going at 8.33 m/s, which allowed us to find out acceleration needed for stopping:

$$a = -\frac{V^2}{L_s} = -1.73\,m/s^2$$

then the stopping force:

$$F_{stop} = MTOW \times a = 2083\,N$$

and the stopping torque:

$$T_{stop} = F_{stop} \times R = 312.5\,Nm$$

We can calculate the hydraulic force this way:

$$F_h = \frac{T_{stop} \times braking\%}{N_s \times N_d \times R_b \times f_b} = 3156.6\,N$$

with $braking\% = 0.5$, number of braked wheels $N_s = 1$, number of discs per wheel $N_d = 1$, lining blocks centroid radius $R_b = 0.66 \times R = 0.01\,m$, and sliding friction coefficient $f_b = 0.5$.

The piston section:

$$S_p = \frac{F_h}{p_h \times g \times N_{p,min}} = 3.22 \times 10^{-4} m^2$$

where $p_h = 0.5 \times 10^6\,kg/m^2$ is the hydraulic pressure and $N_{p,min} = 2$ is the minimum working piston number;

the piston volume:

$$V_p = S_p \times N_s \times N_p \times c_p = 6.44 \times 10^{-6}\,m^3$$

with $c_p = 0.01\,m$ piston stroke and $N_p = 2$ piston number; hydraulic piston flow rate, for piston operating time $t_p = 0.1\,s$:

---

[2] Same as for steering, we assumed only one wheel for forward struct, with a bigger diameter which implicates a braking disc area comparable with the real one.

$$\dot{V}_p = \frac{V_p}{t_p} = 6.44 \times 10^{-5} \frac{m^3}{s}$$

from which finally the required actuation power:

$$W_{brake} = \dot{V}_p \times p_h \times g = 315.6\ W$$

Astrid gave us the following results:

$$W_{p,f} = 312.45\ W$$

$$W_{p,m} = 312.45\ W$$

We used our usual EHA actuators @ 270 V, with an estimated 1.5 kg mass for the forward gear one, and 1.35 kg mass each for the main gear. The total is 4.2 kg.

In order to do that, we interpolated the power data with the known power density of other actuators (found using masses obtained, in turn, by statistical studies) and the result is stated below:
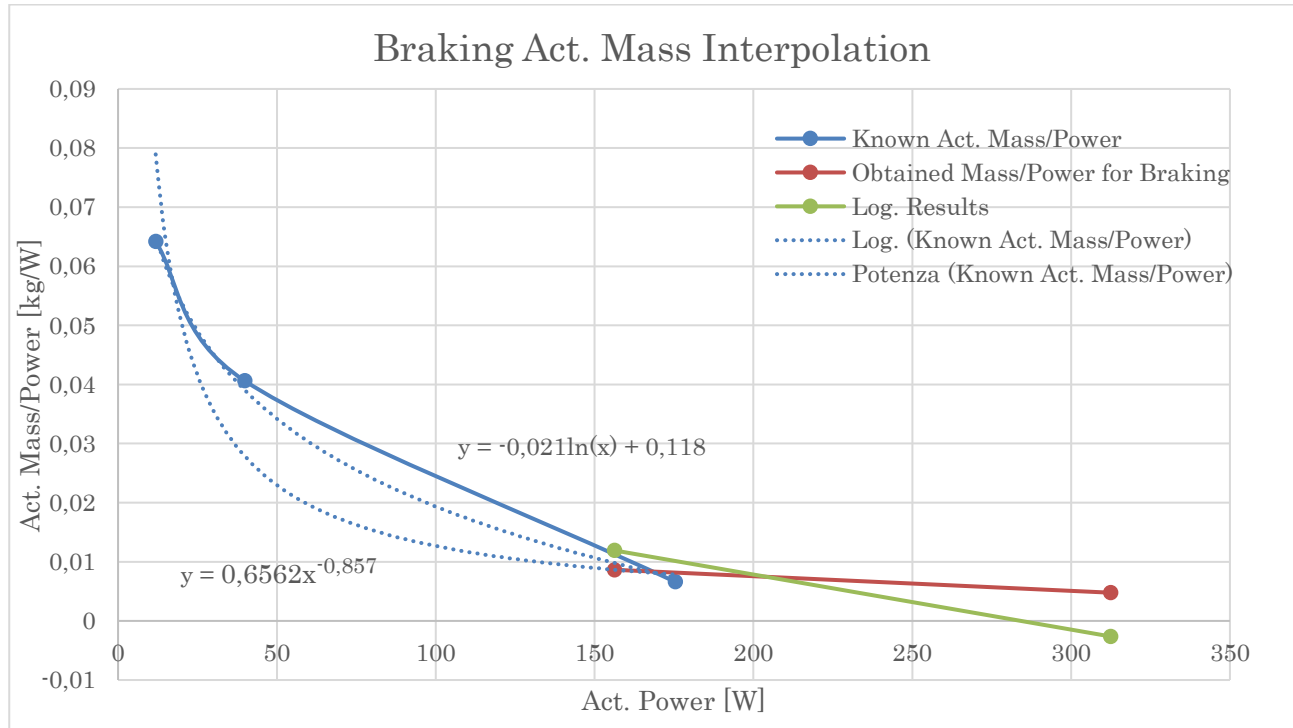
Figure 8.6: We used, as first attempt, a logarithmical law because of better fitting with known values, which unluckily produced a negative result for mass (due to a low number of known data). That's why we employed an exponential fitting and finally obtained the used mass values.

We can estimate the total required power by landing gear:

$$W_{tot,LG} = 0.852\ kW$$

its structure weight:

$$m_{structure} = m_m + m_f = 28.8\ kg$$

its actuators weight:

$$m_{actuators} = 7.74\ kg$$

for a total weight:

$$m_{LG} = 36.54 \, kg$$

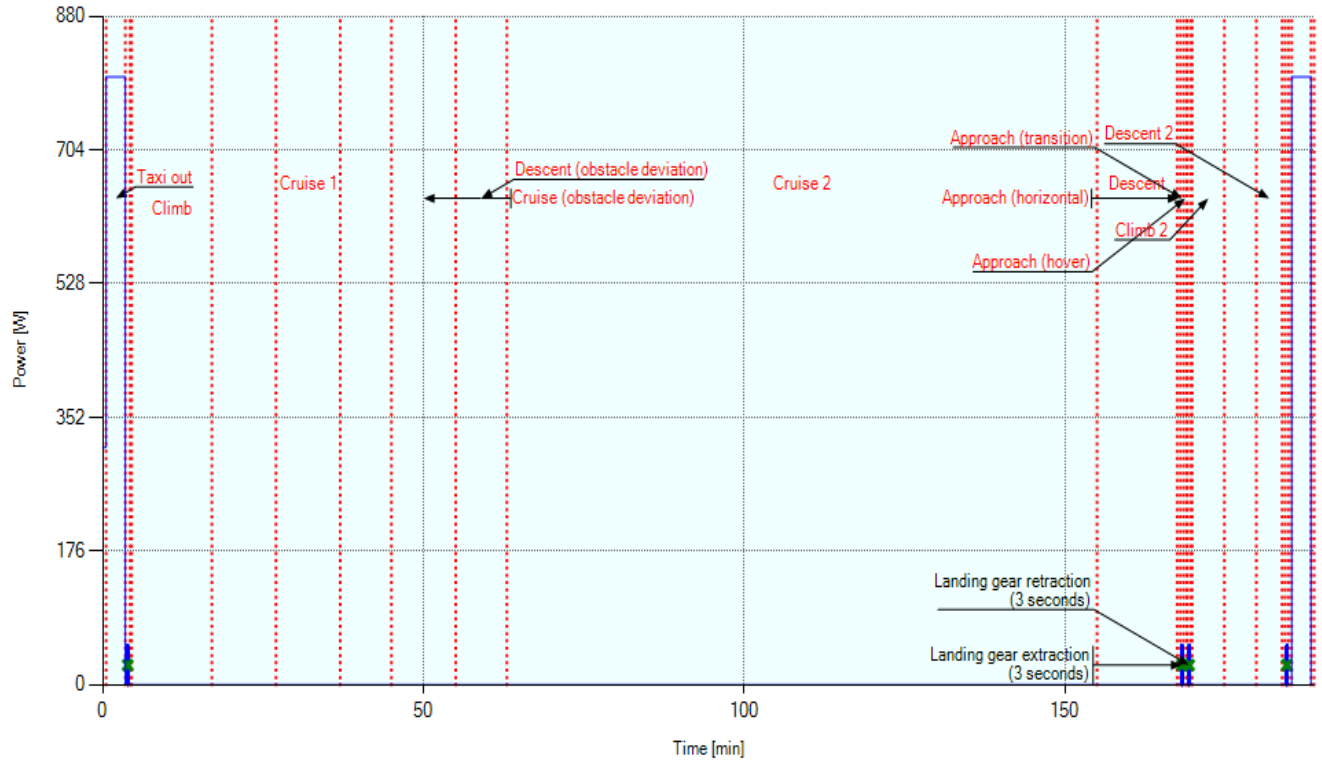The power budget for our mission profile results:

Figure 8.7: During engine start, only the main gear brakes are activated, during both taxi in and out, system requires 800 W since braking and steering are necessary, while during take-off, first landing attempting, landing aborting and final landing retraction/extraction are needed and the related power amount is about 50 W
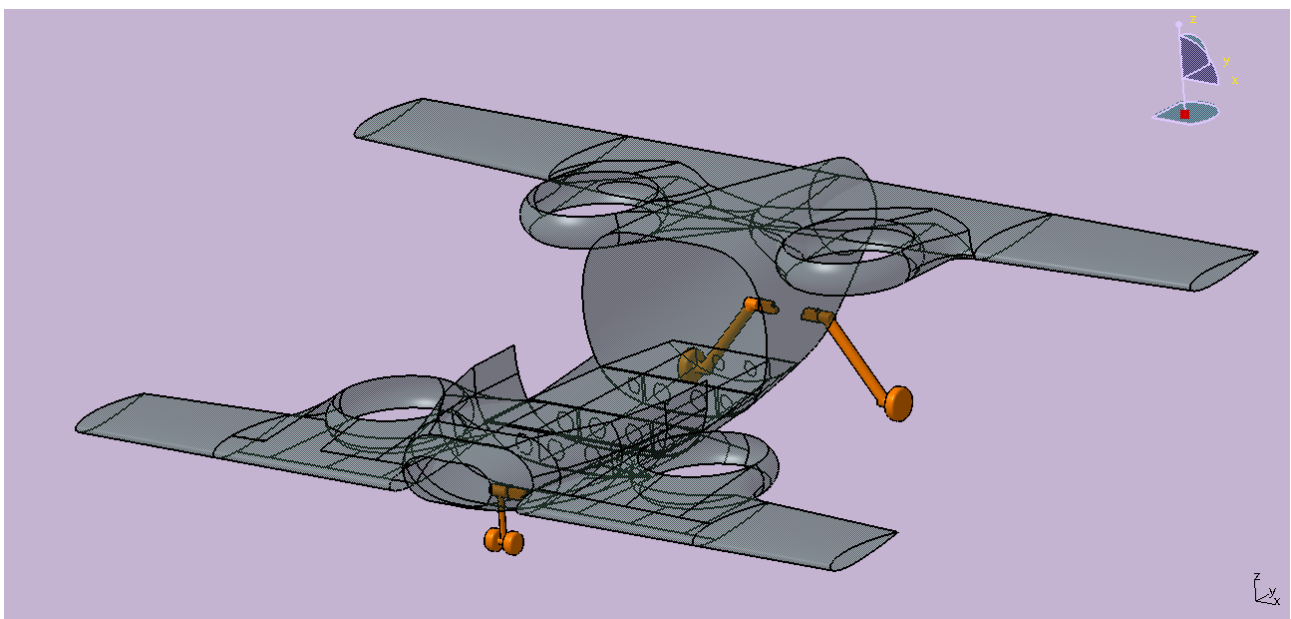
Following the pictures of CAD modeled landing gear with quotes:

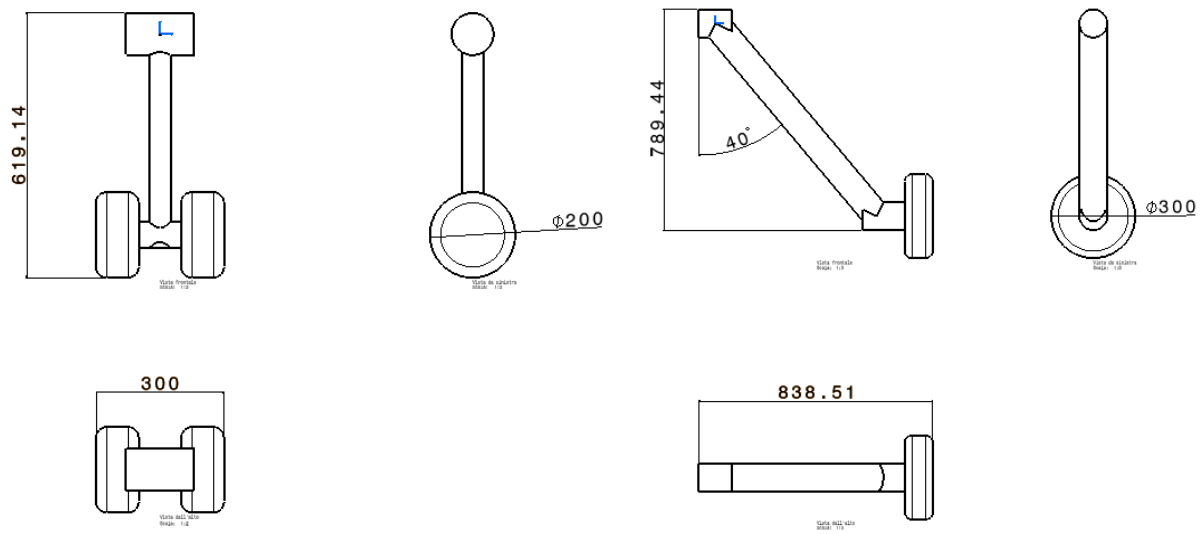Figure8.8: Landing Gear System mockup

Figure 8.9: On the left the forward struct, on the right the main one.
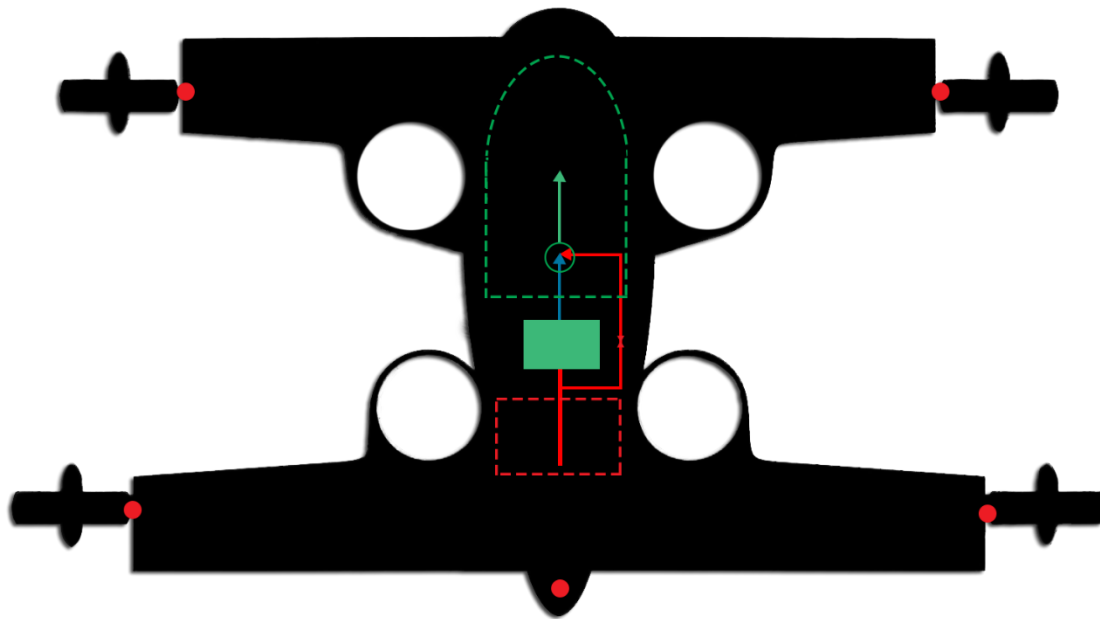
9. Environment Control System

Figure 9.9.1: Scheme of ECS with Cold Air Unit

The Environmental Control System has the function to guarantee a suitable climate inside cabin in every possible condition the aircraft could chance upon. This means that has to be able to control temperature, humidity and, in case of high altitude missions, even to adequately pressurize the cabin.

First step is to evaluate the heat exchange through cabin by considering contributions of conduction q_c, radiation q_r, passengers metabolism q_{met} and systems $q_{sist.}$
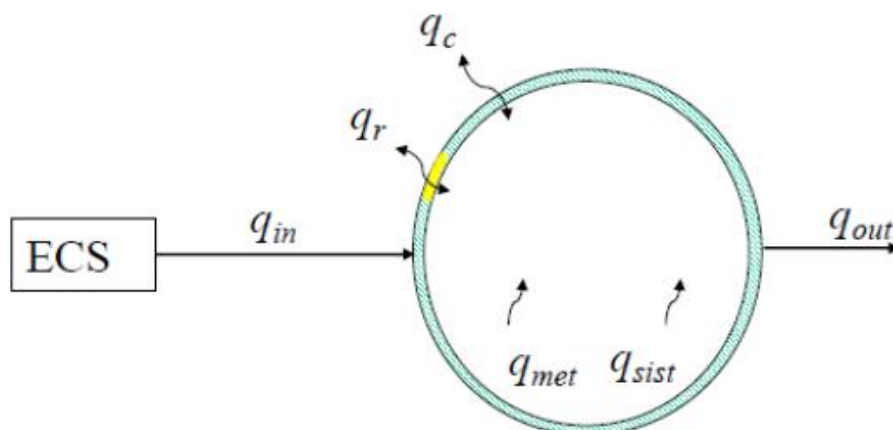

Figure 9.2: Cabin Heat exchange and ECS compensation

Now we can determine the balance of thermal loads given by:

$$W = W_c + W_r + W_{met} + W_{syst}$$

Where:

$$W_c = \mu_c \text{ x } S \text{ x } (T_{cab} - T_{skin}) = \text{conduction heat flow,}$$

$$W_r = \mu_r \text{ x } I \text{ x } S_w = \text{radiation heat flow,}$$

$$W_{met} = 0.1 \text{ x } N_{pass} + 0.3 \text{ x } N_{pilot} = \text{metabolism heat flow}$$

$$W_{syst} = (W_{eq1} + W_{eq2}) \text{ x } K_{eq} = \text{system heat flow,}$$

with:

μ_c = conductivity transmission coefficient

μ_r = radiation transmission coefficient

S_w = cabin wetted surface

T_{cab} = cabin temperature

T_{skin} = external skin temperature

I = solar intensity

S_w = windows surface

N_{pass} = passengers number

N_{pilot} = pilots number

W_{eq1} = avionics contribution -> $f(N_{pass})$

W_{eq2} = interior lights, galleys, passengers service, etc. contribution = $1 + 0.05 \text{ x } N_{pass}$

K_{eq} = 1 during flight, while 0.11 when on ground

It is notable that contribution of W_r is larger on ground than during flight because of heat flow coming from ground.

We size ECS necessary heat flow, by considering the worst condition for both cold and hot cases which are, respectively:

T_{ext} = -20° C, during night, during flight and with no passengers on board;

T_{ext} = 20° C, during daylight, on ground and with maximum passengers number on board.

In particular, we calculated a wetted cabin surface by considering a length of 3.6 m (from engines bottom to batteries front), a 1.5 m diameter and a taper factor K_p = 0.8, thus obtaining:

$$S_w = L_c \times D_c \times \pi \times K_p = 13.57 \; m^2$$

Moreover, considering maximum passengers number of 1, minimum and maximum crew number of 1, $\mu_c = 2.5$, $\mu_r = 0.7$, $S_w = 6 \, m^2$, the maximum flight altitude of 4000 m, cruise speed of 220 km/h, $W_{sist} = 0.519 \, kW$, we obtained the maximum thermal load in heating condition, setting the desired $T_{cab} = 25° \, C$:

$$W_h = 0.86 \, kW$$

While, in cooling condition and with $T_{cab} = 18° \, C$:

$$W_c = -4.24 \, kW$$

Indeed, in hot conditions, heat flow is negative and enters the cabin, whereas in cold conditions the heat flow is positive and leaves the cabin, so that we have the following plot:
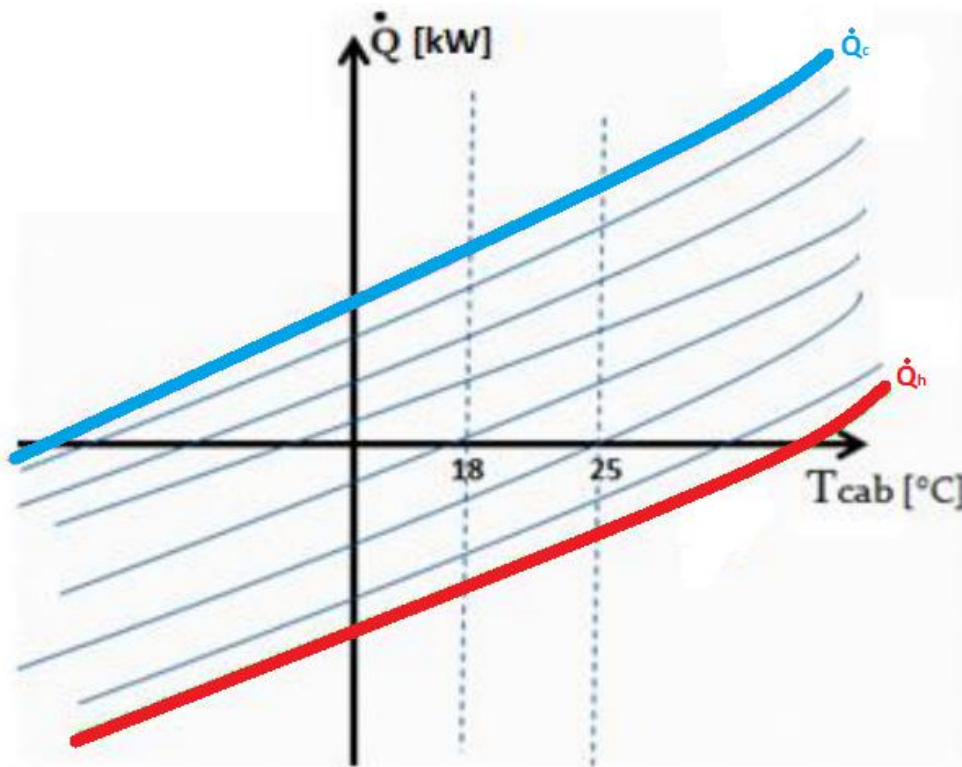

Figure 9.9.2: It's shown the positive heat flow when outside is cold and the negative one when outside is hot, while on the horizontal axis we have cabin temperature. The heat flow is zero when Tcab = Text

All the ECS has to do for reaching the suitable thermal condition, is providing an heat flow equal and opposite to $\dot{Q}$, by injecting in cabin the right airflow rate $\dot{m}$ which depends upon its and cabin temperature conditions. In cold condition, for example, ECS has to provide:

$$\dot{q}_h = \dot{m}_h \times C_p \times (T_{i,hot} - T_{cab}) = \dot{Q}_c$$

with $\dot{m}_h$ = hot airflow, C_p = air specific heat, $T_{i,hot}$ = airflow temperature and T_{cab} = desired cabin temperature.

Since $W_h = \dot{Q}_c$, we can calculate hot airflow rate for keeping $T_{cab} = 18° \, C$:

$$\dot{m}_h = \frac{W_h}{C_p \times (T_{i,hot} - T_{cab})} = 0.1834 \frac{kg}{s}$$

with $T_{i,hot} = 50° \, C$.

The same for hot conditions:

$$\dot{q}_c = \dot{m}_c \times C_p \times (T_{i,cold} - T_{cab}) = \dot{Q}_h$$

where $\dot{m}_c$ is cold airflow rate, C_p is air specific heat, $T_{i,cold}$ is airflow temperature and T_{cab}= desired cabin temperature; by imposing $W_c = \dot{Q}_h$, let's find cold airflow rate for keeping $T_{cab} = 25° \, C$:

$$\dot{m}_c = \frac{W_c}{C_p \times (T_{i,cold} - T_{cab})} = 0.0267 \frac{kg}{s}$$

with $T_{i,cold} = 2° \, C$ (we chose a not sub-freezing CAU).

It is notable and intuitive too, that we can reach higher temperatures by increasing $\dot{m}_h$ in cold conditions and lower temperatures by increasing $\dot{m}_c$ in hot conditions, as shown in figure below:
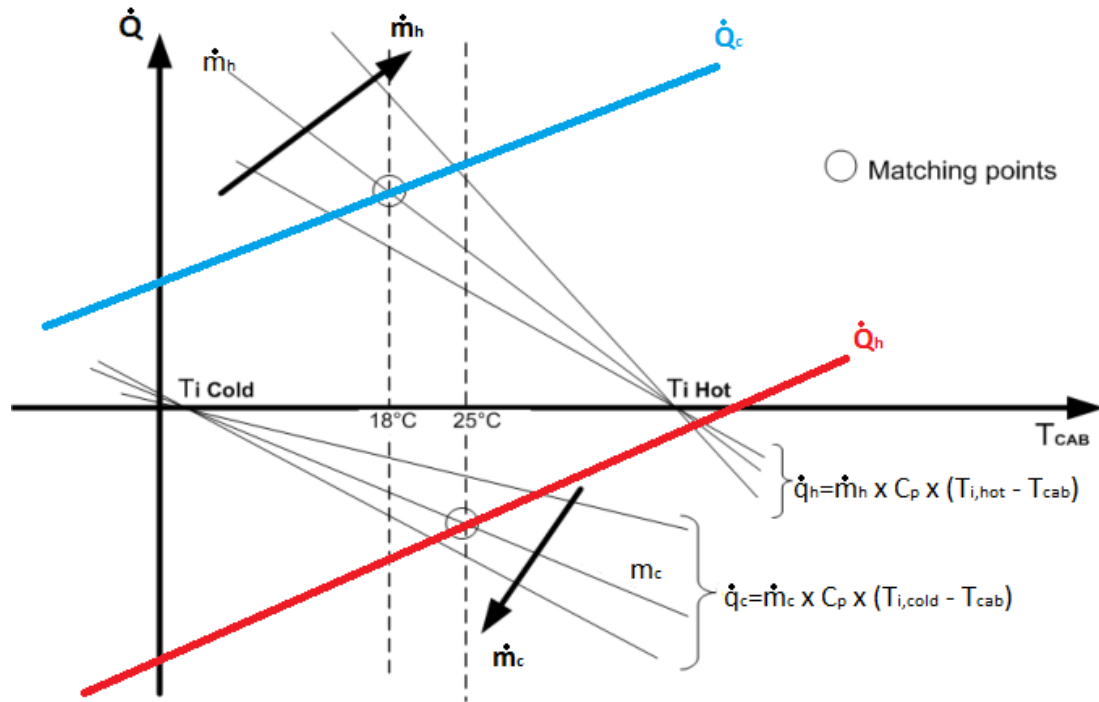

Figure 9.9.3: Matching points making in evidence how q̇ c,h change with ṁ c,h

The heart of environmental control system is the Cold Air Unit (CAU), which is basically a "black box" that receives a hot and pressurized airflow, for providing a cold airflow to be used for cooling or heating the cabin.

In order to accomplish its aim, CAU needs exchangers, turbine and in any cases a dedicated compressor and a condenser; it could be vapor-cycle or air-cycle and sub-freezing or not-subfreezing. The first one needs a condenser and it's not able to

pressurize, which means it can't be used on planes with high altitude missions; the second one needs a compressor in order to accomplish the just explained function; the third provide a sub-zero air temperature drop, which implicates a need to use an anti-ice system before the flow enters the turbine; the last one has a simpler structure, but causes higher consumptions. Their functioning can be schematized as follow:
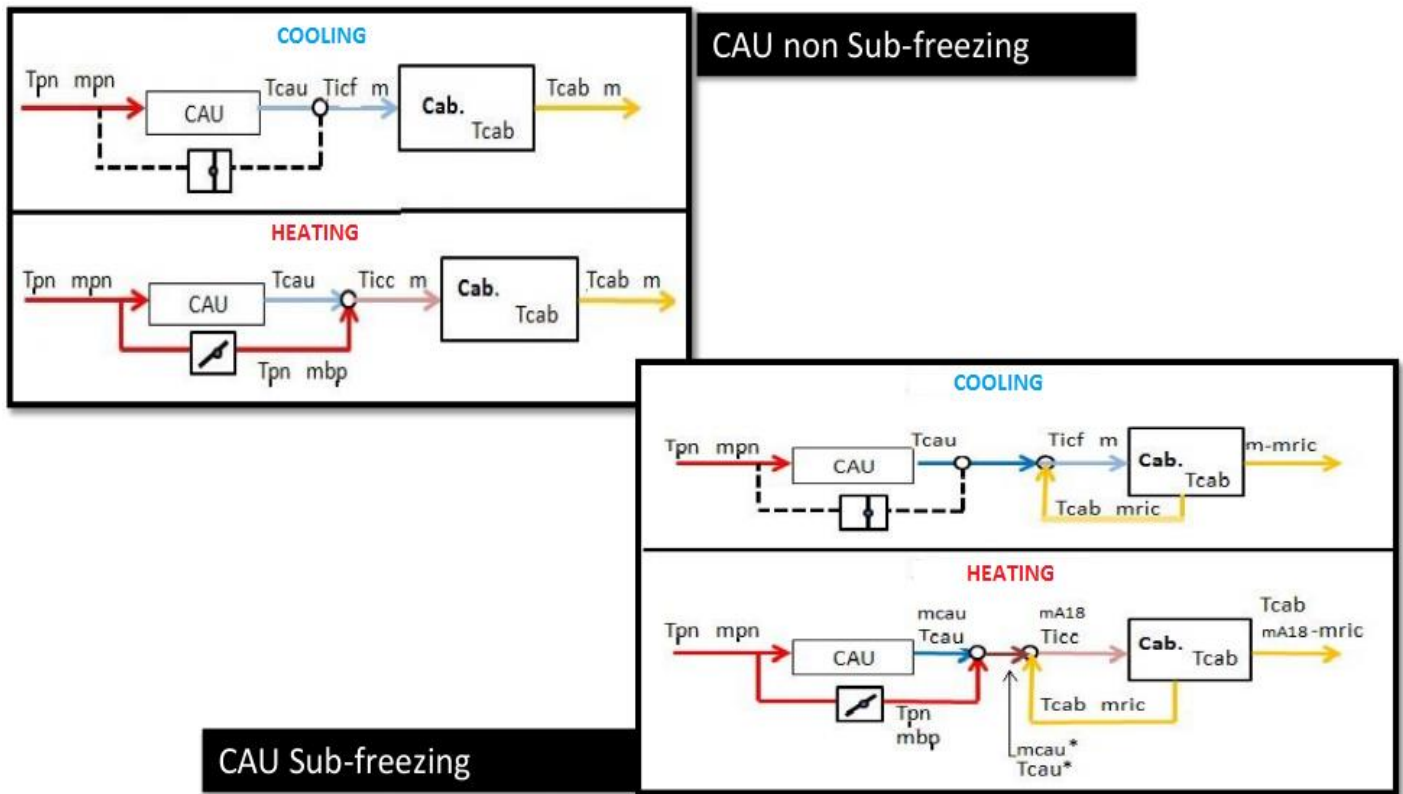

Figure 9.9.4: Functioning differences between sub-freezing and not sub-freezing

A not sub-freezing CAU doesn't need a mixing with its hot air intake before injection in cabin for cooling, because its airflow has an acceptable temperature (2° C), while for heating, it just need that mixing with no further action. In particular we need, for same aforesaid conditions, a 0.0146 kg/s airflow bypass.

On the other hand, a Sub-freezing CAU, although implicates minor consumption (major ΔT, means less airflow needed for reaching same heat flow), implicates a more complex structure and functioning. In fact, for cooling case, we need a mixing with cabin airflow in order to rise the temperature before the injection (otherwise it would be -20° C). Moreover, for heating case, two mixing are required: first one with the hot airflow entering the CAU and second one with the cabin airflow, always before the injection.

Cold air unit can use as intake an airflow coming from engines bleed, or from a dedicated compressor; the last solution allows to have a more precise sizing of intake pressure and, furthermore, doesn't cause an engines power loss, as shown below:
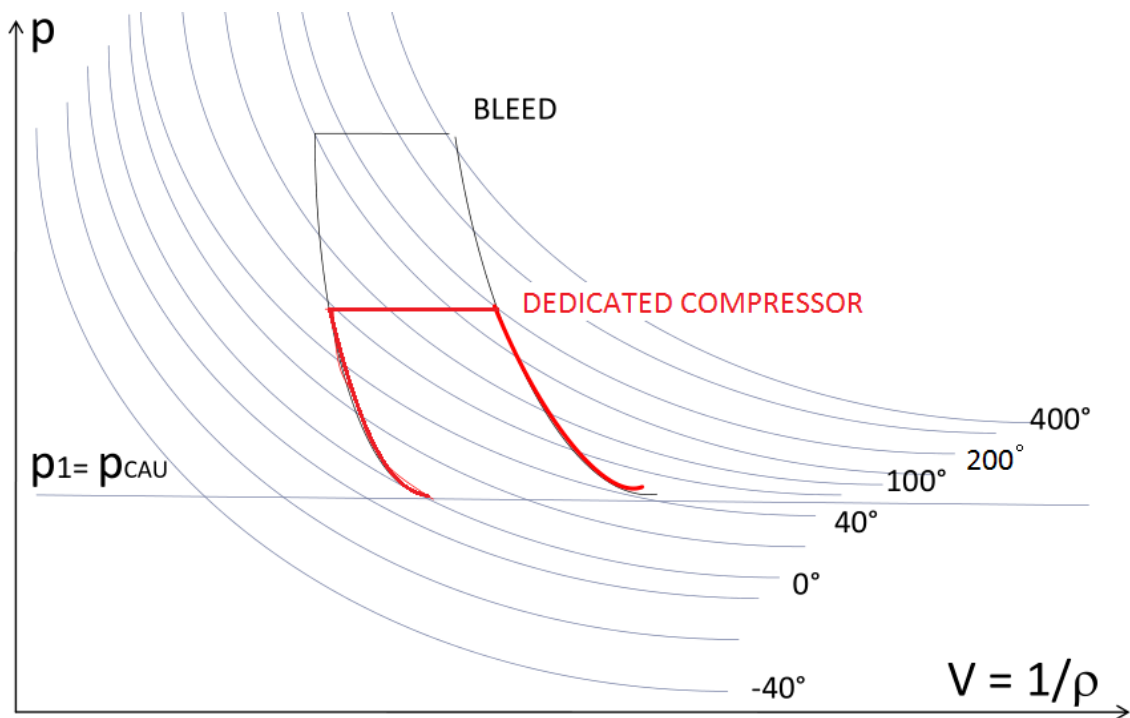

Figure 9.9.5: It's shown how bleed pressure is higher than the pressure provided by a dedicated compressor

We can calculate the power required by airflow bleeding or by dedicated compressor using this equation:

$$P_c = \frac{\dot{m} \times C_p \times (T_{ac} - T_{bc})}{\eta_c}$$

where $\dot{m}$ is the compressor airflow intake, T_{ac} is temperature after compression, T_{bc} the temperature before compression and η_c is the compressor efficiency.

The advantage in choosing a solution with a dedicated compressor, it's clearly shown in the next picture:
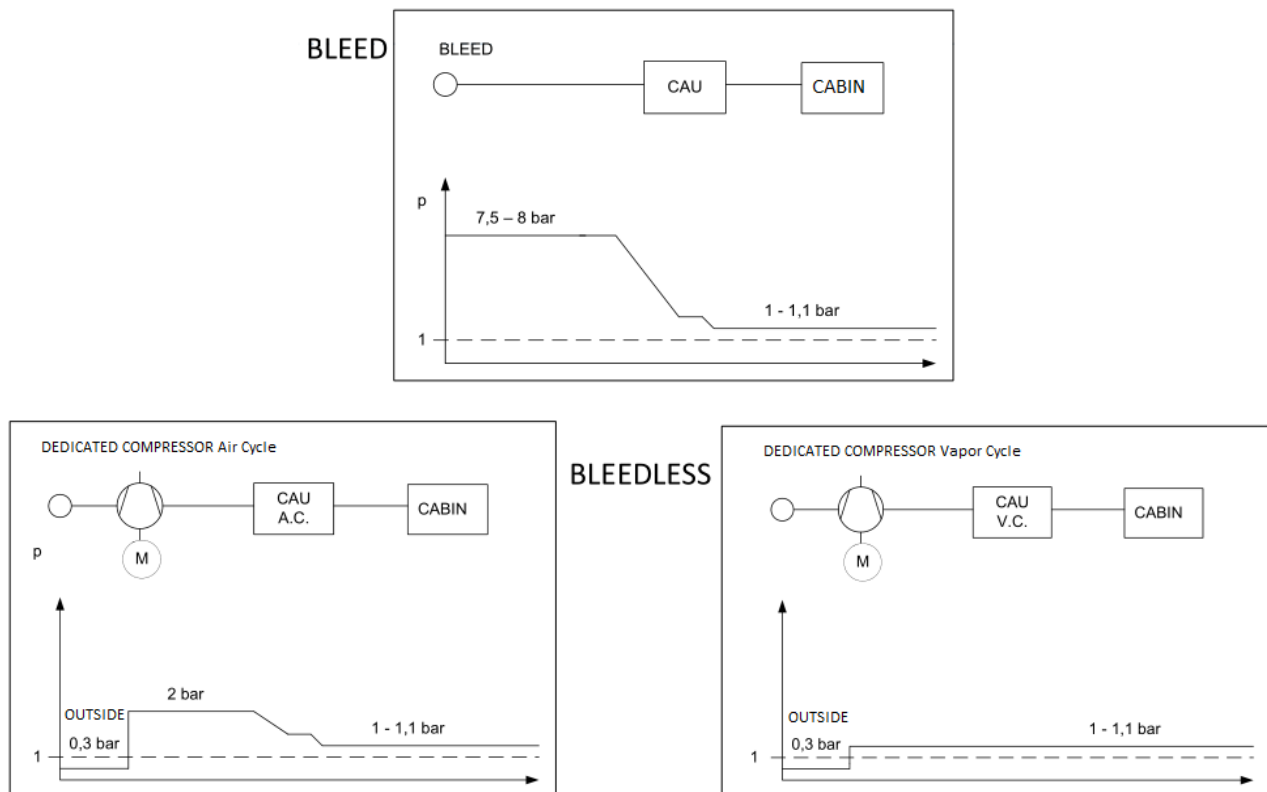
Figure 9.9.6: Comparison between air pressure evolution for a bleeding system and bleedless air-cycle and vapor-cycle

We chose, for our application, to install an all-electric, existing ECS with a dedicated compressor and a vapor-cycle, not sub-freezing CAU, already integrated with G 1000 and used on airplanes such as Cessna 172 and 182 series:
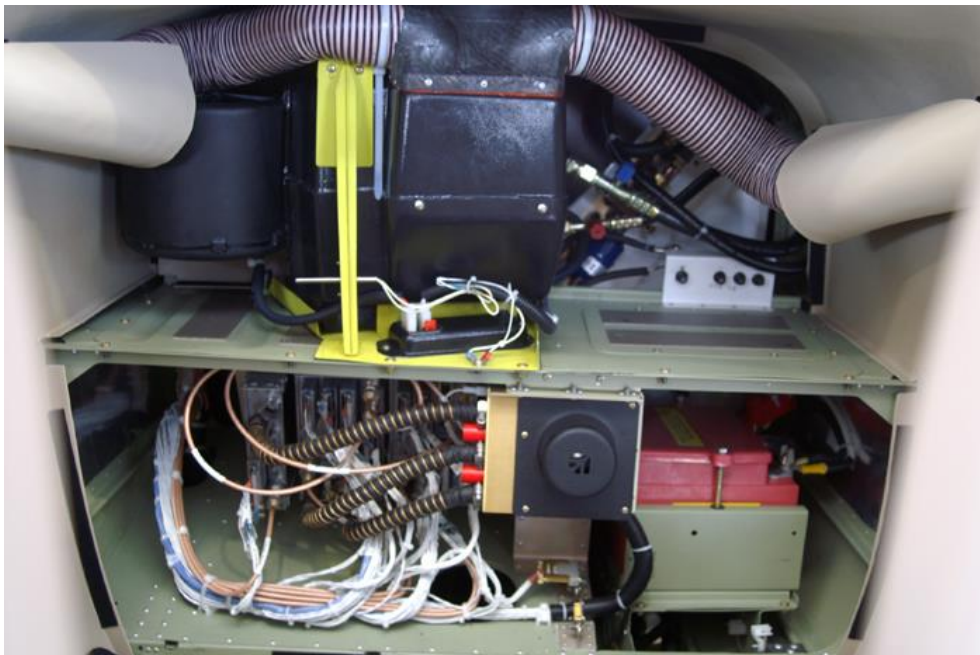

Figure 9.9.7: Kelly Aerospace Thermacool integrated with G 1000 installation on a Cessna 182T

ThermaCool is an air conditioning system with a trouble-free hermetically-sealed brushless DC motor/compressor that is powered by either the aircraft electrical system or a 28 V DC ground power cart. Has a 33 A nominal run, a 22.2 kg mass, an optional

back-up alternator could be installed, a 12.7 kJ cooling energy and a maximum airflow of 550 CFP (0.2 kg/s with air density of 1.225 kg/m³) which is largely enough for our application. Among the other performance, we can find: providing a 20 degree cabin temperature drop in just 5 minutes at the touch of a button, during ground pre-cooling and a cowl mounted piezo-electric switch activates the system without ever opening the cabin door, when connected to ground power.

Along mission profile, the ECS is always activated except during phases with hover rotors running, in order to avoid engines overloading, and its nominal consumption is given by:

$$V \times I_n = 28\,V \times 33\,A = 0.924\,kW$$

For the environmental control system, we obtained the following mock-up
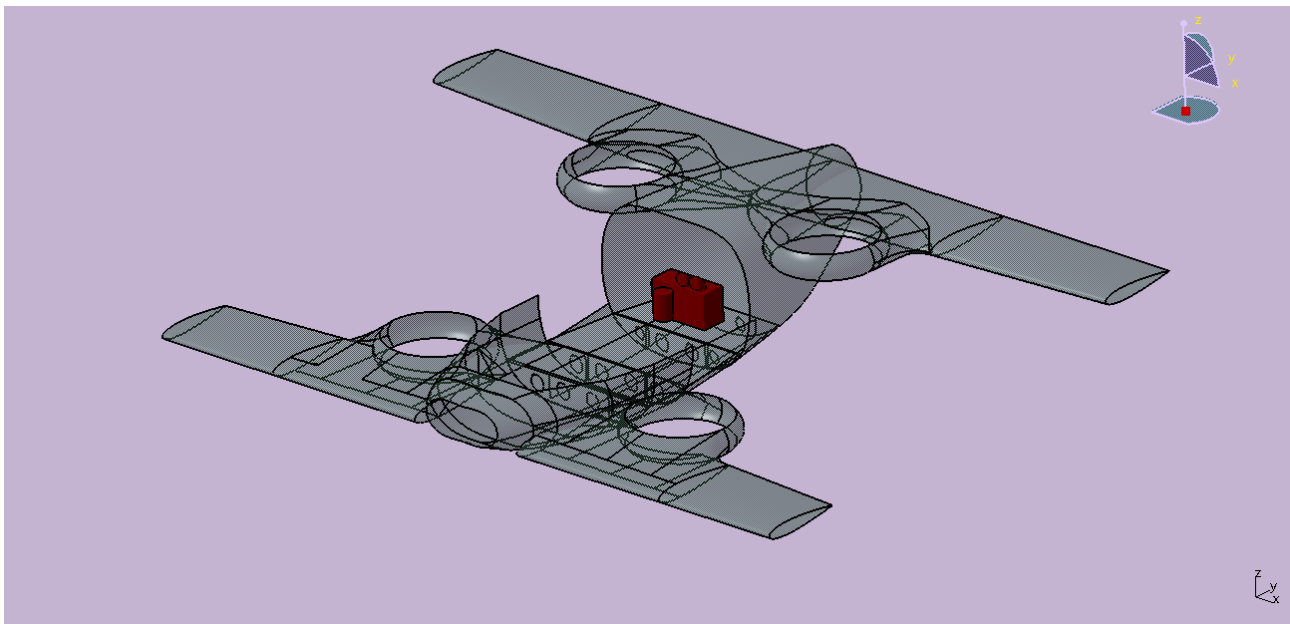

Figure 9.9.8: CAD collocation of the ECS
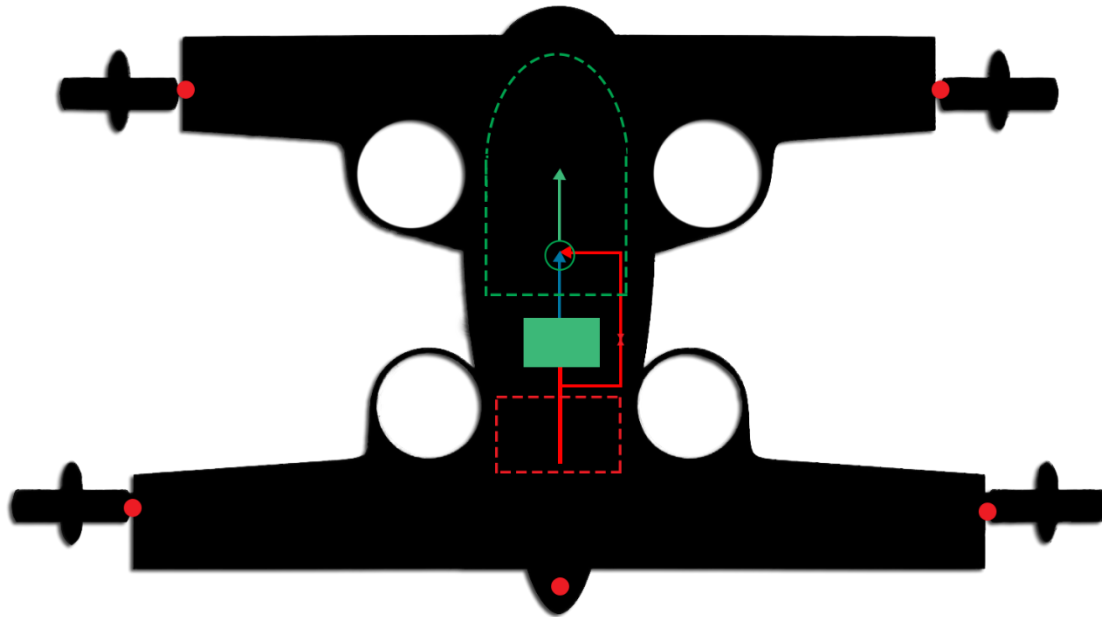
10. Anti/De-icing System

Figure 10.10.1: Architecture of ECS and Anti Ice electrothermal resistance for mobile surfaces hinges (red dots).

The anti-ice system could be fundamental in particular climatic situations. Indeed, it is essential not just in geographical areas where temperature is extremely low even at sea level, but it could be also vital in case of super-cooled rain, when the water remains in a liquid state though temperature is lower than 273 K because of drops very small dimensions and of surface tension. This situation is very instable, in fact as soon as raindrops touch something, freeze and may cause formation of an ice layer with bad consequences for the aircraft.

There are different types of anti-ice system, but all of them protect leading edges and mobile surfaces hinges, for obvious reasons.

The Electro-Thermal anti-ice system exploits jowl effect by using simple electrical resistances, in order to warm the critical areas and thus preventing ice formation. As shown in the figure below, we can efficiently warm up a huge area (wing leading hedge for instance), by heating continually a little part of it, and cyclically the remaining.
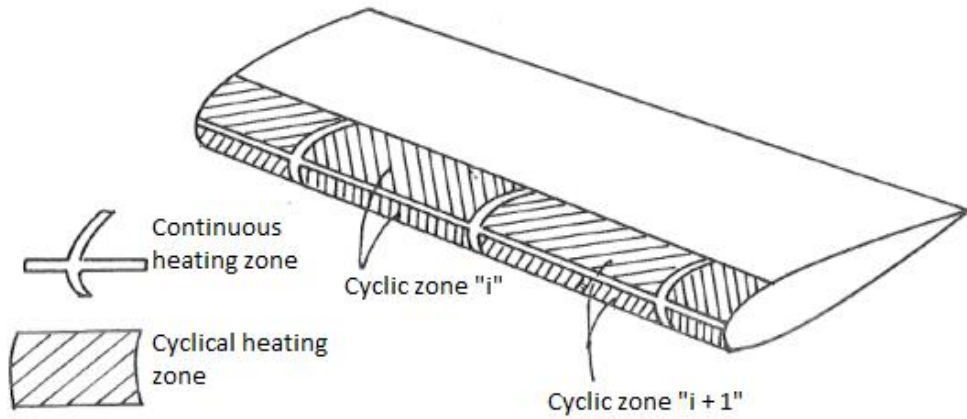
Figure 10.10.2: Cyclic and continuous heating areas

We have a 28 kW/m² and a 21 kW/m² thermal flow respectively for cyclic and continuous areas, thus the total dissipated power P_h is given by the following:

$$P_h = \sum_{i=1}^{n}(A_{cy,i}) \times 28 + A_{co} \times 21$$

where $A_{cy,i}$ is the i-th surface cyclically wormed up, and A_{co} is the total continuously warmed surface.

It is clear that, in order to calculate the anti-ice system power budget, we have to know the extension of the areas we want to heat and we will estimate them as following:

$$A_{tot} = p \times L$$

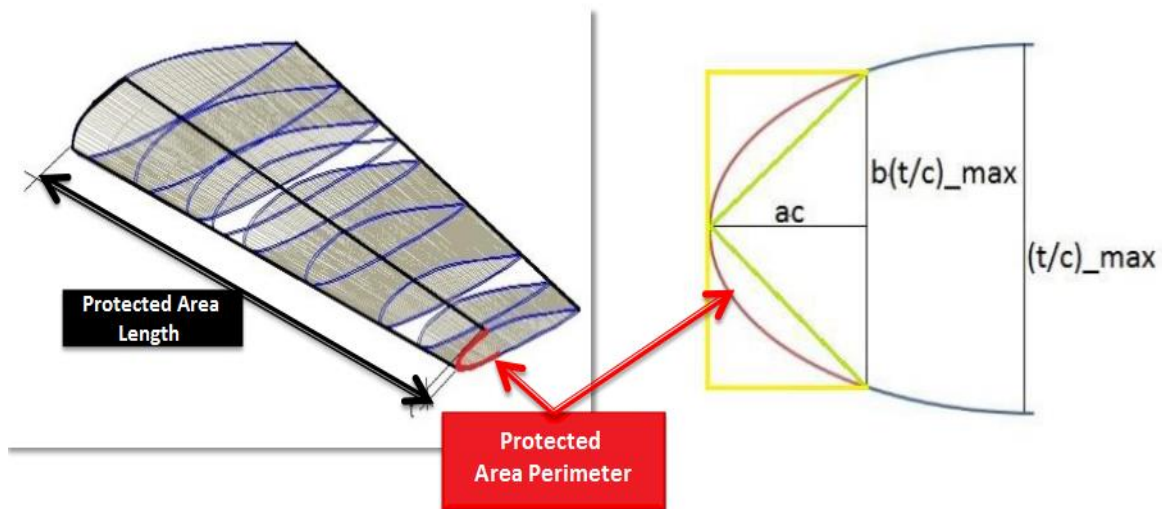with p heated area perimeter, and L length of it as shown in the next figure.

Figure 10.10.3: We can see that perimeter is estimated by calculating the hypotenuse of a triangle whose sides are given by b(t/c_max)/2 and ac

$B(t/c\_max)$ and ac, are respectively given in terms of maximum wing thickness and chord percentage.

Next step is calculating the continuous area extension as follow:

$$A_{co} = [L + (p \times n_p)] \times t_{co}$$

where n_p is the number of vertical continuous zones, and t_{co} their thickness.

We can now calculate the extension of the i-th cyclical area, in this way:

$$A_{cy,i} = \frac{A_{tot} - A_{co}}{n}$$

where n is the number of cyclical areas, and finally find out the total required power P_h.

By setting $p = 0.25\ m$, $L^3 = 4.37\ m$, $t_{co} = 0.025\ m$ and $n = 21$ (which means $n_p = n - 1 = 20$), the result is:

$$P_h = 9.54\ kW$$

It is clear that such value is too high for our application, indeed it represents about the 4.5% of available power during cruise and that's why we decided to heat only rudder and tiltable rotors hinges, by heating continuously their entire estimated surface, $A_h = 0.04\ m^2$. The result is:

$$P_h = 0.88\ kW$$

We assumed the anti-ice is activated when at maximum quote and, in case of necessity, during bad weather "on demand". Following the mission power budget diagram:

---

[3] Given by: $b_1 + b_2 - 2*(t_f)$, where $b_1 = 5.74\ m$ is the front wing span, $b_2 = 6\ m$ is the rear wing span and $t_f = 1.5\ m$ is the fuselage thickness.
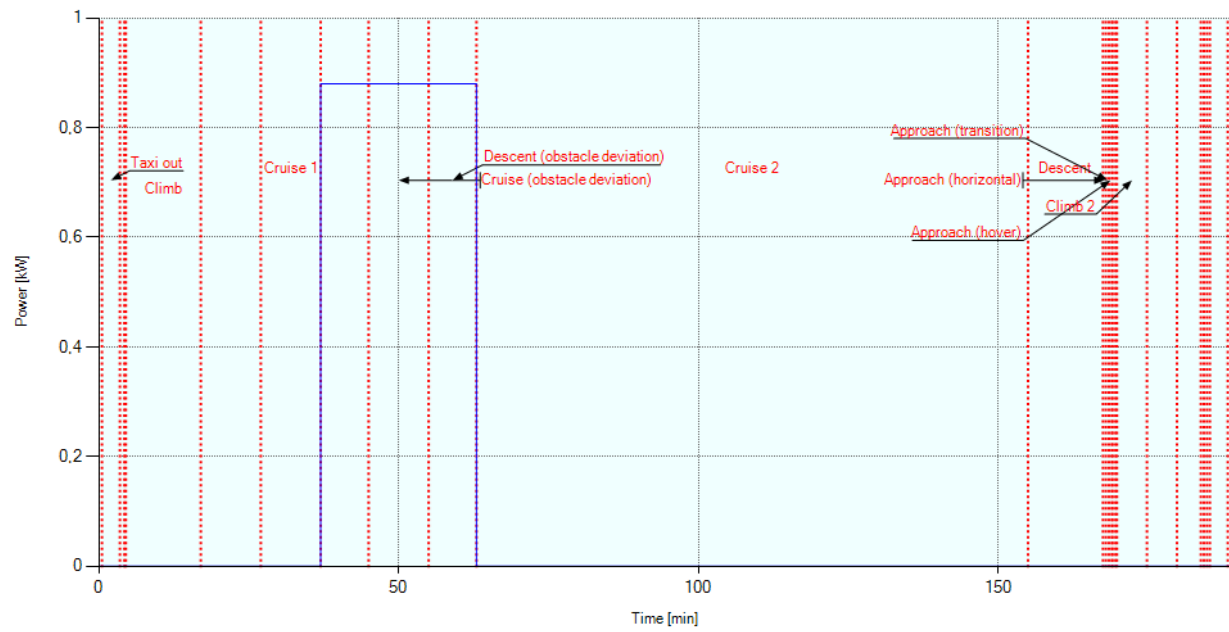
Figure 10.10.4: Anti-Ice power budget
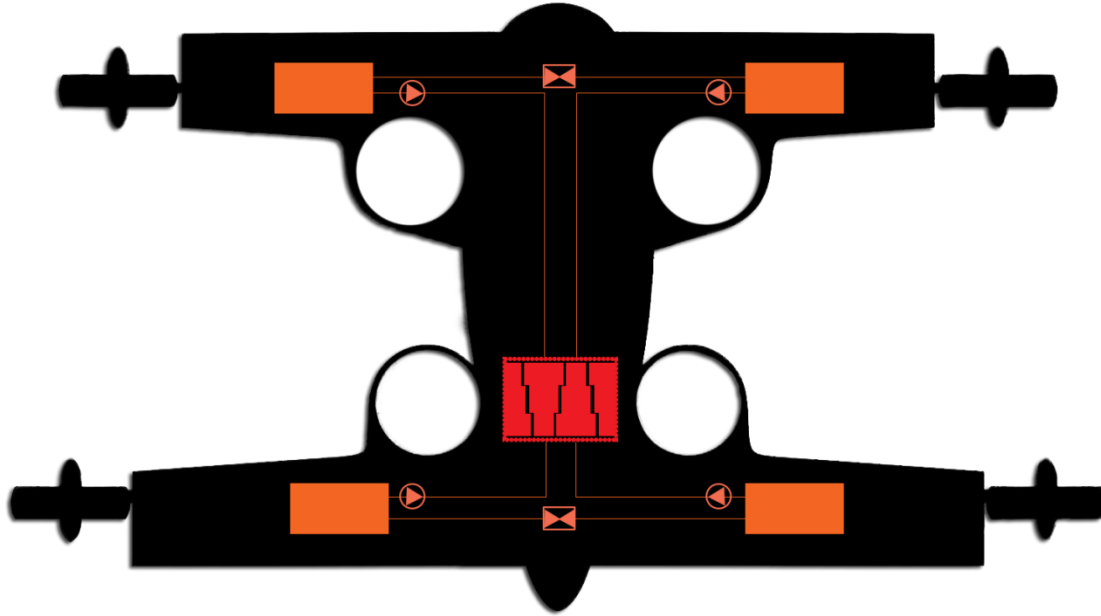
11. Fuel/Propulsion System

Figure 11.11.1: Architecture of fuel system

The fuel system has the target to contain fuel and provide it to the engines so that they can supply the power request of the aircraft. In order to do this task, for the sizing of this system we must determine the request of the engines in term of fuel type, pressure and supply ratio, the size of the tanks and their position in the aircraft, the features of the fuel pumps. Finally, we must verify the refuel operation and the power budget required by the fuel system.

The fuel system could have other auxiliary function such as emergency drain or CoG control but these are not expected for this study.

According with the requirements, the aircraft power is provided by four *Turbotech* fuel generator that will be depth described in the following chapter. These engines has a SFC (Specific Fuel Consumption) of $0.3\frac{kg}{kWh}$ and work at a nominal power of 55kW. Therefore, the engines maximum fuel flow is

$$\dot{m}_{MAX\,FUEL} = SFC * P_{MAX} = 0.3\frac{kg}{kWh} \cdot 55\,kW = 16.5\frac{kg}{h}$$

$$Q_{MAX} = \frac{\dot{m}_{MAX\,FUEL}}{\rho_{fuel}} = \frac{16.5}{0.82} = 20.12\frac{l}{h}$$

One other feature of these engines is that they burn Jet-A fuel that as a density of 820 $\frac{kg}{m^3}$. According to the mission profile, we calculate that the total fuel needed for the mission is about 200 liters, which correspond to 164 kg of fuel.

Then, we have to define the engines position on the aircraft. In the preliminary phase of this project, we wanted to position the engine in the front bay of the aircraft in order

to simplify cooling and improve the maintainability. The problem of this solution was that we want use a different engines, smaller than the chosen *Turbotech* but with less power. Using the *Turbotech* engines, we need more space so we put them in the rear bay, behind the cabin, and we set the maximum and minimum pressure for the Fuel Control Unit at 1,2 and 2 bar respectively.

Once certain characteristics, we defined the number, type, and position of the fuel tank. We choose to set one internal tank with the capacity of 50 liters for each wing. With the purpose to limit complexity and weight of the system and improve reliability, we choose to use integral tank rather than bladder or discrete ones. In fact, the bladder tank are less reliable because the case could have some leak. The following is picture representative of an integral tank
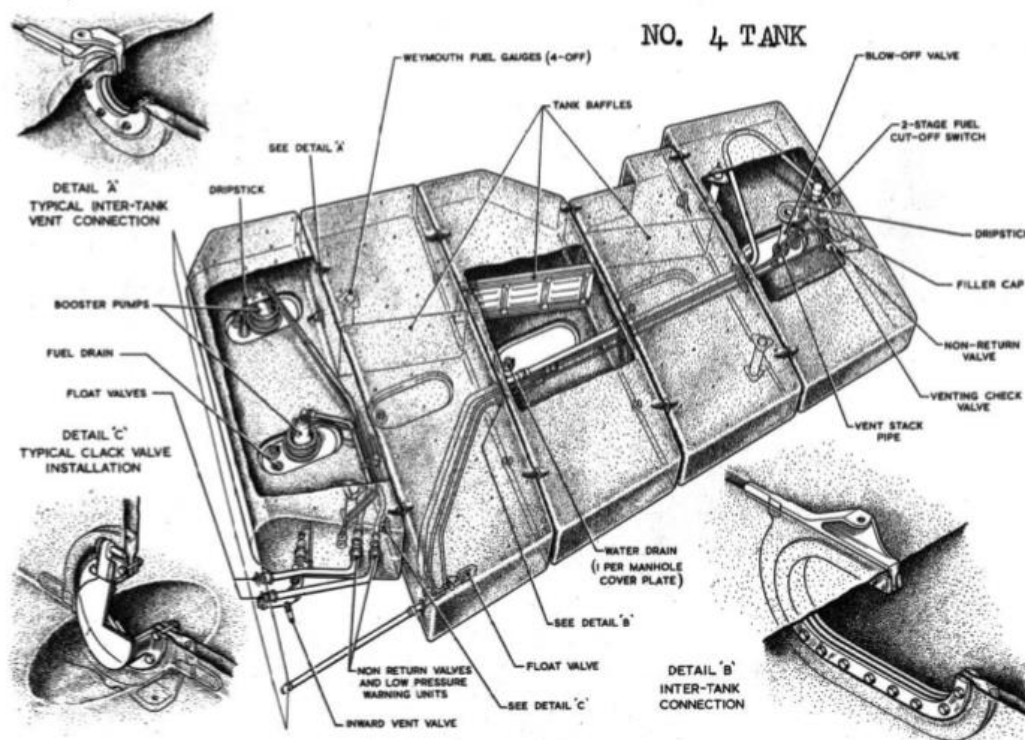

Figure 11.11.2: Integrated fuel tank

In this scheme we could focus on the inter-tank connection that allow the fuel to flow through the wing boxes, the fuel pumps, the non-return valve and clack valve, simple but fundamental equipment that fuel to flow in only one direction. Our solution is slightly different, but the peculiarity are the same.

We choose to not put fuel in the tail-cone or use some internal tank because of the total amount of fuel could be stoked in the wing without any problem.

Once defined the features of the tank we must size the fuel pump. To improve safety we choose to use two electric booster pump for each tank in order to guarantee the proper function of the fuel system. Then we set the position of the fuel collector close to the tank in order to avoid any suction problems.

Defined the pump location, we calculate the maximum and minimum fuel flow and the supply pressure. We set the alimentation pressure at 1.2 bar and we calculate the fuel

flow of the pumps in the worst case, which is when a single pump have to supply fuel to two engines instead of one. The maximum fuel flow in this case is:

$$m_{MAX_{FUEL}} = N_{mot_{ass}} * SFC * P_{MAX} = 2 \cdot 0.2238 \cdot 73.7562 = 33.013 \frac{kg}{h}$$

$$Q_{MAX} = \frac{m_{MAX_{FUEL}}}{\rho_{fuel}} = \frac{33.013}{0.82} = 40.26 \frac{l}{h}$$

We could have supposed that a single pump have to provide fuel to all the engines, but considering that we have a double redundancy of fuel pump for each tank, we supposed that, in the worst case a pump have to provide fuel to a maximum of two engines.

The last step for the sizing of the pumps is the definition of the pressure drops that is estimated from length, diameter and type of the conduct. We choose a sketchy value for the conduct length considering a 4.95 meters pipe from the front tank to the engines and 2.94 meters from the rear ones to the engines. For the type of conduct, we choose a standard aluminum alloy molded tubes with 10mm of diameter. With the aim of have a more reliable solution, we also consider the concentrate pressure drops like entrances, outlets or 90° turns.

This calculation has to be done for the worst case between engines alimentation and fuel transfer. We expected to have a cross-feed valve between the two frontal tank and between the two rear ones in order to guarantee the correct operation of the system. However, the fuel flow and pressure needed for the fuel transfer are less than the ones needed for the engines alimentation so we set this last case as the reference for the sizing.

Relying on the required fuel pump features, we choose to use a FACET solid-state electronic fuel pump with the following characteristics

Fuel flow [l/h]	26,4979 - 151,416
Pressure [bar]	0,0689 - 1,0342
Volt [V]	24
Ampere [A]	1.4
Weight [kg]	~0.5

Figure 11.11.3: FACET electronic fuel pump

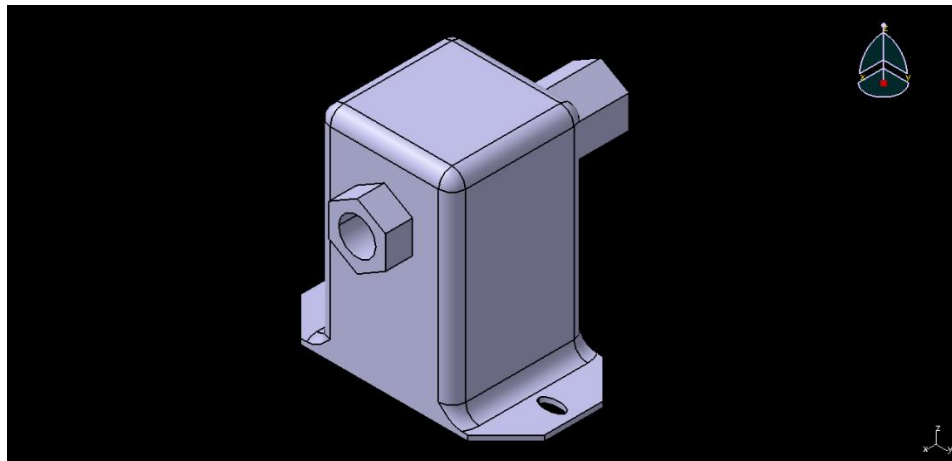We also realize the CAD model of the fuel pump

Figure 11.11.4: Fuel pump CAD model

The next step of the design of the fuel system is the validation of the re-fuel operation. Considering the nature of this project, we think that the user should not need special equipment for the refuel so we set that refuel pressure at 1.2 bar and we put the refuel filler on the top of the rear wing. In this way, the owners can refuel the Mini-bee at a normal gas station, without having extra refuel pressure to do a pressurized refuel operation. They just need a little ladder to get on the top of the aircraft. We also consider that the refuel operation duration is about 15 minutes. Considering this features and the maximum pressure drops calculated on the farthest tank from the filler, we obtained the following results.

Refuel fuel flow [kg/h]	656
Minimum refuel piping diameter [mm]	4.85
Tank-fuel filler altitude gap [m]	-1.10
Pressure gap [bar]	1.01

The final step was to define the power budget for the fuel system. The fuel pump must provide 14.31 l/h of fuel in the less critical phase: in this case, the electric power absorbed by the pump is about 111 W. In the more critical phase, the fuel flow requested grow up to 20.10 l/h so the power required is about 156.4 W.

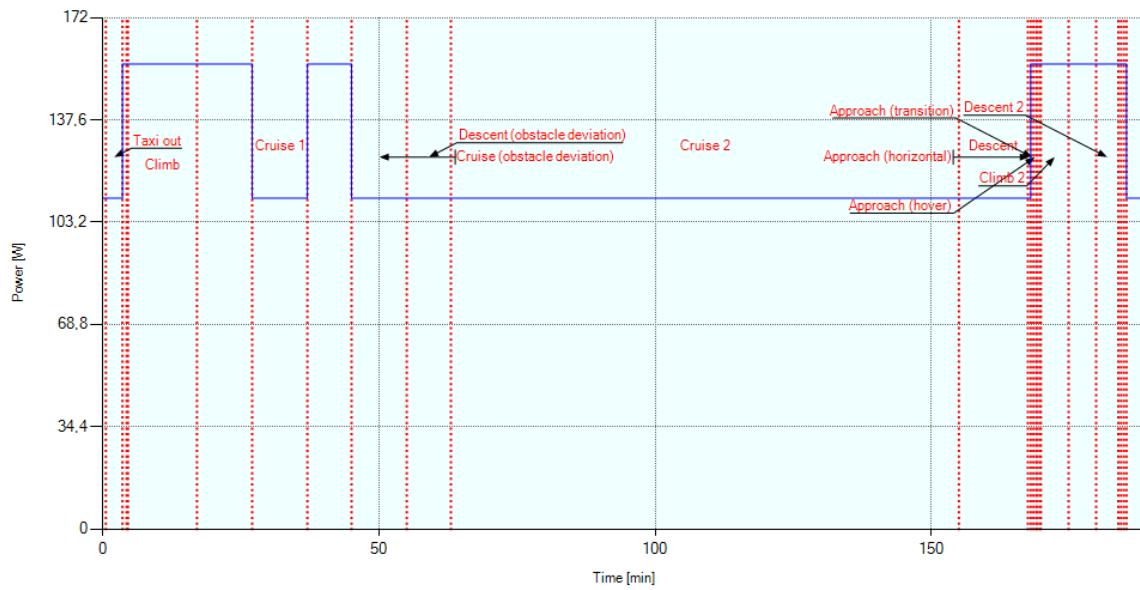Based on these data, we obtained the following power budget for the fuel system.

Figure 11.11.5: Fuel system power budget

Once the all system is designed, we create the CAD model of each component and we installed on the aircraft model. We cannot realize the correct shape for the integrated tank, so we realized a simple parallelepiped whose volume is the same of the real tank. The result is showed in the figure below.
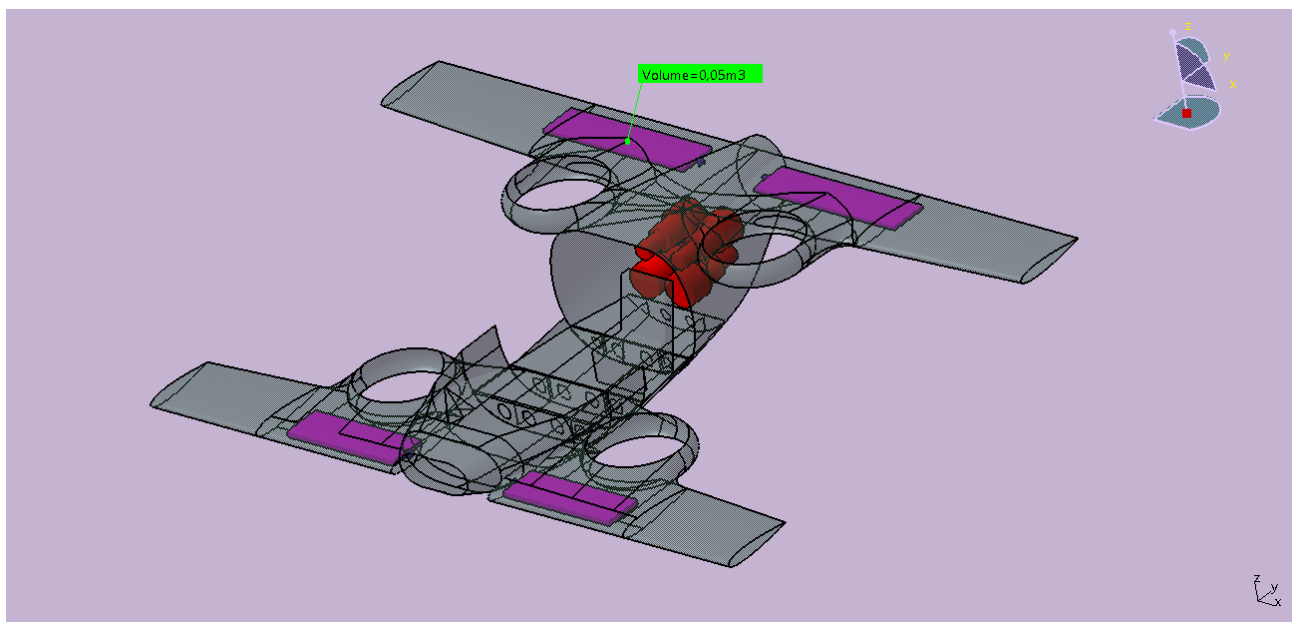

Figure 11.11.6: Fuel system mockup
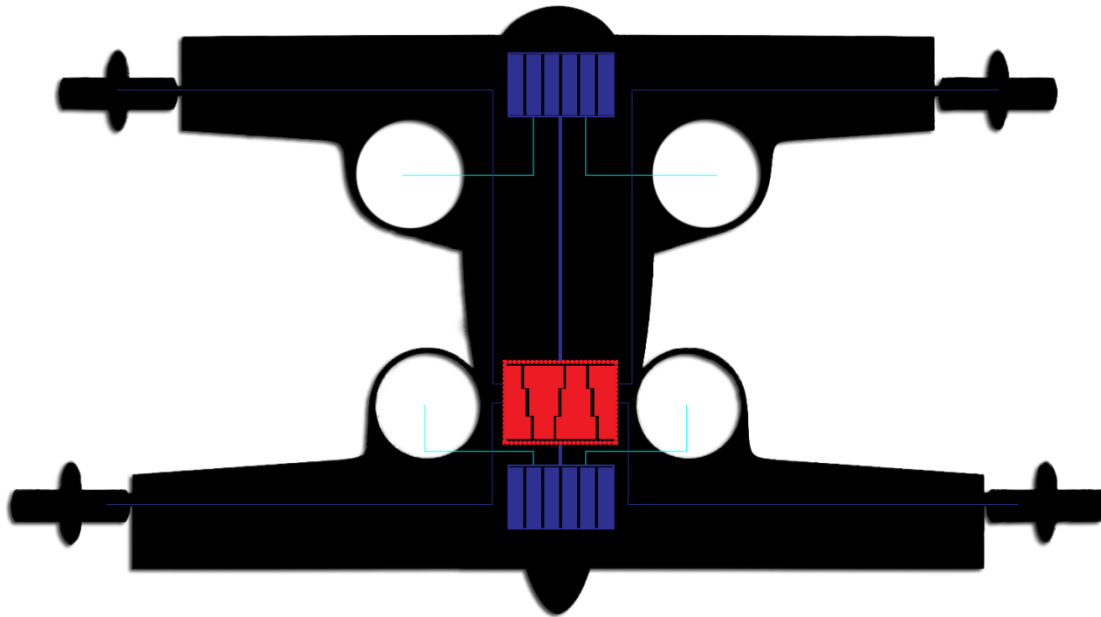
12. Electric System

Figure 12.12.1: Architecture of electric system

The electric system is probably the most important of these aircraft. The Mini-Bee is designed with the more-electric philosophy, so all the equipment installed works with electric power. The more-electric philosophy, or in our case the all-electric philosophy, has the purpose of reduce the weight of the aircraft: replacing the hydraulic supply line with electric cables, the total weight of the aircraft decrease.

For the Mini-Bee, to provide electrical power to the systems, we use four Turbotech. These are experimental turbo-generator specifically designed for the hybrid architectures, with the goal to improve the performance of little turbine.

Figure 12.12.2: Turbotech fuel generator

The developer should realize a prototype with the following features:

Electric Power [kW]	55
Voltage	270-550 VDC
Specific Power [g/kWh]	300

Looking at the generators specs, one particular data is the high current voltage. This solution allow to reduce the weight of the electric cables, in fact, the cable section is inversely proportional to the voltage by the relationship:

$$V = R * I = \rho \frac{L}{S} * I$$

So, at constant current I, length L and electrical resistivity ρ, over the V grows, the more the section S drops and with it the cable mass.

However, the aircraft regulation establish that the aircraft power line has to works at fixed value of tension that are 28V, 115V or 270V so we have to choose one of these tension in order to meet regulations. Choosing the power line tension, we have to face with the fact that many electric utilities need different tension. On the one hand we could chose the weight reduction of the cable given by high tension, and on the other hand the need of transformers to change 270V to 28V. Nevertheless, the only tension that the Turbotech fuel generator could provide, according with the regulation, is 270VDC so we have to use this value.

With this architecture, we provide tension through the aircraft at 270VDC and, only when is needed, we convert it to 28V.

The procedure for the electric system design sees, at the first steps, the definition of the primary electric generation. Based on considerations above, we use the 270VDC. With this selection, we have a switched redundancy electric generator while the engine starter is an electric starter-generator. For the design of these system is also necessary to define the number of engines, which is four, and the number of generators per engines, one. Due to the nature of the Turbotech generators, there are no redundancy for the generator.

Once set the power generation, we calculate the total power requested for each mission phase. To do this, we must define the importance of each sub-systems choosing from Fundamental, Essential and not-Essential. We defined the following set:

Table 12.12.1: Importance of the apparatus in case of emergency

	FCC Athena 311
	Fuel Pump
Fundamental	Garmin G1000
	Rudder's actuator
	Tilt rotors' actuator

Essential	Moving surface hinges
Not Essential	HUD Saab
	Retraction central 1-2
	Retraction forward
	Steering forward
	Breaking strut central 1-2
	Breaking strut forward

Then we have to define the additional users, their characteristics and when they are active during the mission phase. Those are:

- Power Distribution Unit: 200W @ 28VDC, fundamental, active in all mission phases;
- Electric Load Management Center: 300W @ 28VDC, fundamental, active in all mission phases;
- Light (external): 150W @ 28VDC, essential, active in all mission phases;
- Light (cabin): 20W @ 28VDC, not essential, active in all mission phases;
- Electric motors in hover: 440kW @ 270VDC, fundamental, active in hover, transition to climb, transition after descent;
- Electric motors in climb: 200kW @ 270VDC, fundamental, active in climb, climb(obstacle deviation), climb 2;
- Electric motors in cruise and descent: 160kW @ 270VDC, fundamental, active in cruise 1, cruise 2, descent, descent 2;
- Electric motors cruise recharge: 160kW @ 270VDC, fundamental, active in cruise (recharge) and cruise (recharge)2;
- Electric motors obstacle deviation: 135kW @ 270VDC, fundamental, active in cruise (obstacle deviation) and descent (obstacle deviation);
- Environmental Control Unit: 924W @ 270VDC, essential, active in all phases except hover phases;
- Battery recharge: 57kW @ 270VDC, fundamental, active in cruise (battery recharge), cruise (recharge)2, descent 2;

At this point, we have the complete power requested by the aircraft in all mission phases. This is showed in the chart below:
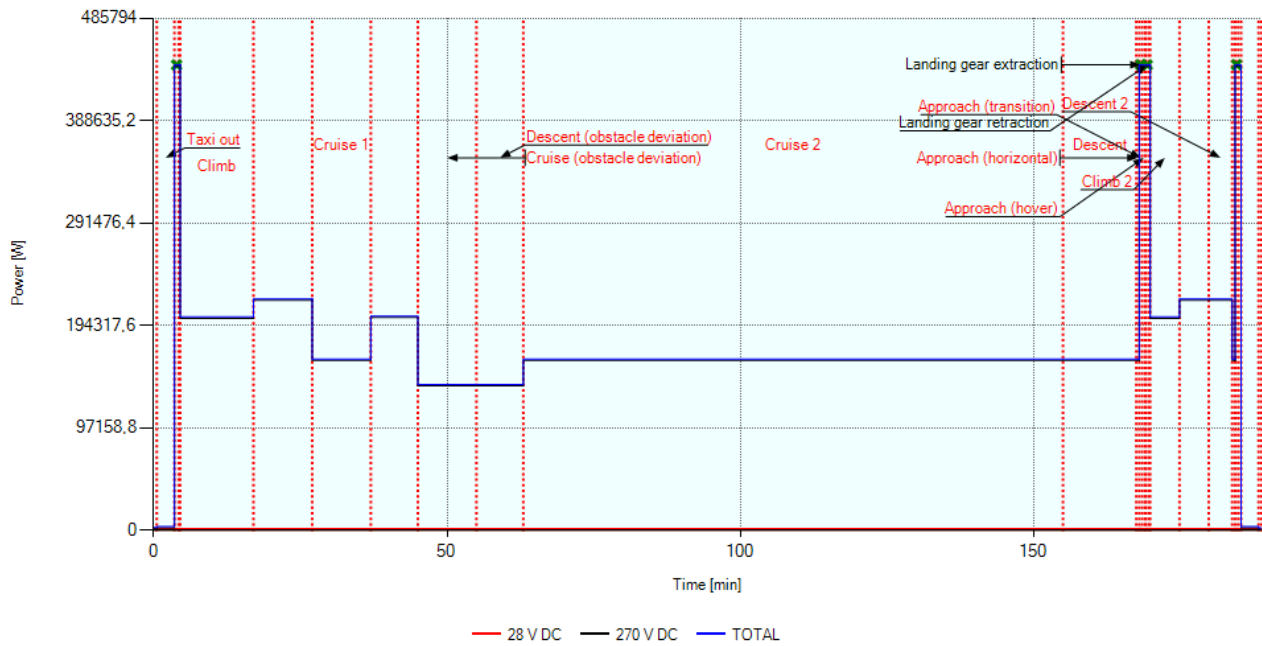

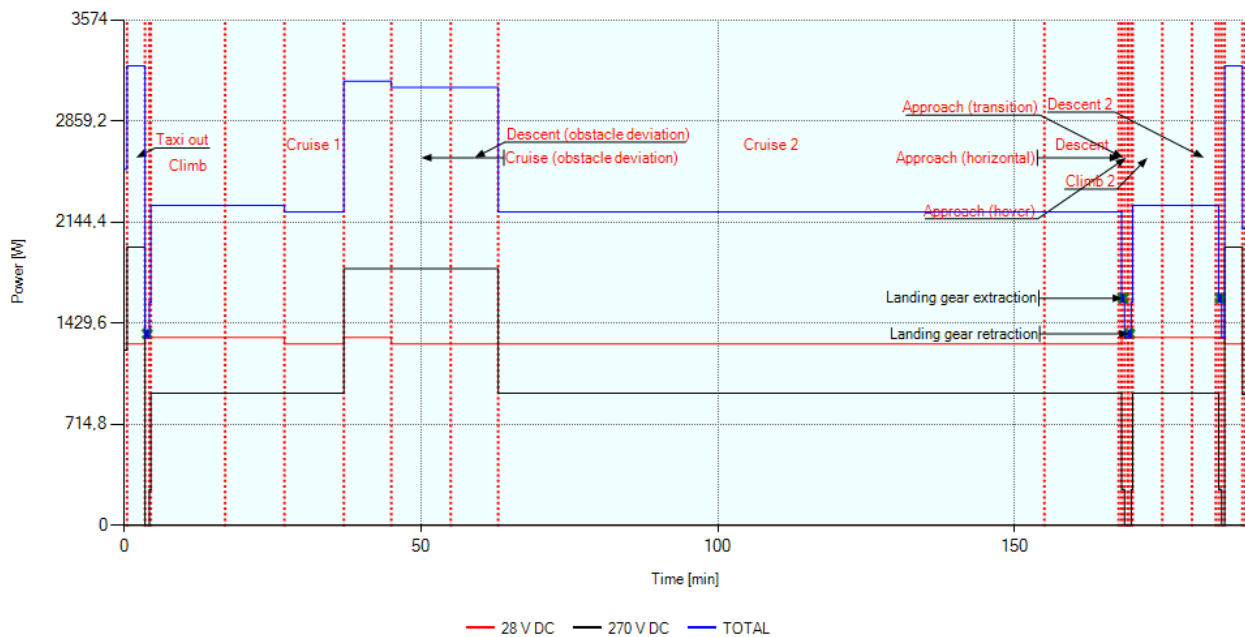*Figure 12.12.3: Electric power budget*

Figure 12.4: Electric power budget without thrust power

As we can see, maximum power load occurs during take-off and landing because of hover rotors activation. In fact, during these phases the amount of required power reaches 441.5 kW that we are able to satisfy thanks to thermal and electric engines capacity to run off-design for a few, even if at cost of an efficiency drop.

The second major power peak occurs during batteries recharge phases, in very first part of cruise and after aborted landing, where the total amount is about 220 kW. In particular, in the

last case, recharge keeps going till the hover turning on for approach, which is the cause of the instantaneous peak from 220 to 440 kW in the right part of the chart.

During climbs, thermal engines have to produce more power than during cruise, that's why the peak load during these phases is around 200 kW.

The cruise phases without recharging batteries have different power consumption because of their different altitude: at 2500 m, we have a 160 kW power requirement, while at 4000 m aircraft requires about 140 kW.

The remaining phases that are not visible due to a much lower power consumption in the graph are characterized by:

- 2.5 kW for engine start-up
- 3.2 kW for taxi in and out due to landing gear steering and braking actuators
- 2 kW during engine shut-down

Defined the power budget, we must verify the electric starter. To do this, we set the type of engines, which is turboprop with 220kW required. Choose the starter, the software verify that the generator power is sufficient for the engines start.

Then, we defined the power converter from 270VDC to 28VDC. From statistical evaluation, the power lost in the conversion is about 442.46 W, while the DC/DC power converter weight 1.04kg.

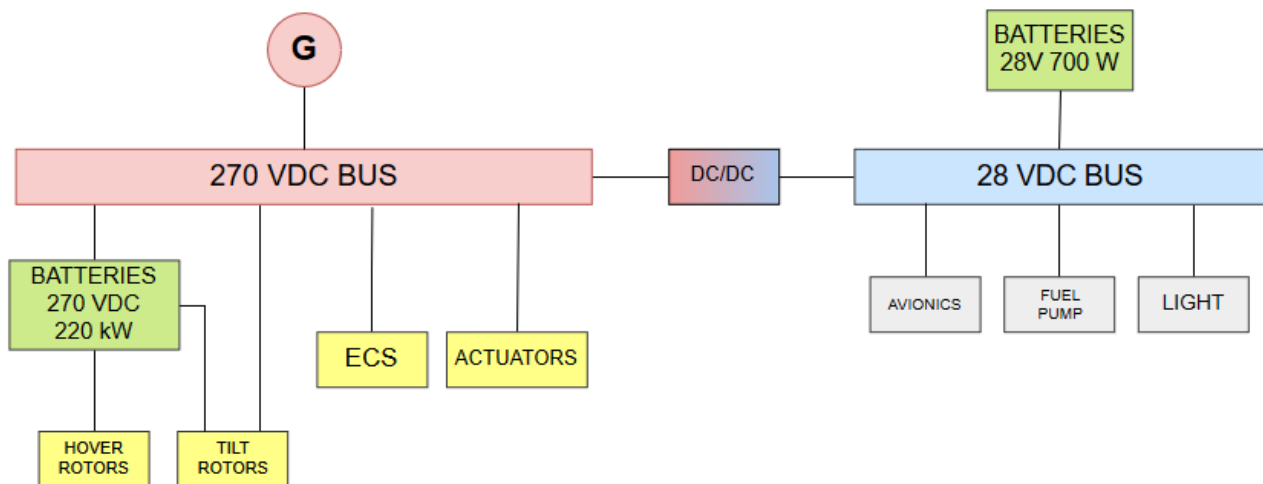So the scheme of the power distribution is

Figure 12.5: Electric system power distribution

Where the total power distributed at 28 VDC is 1.32 kW, while the remaining 440.615 kW are supplied to the system at 270 VDC.

12.1.   Batteries sizing

The choosing of Li-Ion batteries for our needs is to be found in high energy density (both with respect to mass and volume) and reliability. Indeed, among the multiple benefits, we can notice more than 1000 charge/discharge cycles, a huge operational temperature range, a long lifetime, high efficiency and depth of discharge. For our application, we assigned sixty second to the take-off time, which means the hover

rotors must be able to be activated for two consecutive minutes in case of take-off failure and need for emergency landing (and vice versa for landing failure and emergency take-off). Considering that the total required power by electrical engines is 220 kW, we must provide energy equal to:

$$220 \times \frac{120}{3600} = 7.33 \text{ kWh}$$

With electric engines efficiency η_e = 0.95 and batteries efficiency η_b = 0.9, these must be able to produce:

$$\frac{7.33}{\eta_e \times \eta_b} = 8.6 \text{ kWh}$$

which means (with typical energy density values ρ_m = 180 Wh/kg, ρ_v = 400 Wh/L and a D_{od} = 0.94 depth of discharge) a mass equal to:

$$\frac{8.6}{\rho_m \times \text{Dod}} = 50.69 \text{ kg}$$

and a volume occupation of:

$$\frac{8.6}{\rho_v \times \text{Dod}} = 0.023 \; m^3$$

Io order to be conservative, we chose to install 55 kg of batteries, which means 0.025 m³ of volume occupation.

The charging phase takes place in the very first part of the cruise, when only the tilt rotors are running, the speed is about 220 km/h and altitude is 2500 m; in these conditions, the estimated required power for keeping those speed and altitude is given by the following:

$$\frac{D \times V}{\eta_r \times \eta_e} = 158 \text{ kW}$$

where V is the speed, η_r = 0.8 the rotor efficiency, η_e the electric engines efficiency and D is the drag, given by:

$$D = \frac{1}{2} \, c_d \rho V^2 S = 2 \; kN$$

with c_d = 0.058 drag coefficient, ρ = 0.957 kg/m³ air density, V = 61.11 m/s and S = 18.72 m².

During this phase, the nominal available power is given by the turbo engines, which are able to provide 55 kW each, for a total amount of 220 kW, while the estimated residual power available for charging batteries and powering other systems is:

$$220 - 158 = 62 \text{ kW}$$

If the whole amount of residual power would be used for charging batteries, the estimated recharging time would be:

$$\frac{\rho_m \times W_b \times D_{od} \times \eta_b}{62} = 0.13 \text{ h} = 8.06 \text{ min}$$

where W_b is the batteries weight.

We have to make in evidence that the aircraft is not able to reach the required maximum speed of 300 km/h only powered by thermal engines, indeed for that, there would be required a power of about 400 kW, which means the gap should be erased by additional 180 kW, eventually provided by batteries. In these conditions, in theory we can reach the desired speed for about 3.5 minutes and, before attempting a landing approach, we have to recharge batteries again, but we have to take into account that the electric motors are designed to provide 55 kW and about 15 kW more each just for a few, which means that we are definitively not able to reach maximum speed.

We can suggest that a reasonable value of maximum speed could be 250 km/h. Indeed, we would need around 230 kW and, since batteries are be able to provide 10 kW plus for about 50 minutes, we could charge them again before landing, but we should also put in evidence that this condition would unavoidably cost an electric motors efficiency drop due to their running in an off-design condition. Moreover, at the maximum altitude of 4000 m, we could reach the suggested maximum speed and charge batteries in 22 minutes (22 kW of residual power).

Otherwise, for reaching 300 km/h we could propose the following solution, even if it doesn't seem that convenient:

Installing more powerful thermal engines (totally 400 kW) and electric motors (100 kW each), without oversizing batteries, but at cost of a larger weight (290 kg instead of 160 kg for *Turbotech*, and 80 kg instead of 44 kg for electric motors).

The procedure utilized to realize the batteries sizing via software is described in the following paragraph.

12.1.1. Emergency battery

For the emergency case, the software calculates the required electric power in emergency case summing the power required by the fundamental equipment. However, the Mini-Bee is an all-electric aircraft, so all motors and actuators are fundamental for a successfully mission. Due to this aspect, the total power needed in case of emergency is 441652.7 W. Then, we set the discharge time of the emergency batteries at 15 minutes-that are 0.25h. In order to size the emergency batteries for their real purpose, we have to use a fictitious batteries capacity/fuel ratio so that the energy stored in the batteries and their weight are more realistic. We set the batteries capacity/fuel ratio at 51972 Wh/kg so we obtained the following energy stored and battery weight.

$$Energy\ stored = Required\ power * discharge\ time = 441652.7 \cdot 0.25$$
$$= 110413.175\ Wh$$

$$Battery\ weight = \frac{Energy\ stored}{Battery\ capacity/weight} = \frac{110413.75}{51972} = 2.124\ kg$$

12.1.2. Hybrid battery

For the hybrid batteries, the software processes many data providing the final feature of the battery. In order to obtain the total batteries weight of 55kg – calculated above – we change the energy storage capacity/energy storage weight ratio considering the statistic data. Setting a ratio of 230Wh/kg we obtained 53.18kg hybrid battery mass.

So the total weight of the batteries is

$$Total\ battery\ weight = Emergency\ battery\ weight + hybrid\ battery\ weight = 55.3\ kg$$
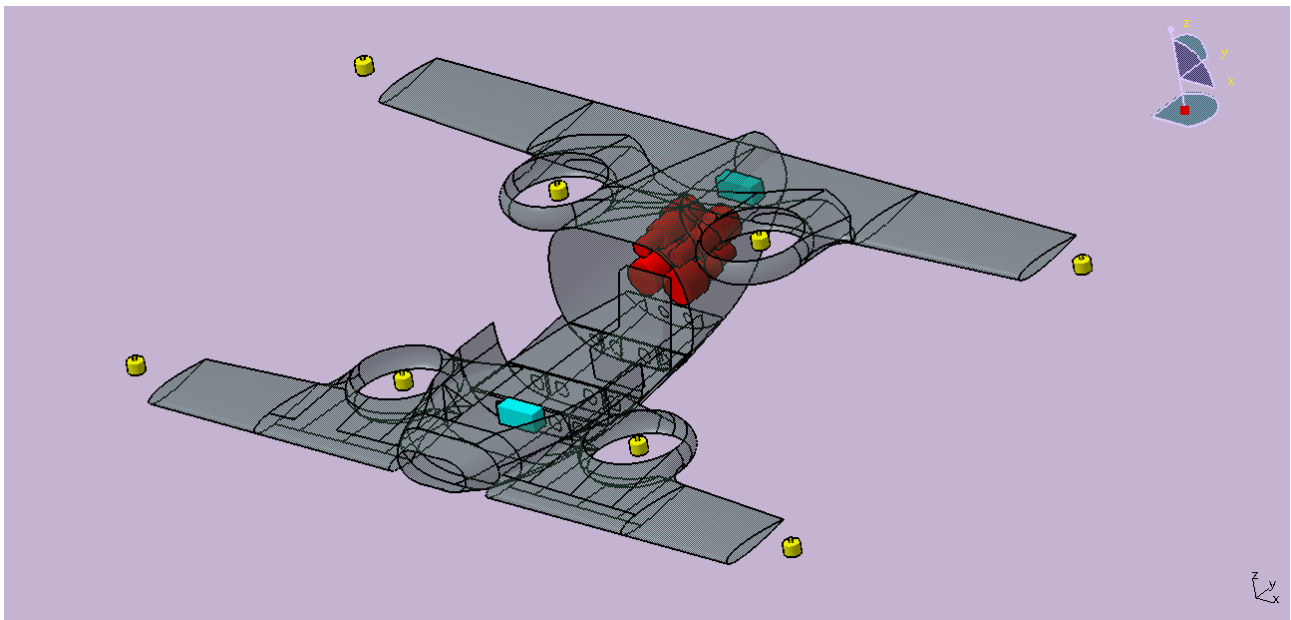
12.2. Electric system mock-up

Figure 12.12.4: electric system mock-up

13. Complete aircraft

The *Supmeca* and *Estaca* teams realize the body and the structure (not available) of the Mini-Bee. We, as system designer, realize the CAD of each equipment and place it in the aircraft shell.
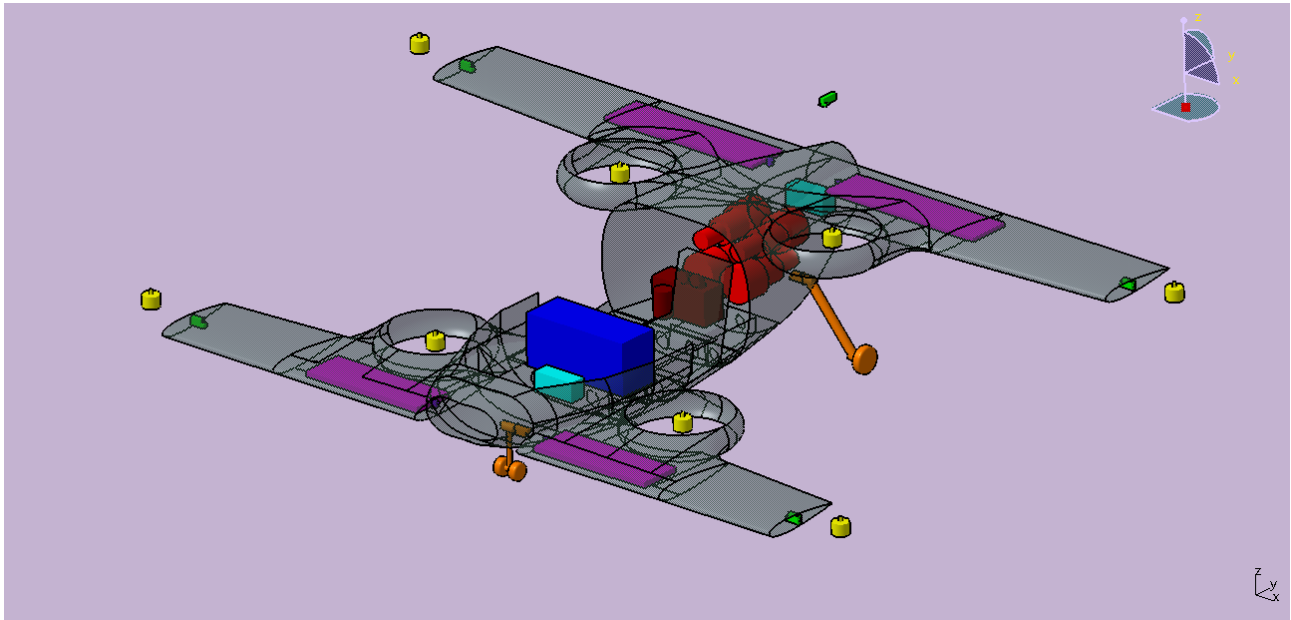
The complete aircraft mock-up is the following
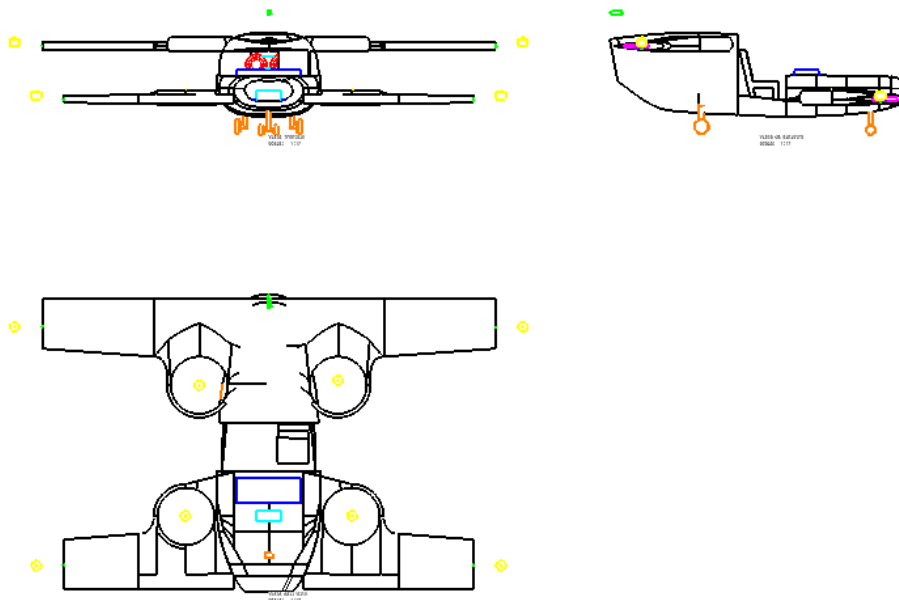

Figure 13.1: Complete aircraft mock-up

Figure 13.2: Complete aircraft three-view

We obtained the following weights:

Table 13.13.1: mass budget of on-onboard systems

System	Weight [kg]
Avionic	49.8
Flight Control	31.8
Landing Gear	61.93
Environmental Control	22.2
Fuel	12
Power Generation + Motors	307.2
Total	485.13

14. X-Plane

First step of X-Plane implementation is modeling the plane mock-up through plane maker and the help of its three sight view conveniently scaled, as shown in the figure below:
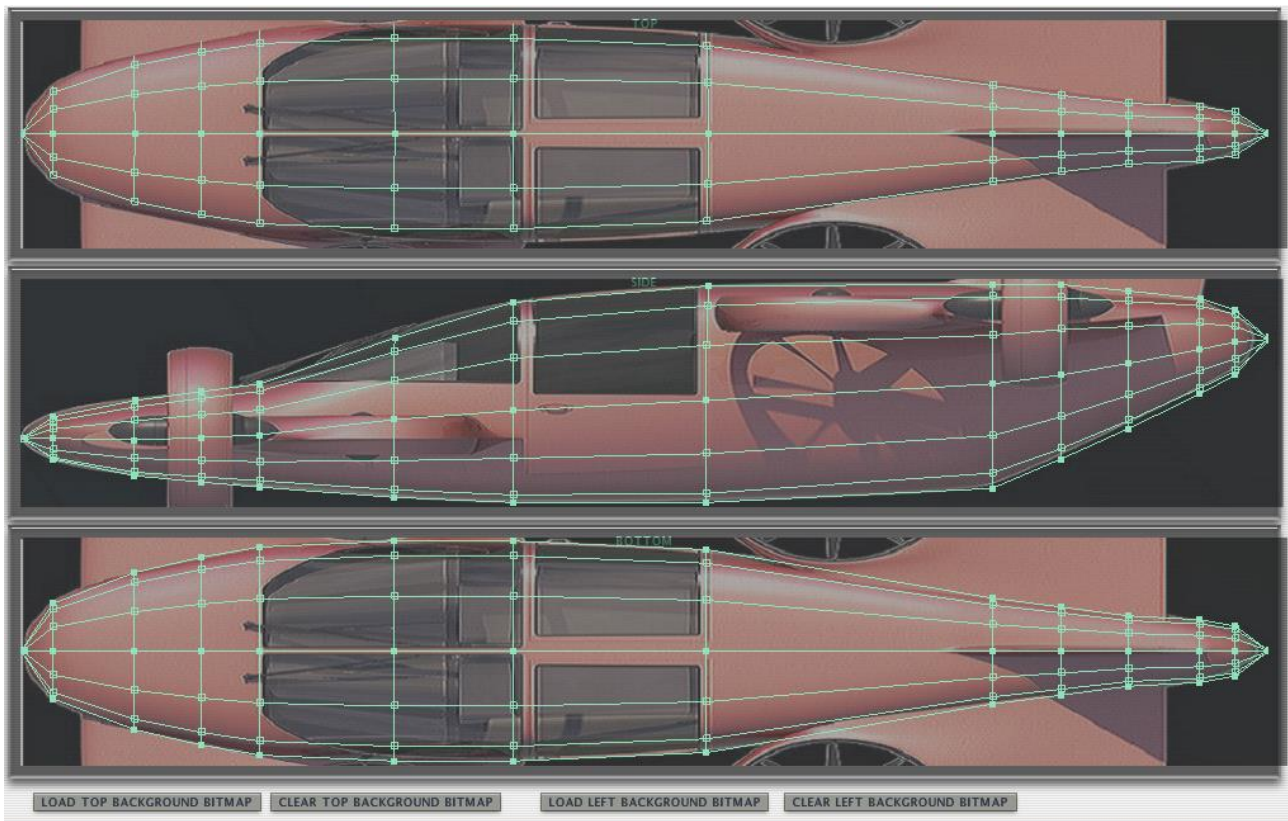

Figure 14.14.1: Fuselage modeling in Plane-maker

After we established the reference point on the nose of the aircraft, because of fuselage shape, we settled 13 section in order to better fit it; its length is 21.5 ft.

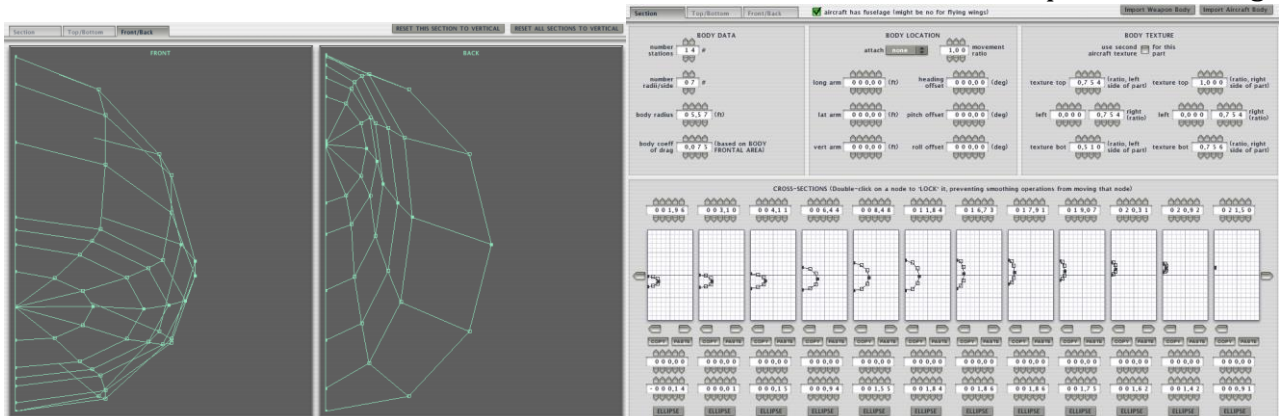Here the section and front-back view of shaped fuselage:

Figure14.14.2: Results of fuselage modeling

Next step was wings modeling; we used a NACA 65(216)412 profile for both, and settled respectively a 20 and 22 ft span for front and rear, same constant chord of 4.92

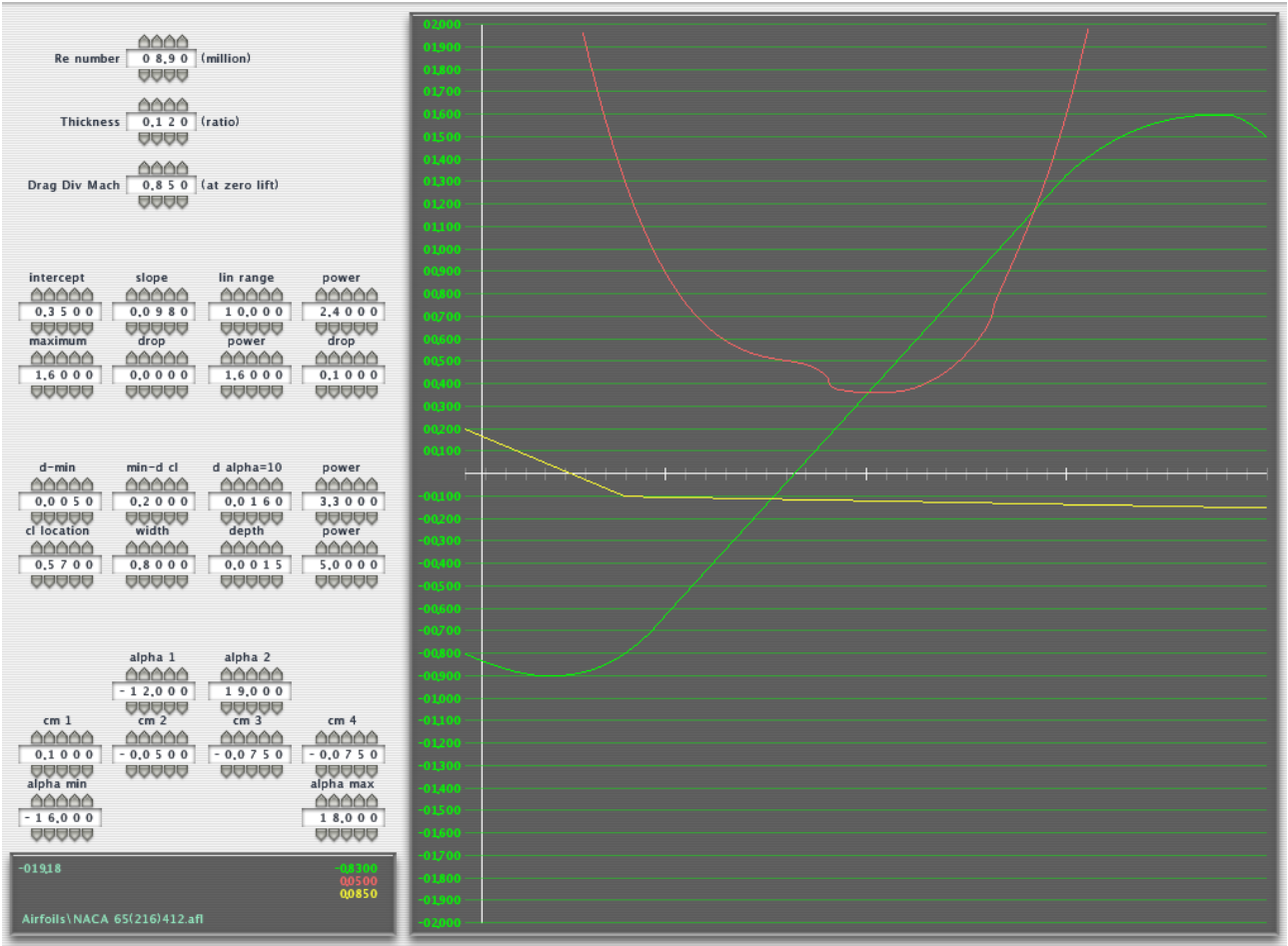ft, and a longitudinal position of 2.8 and 16 ft, while their vertical quotes were -0.8 ft and 1.54 ft.

Figure14.14.3: The airfoil maker of chosen profile

As we know, the only one control surface of our aircraft, is the rudder that we of course integrated on the vertical stabilizer modeled this way:
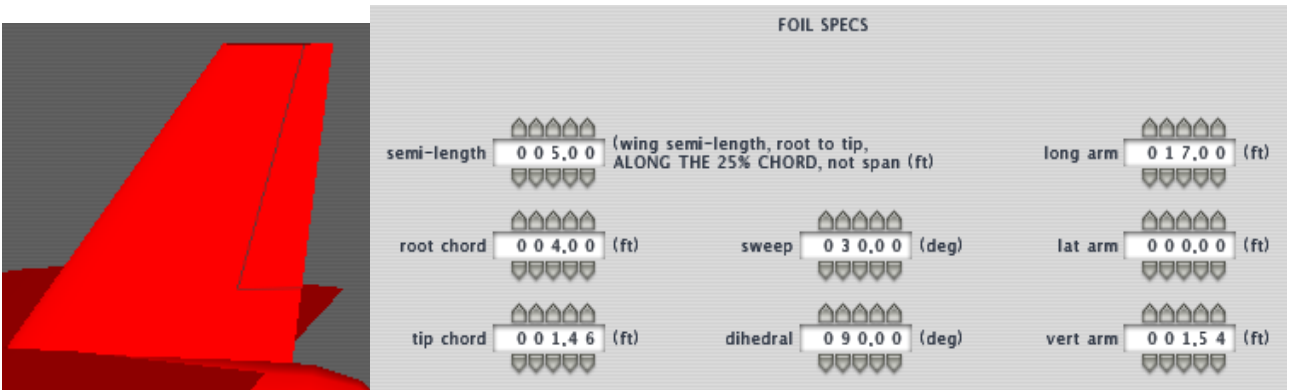

Figure 14.14.4: Vertical stabilizer and rudder

Then it was the time for landing gear that we tried to modeling as accurately as possible and here the result:

Figure 14.14.5: particular of Landing Gear

It is retractable too.

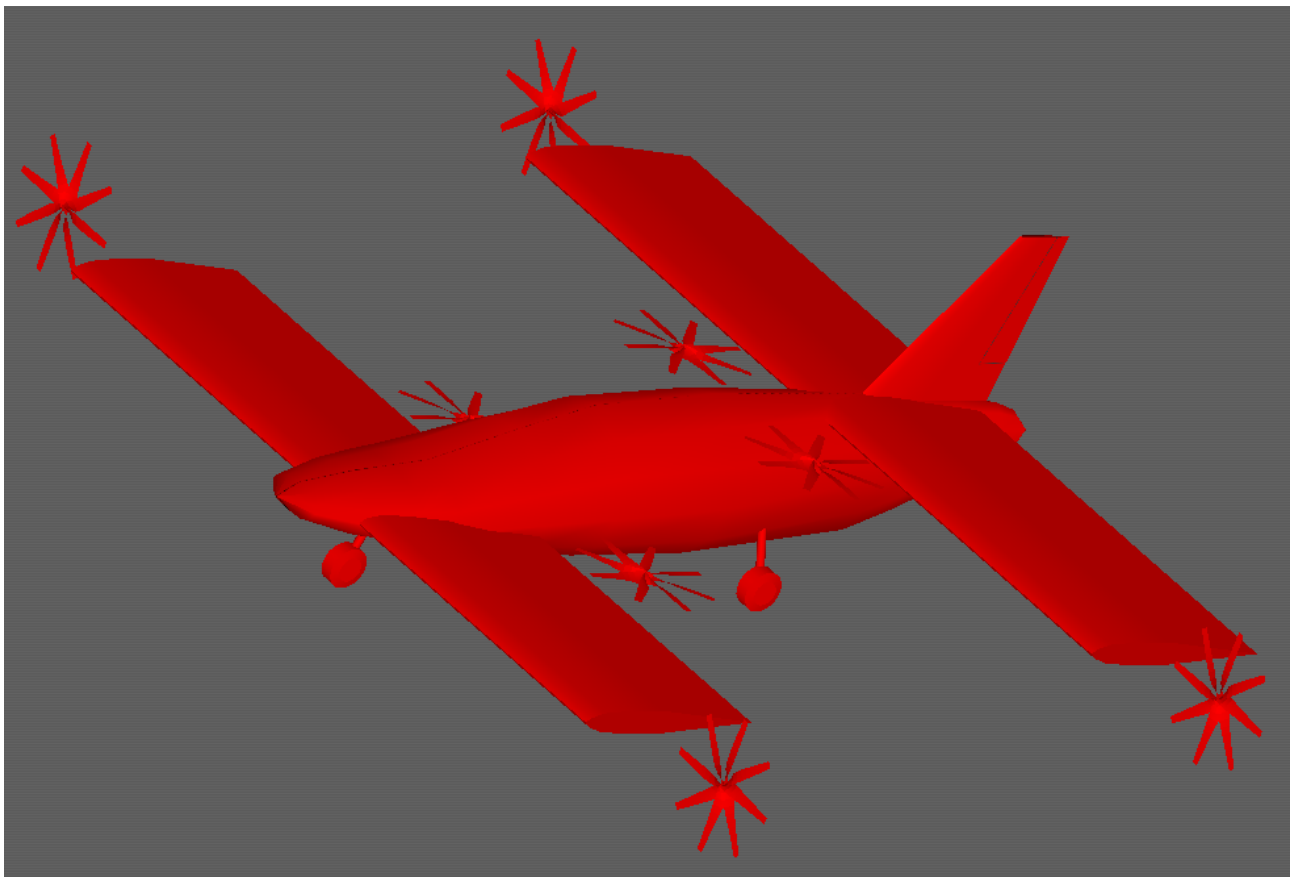Final step for the "exterior" modeling were engine and rotors:

Figure 14.14.6: Complete mock-up with the rotors configuration

Since X-Plane doesn't support the hybrid configuration, we had to set a turboprop engine for simulating our Turbotech and fuel consumption. We settled the wing-tip rotors as tiltable and the remaining as fixed, while the other data are:
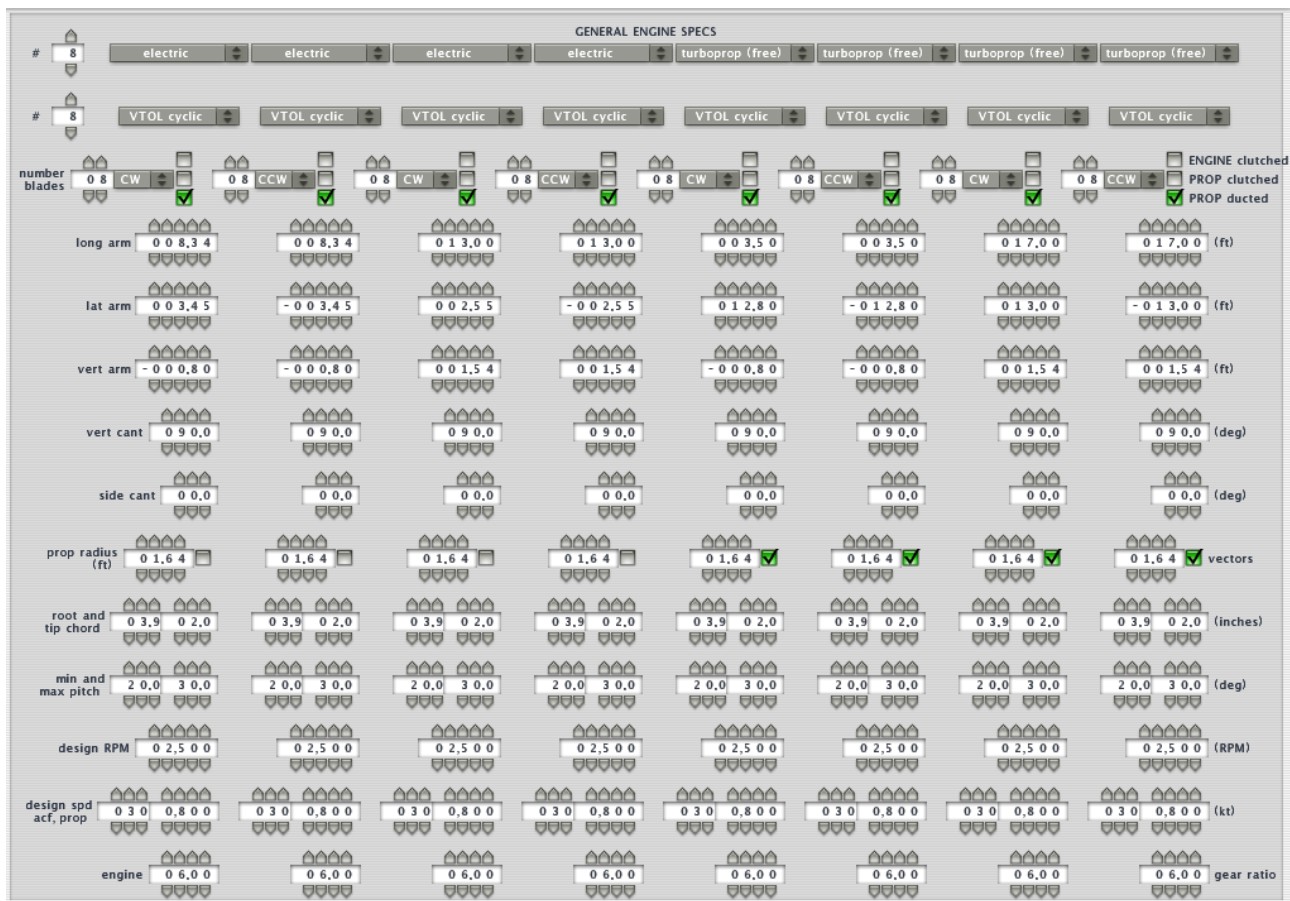
Figure 14.14.7: Rotors data

Finally, we imposed the center of gravity at 10.46 ft and tanks in the wings, each with 25% of total fuel mass (360 lb).
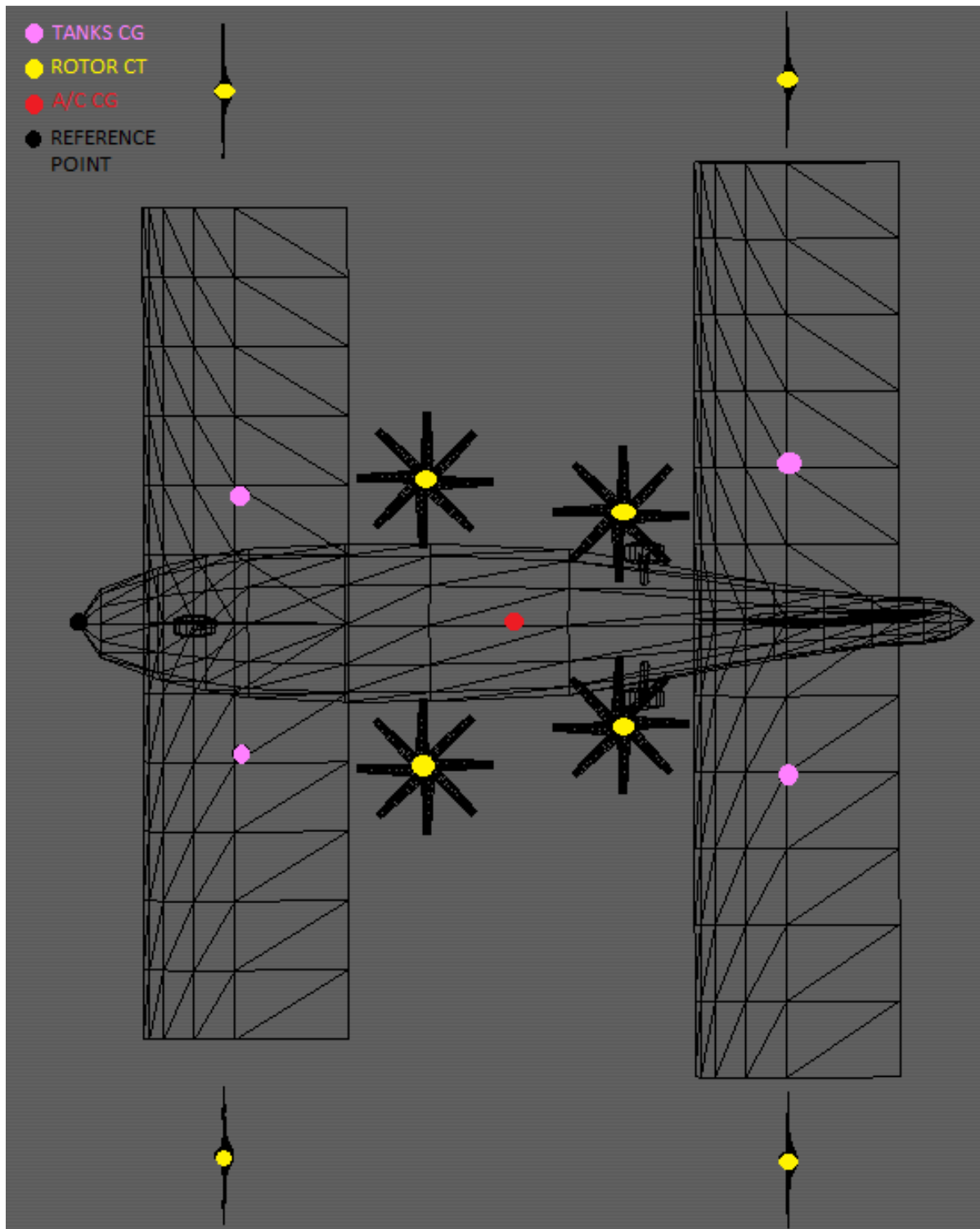

Figure 14.14.8: "Dotted" view of A/C
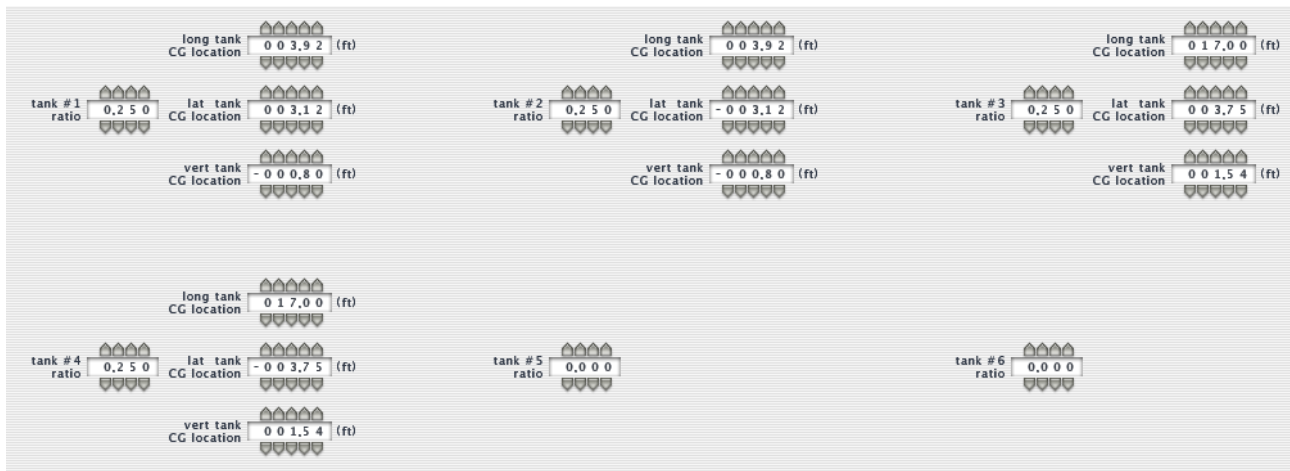
And, following, the data:
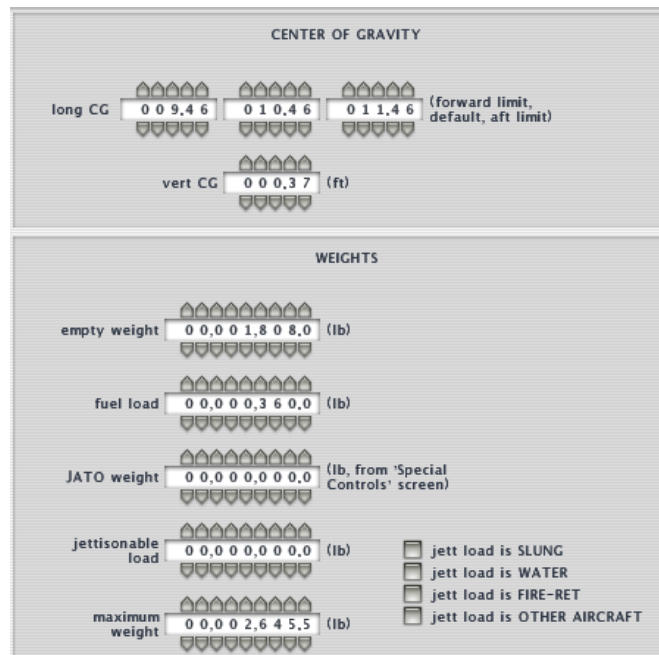
Figure 14.14.9: Mass, balance and tanks data

Since this plane is supposed to be piloted by "common people", it's strictly necessary the development of an ad-hoc flight control system with an automatic control, which means to differentially distribute thrust and tilting among the eight rotors, even because these are the only ways to operate di A/C, seen the lack of control surfaces. Forasmuch as there's no way to implement that kind of system on X-Plane, what we did was letting the rotors total center of thrust (TCT) coincide with aircraft center of gravity, in fact, by calculating CTC

$$CTC = \frac{8.34 + 13 + 3.5 + 17}{4} = 10.46\,ft$$

we can see that coincides with center of gravity. Same for fuel tanks which are located inside wings:

$$CG_t = \frac{3.92 + 17}{2} = 10.46 \, ft$$

These statements ensure stability at least during vertical motion but, as already said, it's really difficult to steer the airplane during flight because of lack of a control system.

Finally, here is the cockpit view of our model, where we can find all the essential components and the thrust vectoring handle:

Figure 14.14.10: Panel details in X-Plane with indication of thrust vectoring handles

As we can see, we settled two MFD, one with HSI and the other with navigation display function. Following the detail on the HUD:

Figure 14.14.11: HUD focus

We run just two kind of simulation, which are vertical take-off and a horizontal take-off in case of hover rotor failure. Indeed, we were not able to evaluate a cruise or landing phase because of aforementioned stability problems. In fact, as stated in x-plane video of vertical take-off simulation, the aircraft could accomplish vertical take-off and transition to horizontal flight, without any problems but control is lost just after same transition.
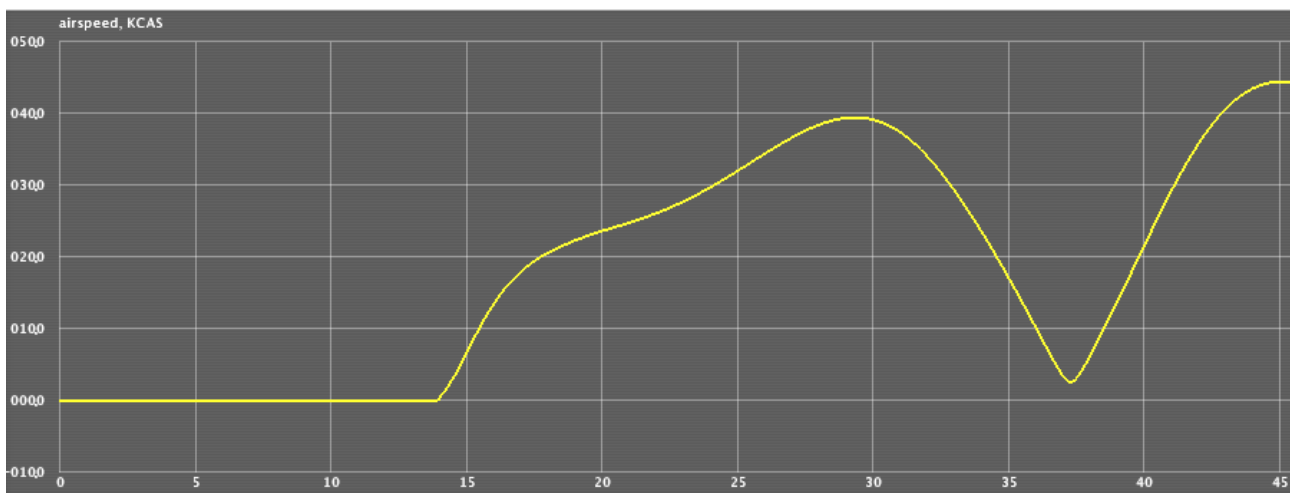
Figure 14.14.12: As we can see, the airspeed during vertical TO, grows smoothly during the vertical phase, than decreases during transition and gradually grows again for horizontal phase.

In the ghaph we can read the total time along which hover rotors are running and result is about 30 s, which means the take-off duration assumed for batteries sizing (60 s) is sufficiently conservative. Because of unknown issues with x-plane, we unluckly were not able to plot information such as specific fuel consumption, and other parameters. Indeed it was impossible to have the "data.out" file correctly compiled with such information. Other useful datas we could evaluate where:

- left and right thrust

Figure 14.13: Left thrust
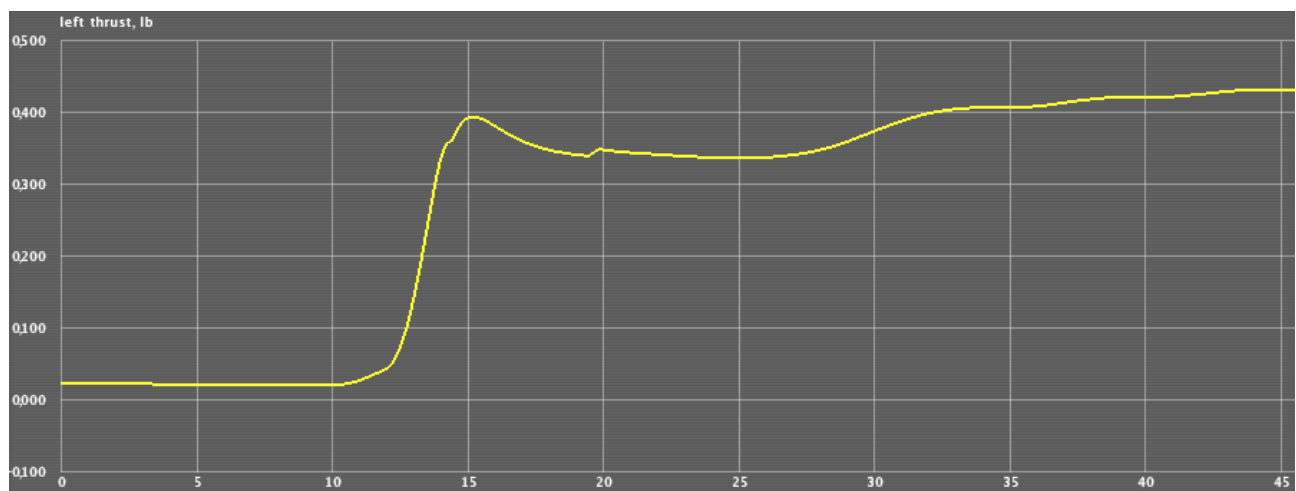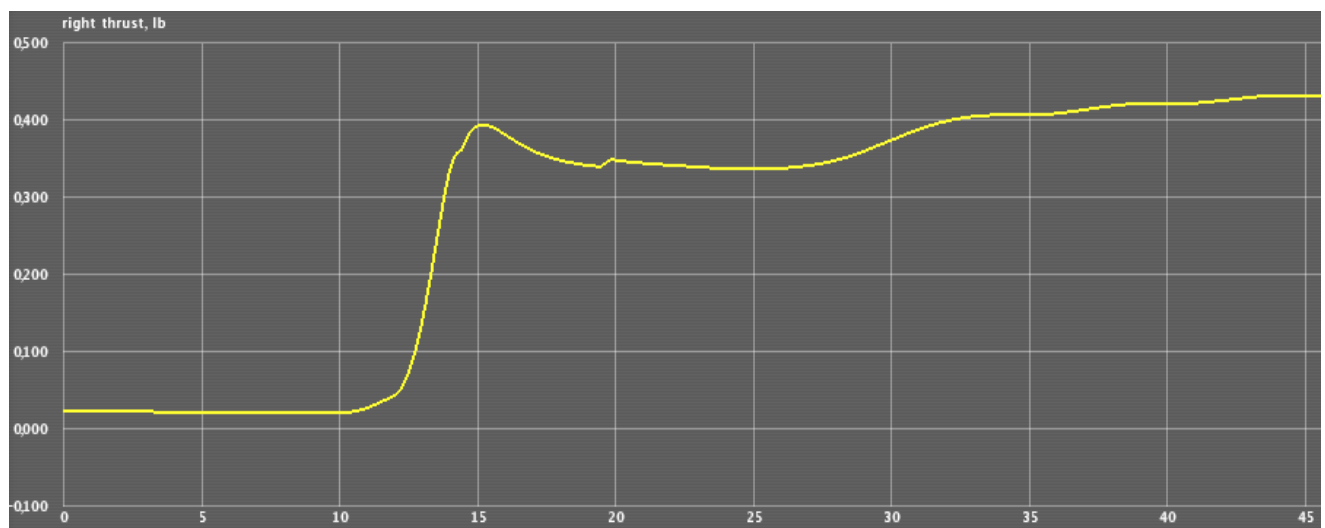

Figure 14.14.13: Right thrust

- Landing gear retraction/extraction
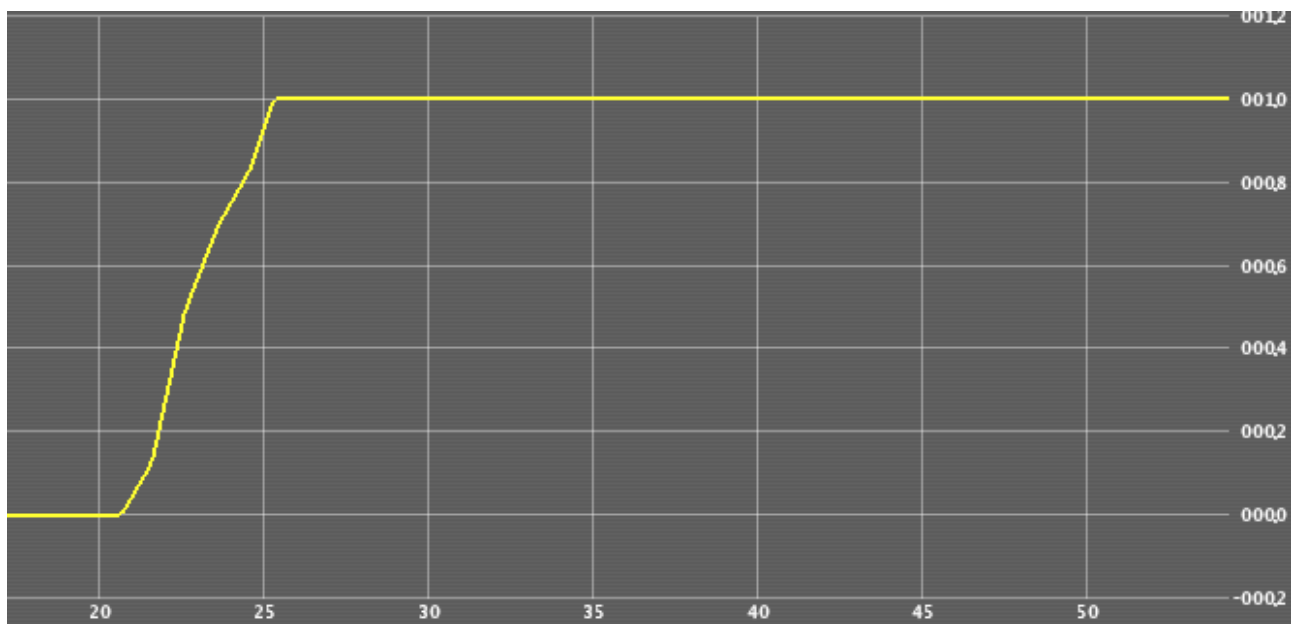
Figure 14.14.14: Retraction. The 3 s required time is fullfilled
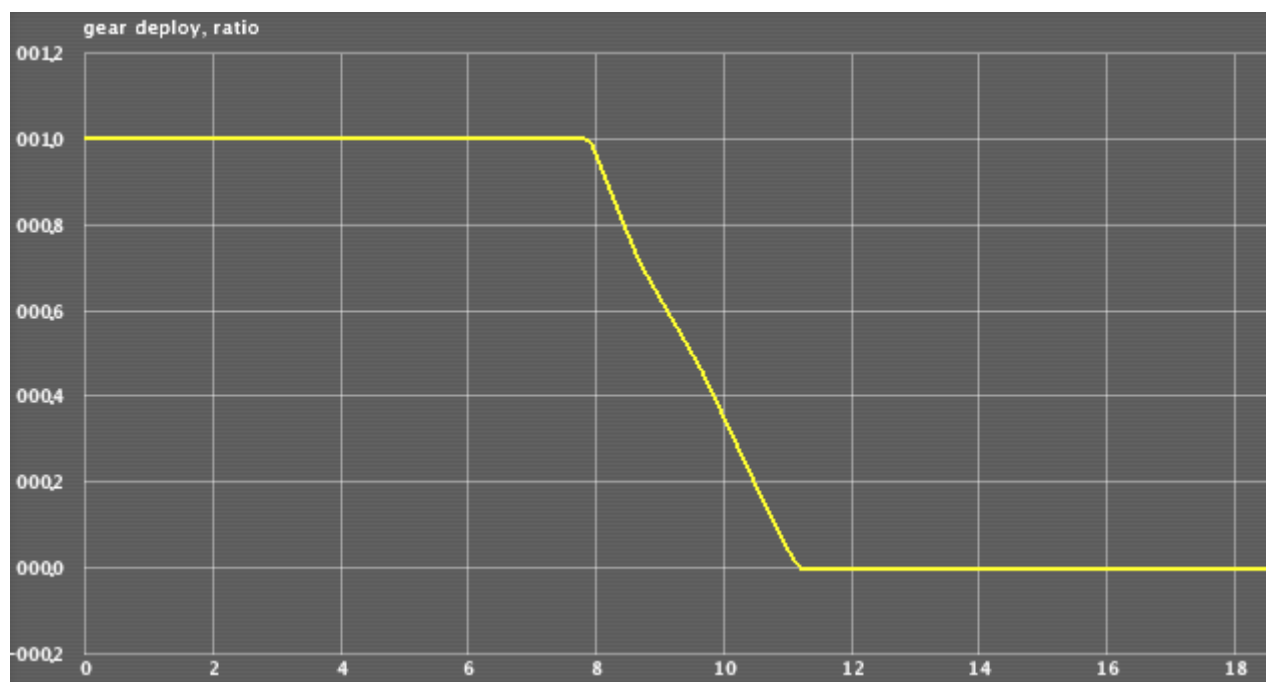
Figure 14.14.15: Extracion. Even in this case required extraction time is achieved

For, horizontal emergency take-off, the results were as followig:

- Airspeed
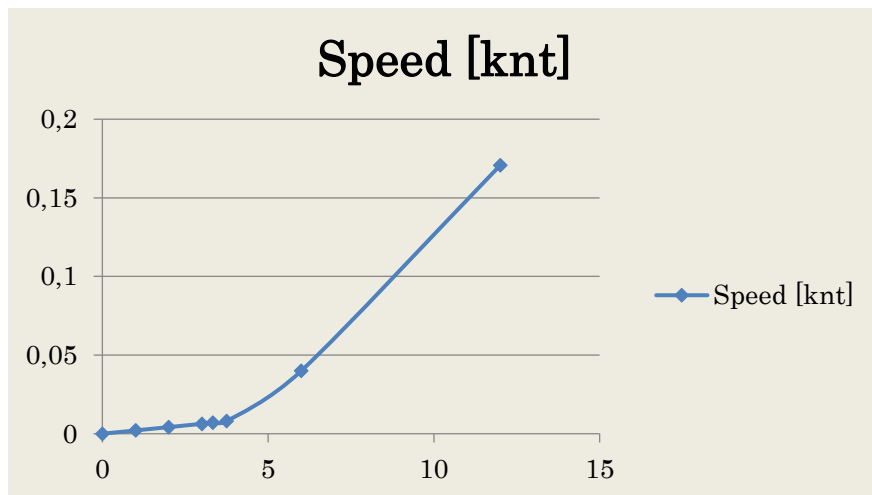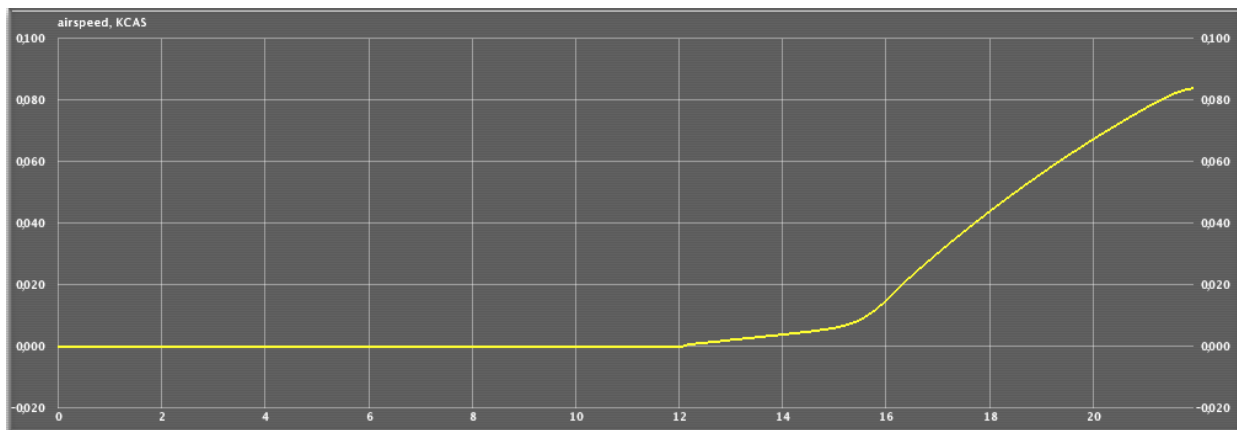
Figure 14.14.16: We had to manually calculate take-off distance and, since TO time was around 12 s, we approximated speed as stated in the graph upside

From 0 to 4 seconds the motion equation is:

$$s_1 = \int_0^4 2.1 * 0.5 * t \, dt = 4.2 \, m$$

While from 4 to 12 seconds:

$$s_2 = \int_4^{12} 14.2 * 0.5 * t \, dt = 56.8 \, m$$

And total TO distance:

$$s_1 + s_2 = 61 \, m$$

We suppose the cause of that low value is due to the high wings surface.

15. RAMS and Cost

15.1. COST

The gross cost is estimated by a parametric method, which is reliable enough in the Concept Refinement and Technology Development phases. The cost estimation is based on a database from which the parameters of the costs are taken.

The parametric method, in this case, is based on the CERs (Cost Estimating Relationships). The CERs are statistic equations that link costs to the designed parameters.

An example of CER may be the following equation:

$$Cost_i = A_i \cdot W_i^b \cdot X_i^c \cdot Q^{-k}$$

In which:

i = subsystem or component
A = constant cost related to the mass unit of which component or subsystem
W^b = subsystem or component size characteristics, which includes mass, dimensions and volume
X^c = performance characteristics of the subsystem or component (i.e. power, speed, ecc)
Q^{-k} = learning curve which depends on the quantity of the components produced

Using as an initial parameter the MTOM (Maximum Take-Off Mass equal to 1200 kg or 2645.55 lb) it is possible to find a statistic price **P'**. Using the graphic indicated in the figure below, we found $ 120.000,00.

The other coefficients considered are:

- The discount factor (equal to 2,08 in 2017)
- Technological coefficient (equal to 2 because of the concept of VTOL conceptual aircraft)
- Turnkey Coefficient (equal to 1,6)

So, the purchase price **P** estimated is the following:

$$\boldsymbol{P} = P' \cdot 2{,}08 \cdot 2 \cdot 1{,}6 = \$\,\boldsymbol{798.720,00}$$

P' is the statistic price calculated from the following statistical plot (*Jan ROSKAM " Airplane Design"- Part 7: Airplane Cost Estimation*):

Figure A4 Effect of Takeoff Weight on the Price of
Single Engine Piston Airplanes
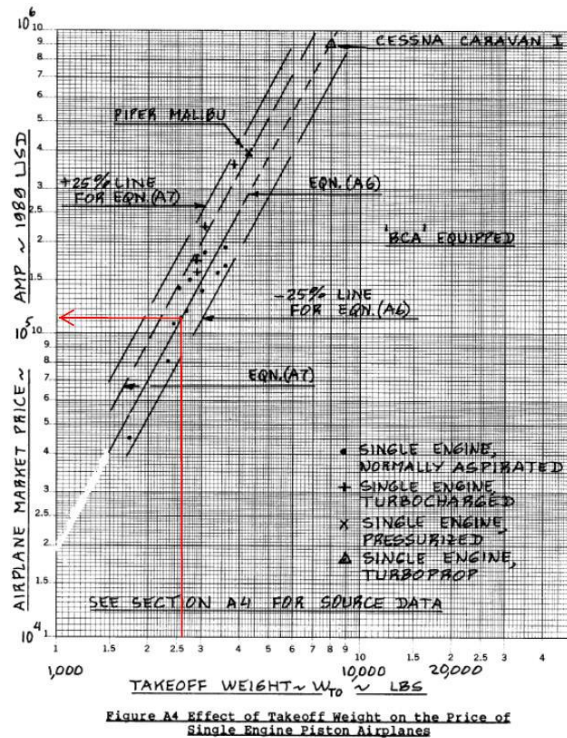
Figure 15.1: Weight vs cost curve

The purchase price is a little bit higher than that calculated in the previous Mini-Bee versions. This aspect must be discussed as it is crucial to understand if the cost is a requirement that not admit a large margin.

The percentage breakdown of the main components cost is indicated in the chart below:

Table 15.15.1: Cost % of the main components
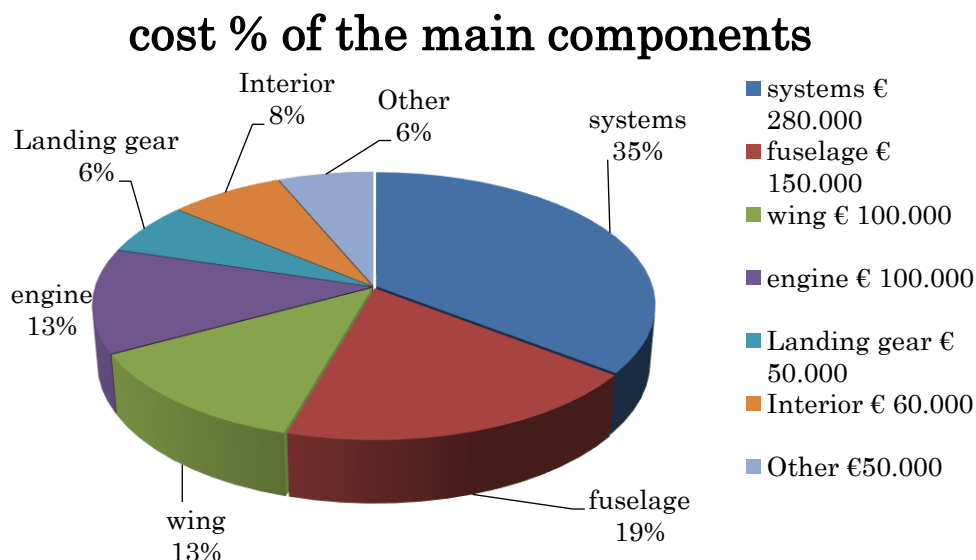
In a gross estimation, it is well to know that the cost of the systems sensors is approximately 8000 $/*lb* and the cost of the avionics is about 5000 $/*lb*.

15.2. RAMS Considerations

RAMS stayed for Reliability-Availability-Maintainability-Safety. For an efficient aircraft design, it is necessary taking into account all the RAMS aspects because they will influence strongly not only the aircraft's operational costs but also the cost of the aircraft itself, without considering the safety and reliability itself.

During a preliminary conceptual design, it is difficult to calculate a reliable Failure Rate (λ, [failures/1000 h]). So, the approach we made was to consider a "top-down" analysis, with reference to a unfortunately poor statistical database.

15.2.1. Failure Rate estimation

Considering a statistical "top-down" approach, the equation used to evaluate the failure rate λ is:

$$\lambda = \left(\frac{\lambda}{MEW}\right) \cdot IR \cdot IC \cdot IA \cdot MEW$$

With the following parameters:

Table 15.2: coefficients used for failure rate estimation

Coefficient	Symbol	Value	Note
$\left(\dfrac{Failure\ rate}{Manufacturer\ Empty\ Weight}\right)$	$\left(\dfrac{\lambda}{MEW}\right)$	1,8	[failures/1000h/tons] from statistics
Role coefficient	IR	1	A more complex role, higher is the role coefficient
Complexity coefficient	IC	1,2	Was considered a medium-high complexity
Technological age coefficient	IA	0,5	Ages: 2015-2020
Manufacturer Empty Weight	MEW	0,82	tons

Which leads to:

$$\lambda = 0,88\ \frac{failures}{1000\ h}$$

15.2.2.   Maintainability estimation

The approach used is the same as for the Failure Rate estimation. The parameter considered to evaluate the maintenance cost is the ratio between the man hours of maintenance (Maintenance Man Hours, MMH) and the hours of the aircraft flight (Flight Hours, FH).

The equation used is the following:

$$\frac{MMH}{FH} = IMR \cdot CDTM \cdot IC \cdot IA \cdot MEW^{0,25}$$

With:

Table 15.3: the mass, power and volume budget of the Avionic System

Coefficient	Symbol	Value	Note
$\left(\dfrac{\textit{\textbf{Maintenence Man Hours}}}{\textit{\textbf{Flight Hours}}}\right)$	$\left(\dfrac{MMH}{FH}\right)$	To find	Indicator of the maintainability and reliability
Role coefficient for the maintainability	IRM	1,3	A more complex role, higher is the role coefficient of the maintainability
Influence of the maintenece du the design coefficient	CDTM	1	Design To Maintain Coefficient depends in the stress put on the Maintainability
Complexity coefficient	IC	1,2	Was considered a medium-high complexity
Technological age coefficient	IA	0,5	Ages: 2015-2020
Manufacturer Empty Weight	MEW	0,82	tons

Which leads to the following result:

$$\frac{MMH}{FH} = 0,74$$

16. Conclusions

16.1. System Mass Budget

Once determined the mass and power budgets of all the main subsystems, it is necessary to draw some conclusions. The total power budget is indicated into the Electric System as the aircraft is all-electric.

The total mass of all the systems is about 459,54 kg. Here are not considered the rotors weight.

Table 12.1: Percentage of each subsystem

SYSTEMS MASS BREAKDOWN

Avionic 49,8 kg
10%

Flight Control 31,8 kg
7%

Landing Gear 36,54
13%

Power Generation 219,2 kg
45%

Environmental Control 22,2 kg
5%

Fuel 12 kg
2%

Electric Propulsion 88 kg
18%
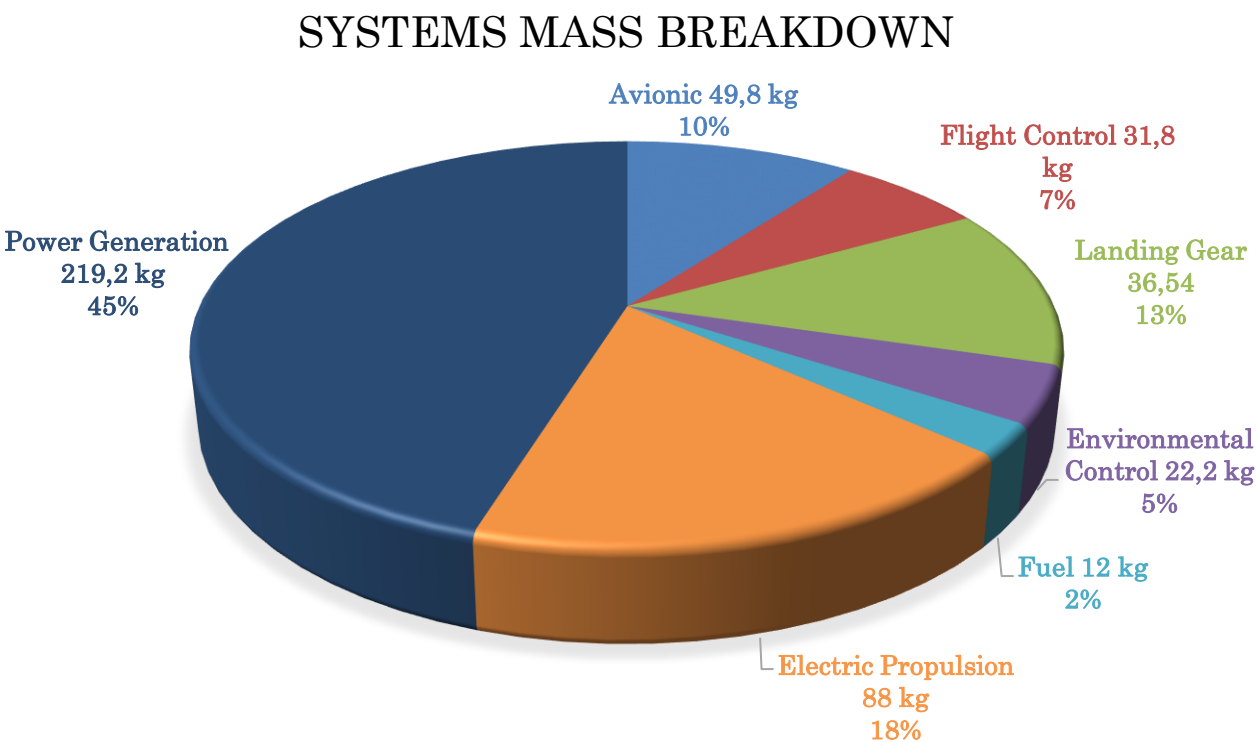
The estimations calculated are in trend with previous estimations.

OVERALL AIRCRAFT MASS BREAKDOWN

- Payload 220 kg
- Structure 291,34
- Landing gear system 36,54
- FCS system 31,8
- Electric and Propulsion system 376,32 kg
- Fuel system 12 kg

Table 12.2: Percentage of all main systems and components on the Mini-Bee

16.1.1.   Comparison with preliminary design configuration

Now we compare the results of the obtained mass distribution of the overall aircraft with the one obtained after the preliminary design of the Mini-Hornet. We get the following results:
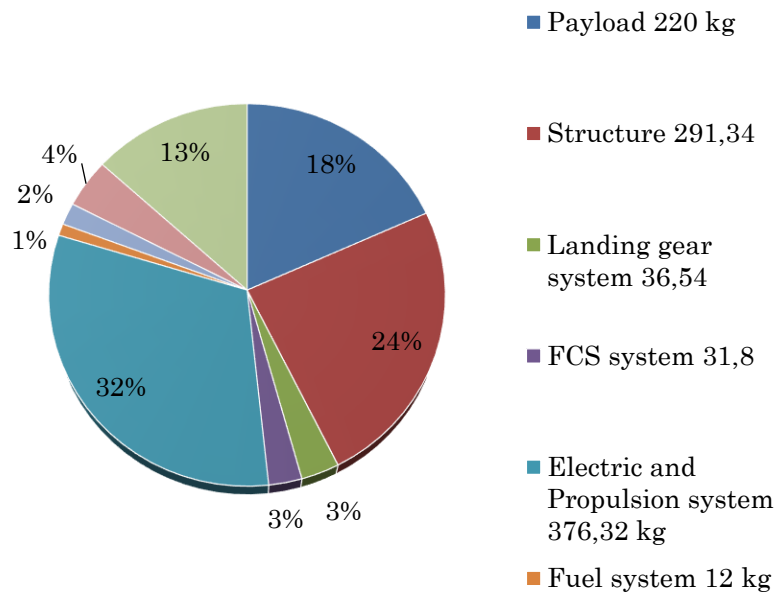
Table 16.1: mass distribution comparison between Mini-Hornet and Mini-Bee

|	Mini-Hornet (preliminary)		Mini-Bee (system design)	
	m [kg]	% mtow	m [kg]	% mtow
Payload/crew	220	24.44	220	18.33
Structure	177.49	19.72	327.88	27.32
Wing	*44.18*	*4.91*		
Tail	*13.25*	*1.47*	*291.34*	*24.28*
Fuselage	*93.08*	*10.34*		
Landing gear	*26.98*	*3.00*	*36.54*	*3.05*
Systems	452.42	50.27	492.12	41.01
FCS	*35.97*	*4.00*	*31.8*	*2.65*
Electric + Prop. systems	*344.51*	*38.28*	*376.32*	*31.36*
Fuel system	*13.49*	*1.50*	*12*	*1.00*
ECS	*4.5*	*0.50*	*22.2*	*1.85*
Avionic system	*53.95*	*5.99*	*49.8*	*4.15*
Empty weight	629.91	69.99	820	68.33
Fuel weight	50.12	5.57	160	13.33
Payload weight	220	24.44	220	18.33
MTOW	900	100.00	1200	100.00
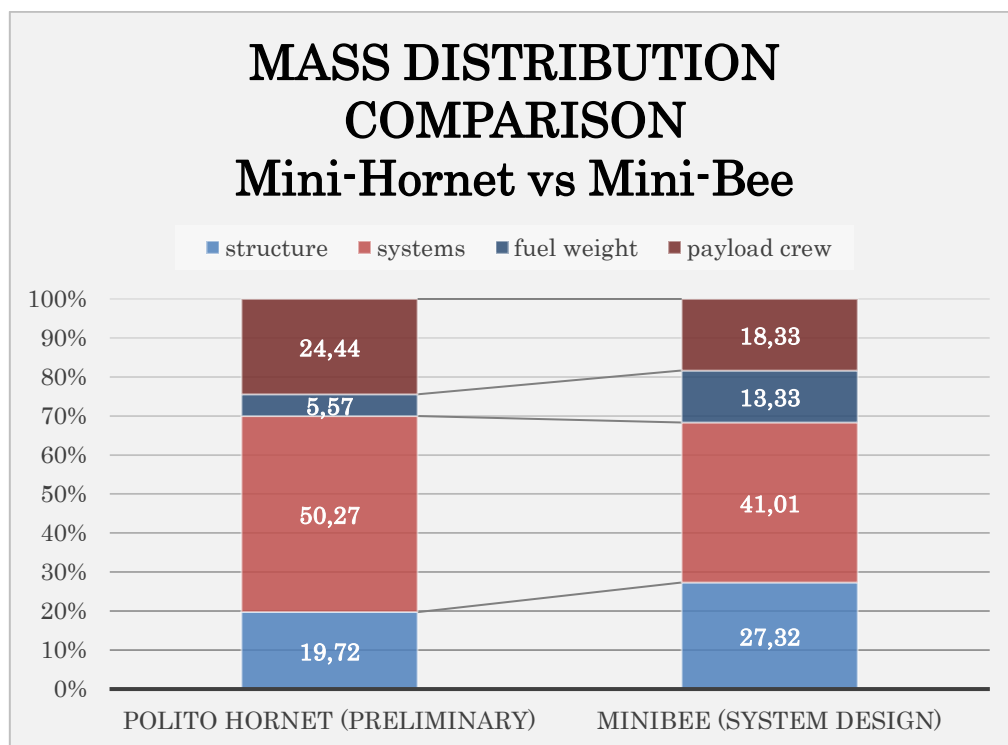
Figure 16.1:mass distribution comparison between Mini-Hornet and Mini-Bee

As a reminder, the structure is mainly made of composite materials. The landing gear is a classical tricycle. Its weight is about 3% of the Maximum Take Off Weight, which is in trend of the classical method of weight estimation (Stanford University estimates it at 4%). The fuel is located into the integrated tanks.

The collocation of the systems is a trade-off between many parameters. One of the most important is the position of the center of gravity, essential for the aircraft stability.

In the figure below is indicated the C.G of all the systems:
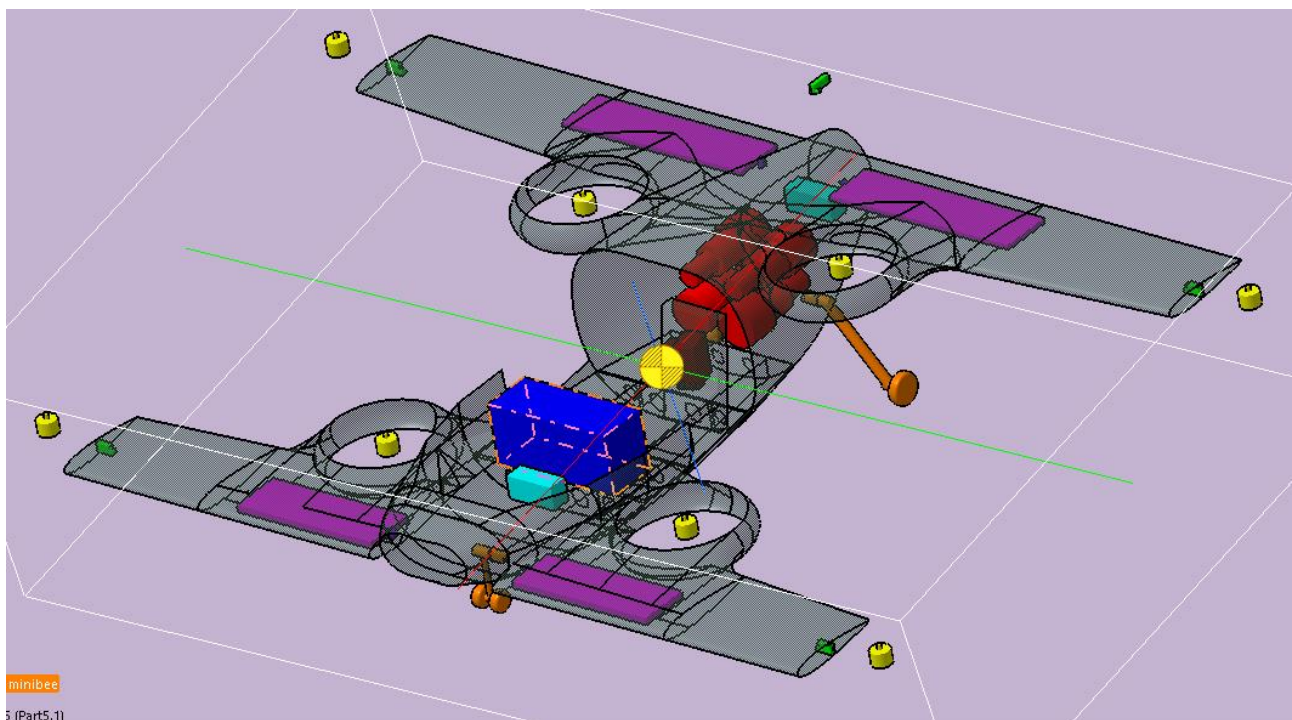
Figure12.1: systems C.G. location

The trend is to have a more integrated configuration of the aircraft systems.

16.2.   Remarks
Air intakes

We found that on the Mini-Bee configuration the air intakes are not present. As the primary source of power is an axial thermal engine it is necessary to provide airflow to aliment these engines. Furthermore, it is the necessity to provide cold air to cool the subsystems and in particular to aliment the Environmental Control System.

At this point it is possible to design a cooling subsystem and to estimate its mass and power budget.

The same thing has to be done concerning the exhaust pipe.

Location of maintenance doors

It is worth to note that a good position of the maintenance doors rises up the Maintainability, so the MMH/FH goes down and in general operational costs lowers.

In the following figure it has been hypothesized a location of the maintenance doors.

Figure 12.2: Maintenance doors location on Mini-Bee

17. Other Themes

In this chapter, we present a short description of what our classmates had designed and project.

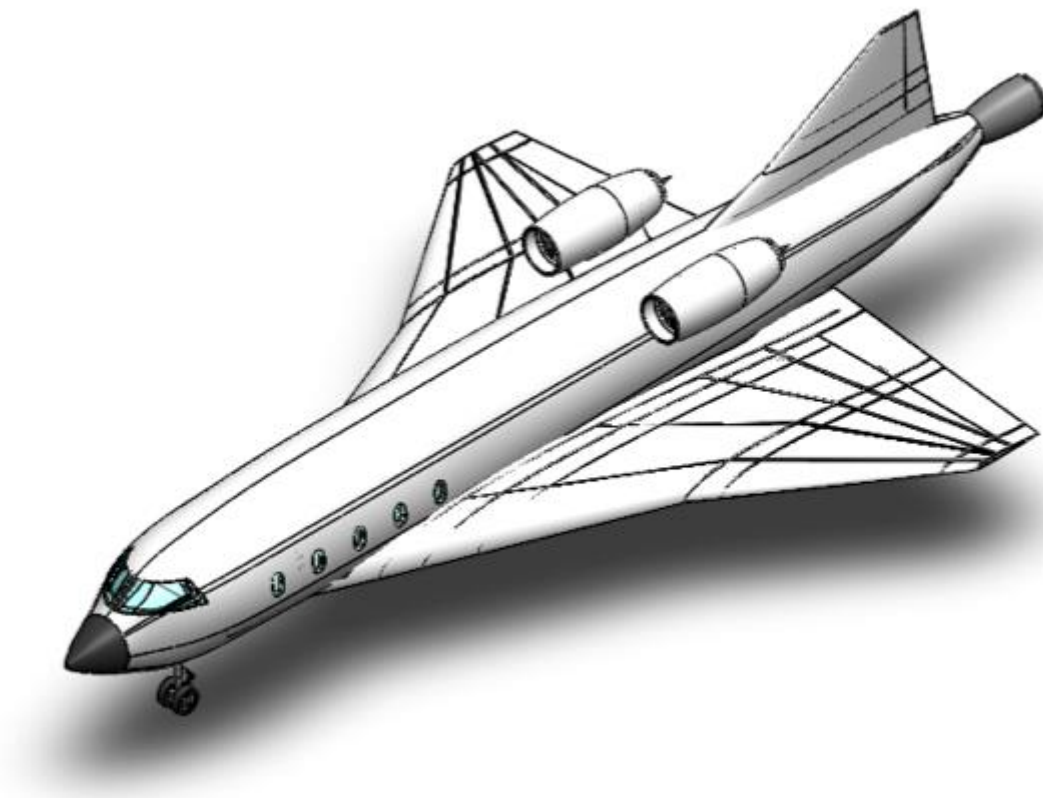## 17.1. SUB-ORBITAL TRANSOPORT FOR PARABOLIC FLIGHT WITH HTOL

Figure 17.1: Sub-orbital transoport for parabolic flight with HTOL

The purpose of this study is to realize a sub-orbital touristic aircraft in order to reach the altitude of 100 km. The requirements for this project sees are: HTOL, air-breathing engines to reach 18000m, 50kg of scientific payload, 10 passengers, 2 pilot, 2 minutes in micro-gravity conditions, excellent Earth-view, use of advanced technologies.

The aircraft designed reach the target altitude using two turbofan engines in the first flight phase and an endo-reactor LOX/LH2 engine in the second one, after 18000m. Reached the altitude of 100km, the aircraft stay 2 minutes in micro-gravity conditions and return to the airport with a glide flight.

The aircraft external configuration has a delta-wing and a conic nose in order to allow supersonic flight. The position of the seats in the cabin allow to have much free-space in order to improve passengers' comfort. The sears are could be stocked in order to increase the cabin volume in micro-gravity phase.

The turbofan engines are on the top of the fuselage in order to avoid any aerodynamic problem. The tank for the turbofan fuel are located in the wing while the liquid fuel for the rocket are in the rear part of the fuselage.

The avionic system has the classical civil avionic equipment, a HUD and it include the out-side camera necessary to provide to the passengers a 360° view of the outside. The all-electric flight control system has two control surface for each wing or vertical tail. The FCS works only the atmospheric flight: when the aircraft reach the higher altitude, the FCS is replaced by a RCS. The landing gear has a classical configuration but requires too much breaking power. The Environmental Control and Life Support System has the typical features of a civil aircraft.

The whole external surface of the aircraft has to be realized in high-temperature resistant material.

The estimates made gets an total aircraft cost of about 100000$, while the RAMS analysis lead to the conclusion that the aircraft has a maintainability comparable with a military aircraft.

17.2.   HYPERSONIC P2P TRANSFERT SYSTEM, SINGLE STAGE, HTOL
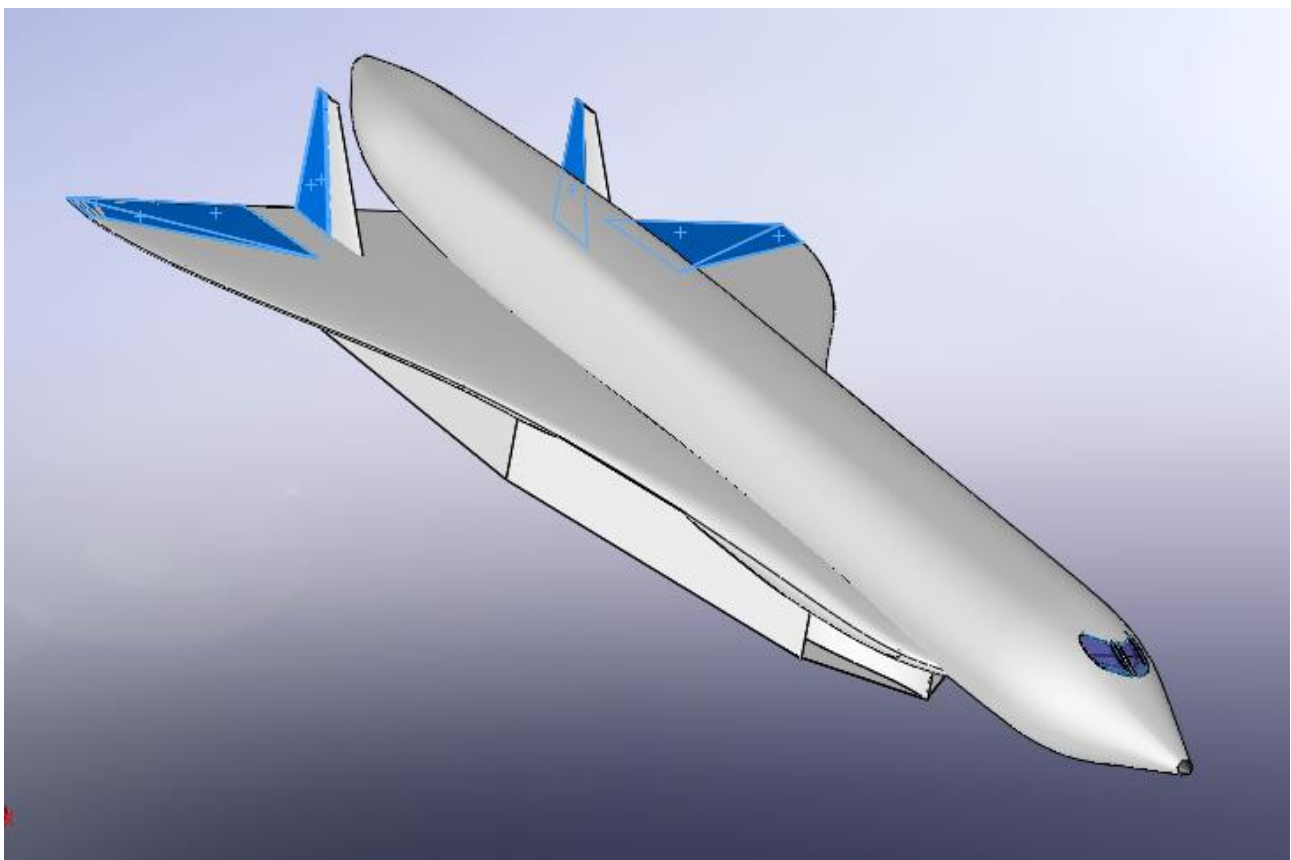

Figure 17.2: hypersonic P2P transfert system, single stage, HTOL

This study aims to design P2P civil aircraft with HTOL, 2 pilot and 300 passengers, cruise altitude 30000-35000m. The aircraft has to cover the route Bruxelles-Sidney in three hours and it work with Air Turbo Ramjet for M<4,5 and with Dual Mode Ramjet for M>4,5.

The preliminary design of the aircraft lead to a MTOW of about 490 tons and a thrust required of 1900 kN.

The configuration adopted for this aircraft sees a delta wing that allow a good efficiency in supersonic flight and it is contained in the Mach cone. It is noteworthy that between the external shell of the fuselage and the internal one there are about two meters difference – in terms of diameter – because of the complex cooling systems that, in order to absorb the heat generated by the supersonic flight, has to use big pipes to reduce the heat generated. Because of this aspect, the aircraft has not windows. The portion of the fuselage not dedicated to the passengers is used as bay for the TEMS and tank for the liquid hydrogen that, in this case, works not only as fuel but also as coolant and steam power for the TEMS. The propulsion system has two different engines unit both located under the fuselage in order to avoid to the fuselage or the wing to reduce the airflow to the engines. The ATR engines works like a turbojet engine in the first phase of the flight and turn in to a ramjet engine at the higher speed. Since M=4.5 the thrust is provided by the DMR: scramjet engines that could push the aircraft to M=8. In the final phases of the mission, the aircraft do a glide flight. The avionic system has no particular aspects. The flight system has two sets of control surface for wing and rudder in order to reduce the actuation power required. The landing gear system is very similar to that of a high MTOW civil aircraft and provide to the aircraft a little pitch angle on order to ease the take-off. During the landing, the required power necessary to brake is too high so the brake system power is reduced to a 30% of the total, the remain power is absorbed by parachute and aero brakes. The Thermal and Energy Management System – TEMS – has a fundamental role in the aircraft because has the task of reduce the high heat flow on the aircraft and produce the electric power for the system. Furthermore, the electric power supply the TEMS fan that works as starter for the engines and all the system of the aircraft. The RAMS & cost analysis led to very high cost and maintenance complexity.

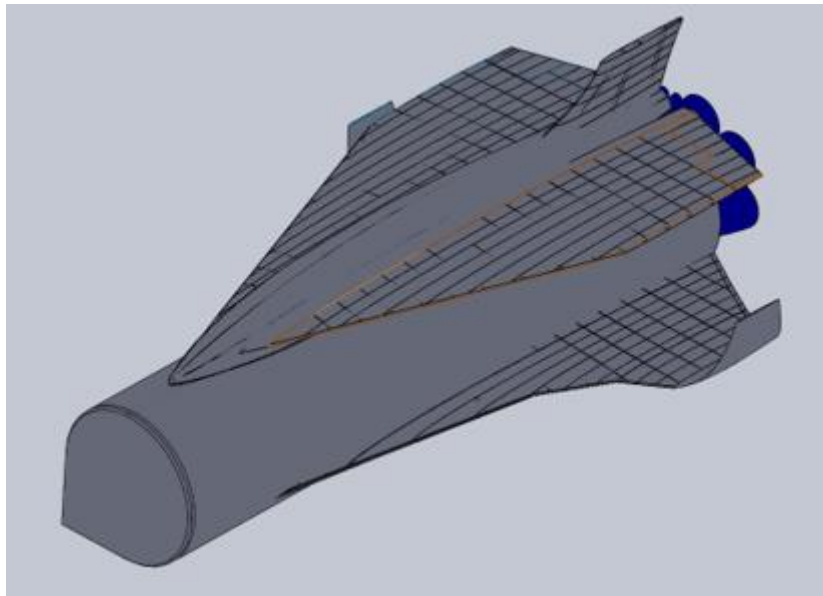## 17.3.   HYPERSONIC P2P TRANSFERT SYSTEM, DOUBLE STAGE, VTOHL

Figure 17.3: hypersonic P2P transfert system, double stage, VTOHL

This project has to study a hypersonic double-stage aircraft that has the aim to cover the distance Bruxelles-Sydney in 90 minutes.

The requirements of this project are: VTOHL, one propulsion system with a LOX-LH2 rocket, service ceiling 80km, maximum Mach 25, 2 pilot and 100 passengers, necessity of a Cabin Escape System for the second stage. The preliminary weight design of the booster, orbiter, cabin and sub-systems is the results of analysis made via Matlab or Excel while the aerodynamic model and the fuel ratio and thrust between the two stages has been studied with Astos. From this analysis emerged that the proper rocket are the RS-25.

The avionic system has to include the typical equipment of civil aircraft, rocket launcher and UAV. The Flight Control System has been studied only for the orbiter where are located the classical control surface. However, the FCS can operate properly only in climb or descent because at the service ceiling they are ineffective; during the cruise, the stability of the aircraft is regulated by a RCS. The landing gear system has to work only in the landing phase where has to absorb the 30% of the brake power; the remaining 70% is absorbed by parachutes and airbrakes. The ECLSS include a suit for each passengers. The TPS is replaced by the TCS with whom both stages can be reused. The aircraft follow the more-electric philosophy and use the electric power for most system. However, is not possible to remove the hydraulic system that is needful for the landing gear. The Cabin Escape System has to be defined. The aircraft cost is estimated about 1.45 billion dollar.

17.4. ADVANCED TURBOPROP

Figure 17.4: Advanced Turboprop

This project has the purpose to study the configuration of an advanced turboprop aircraft with the following requirements: 110 passengers in two classes, 1500 km range, cruise speed of 650km/h, take-off and landing distance 1500m and tail open-rotor engines. Since this requirements, the preliminary design led to a MTOW of 28596 kg, a power required of 252kW and a weight of the systems of 5380 kg.

The avionic system includes the classical components and an ARINC 664: a flight control computer that has better performance. The landing gear system ha the classical tricycle configuration with a simple retraction system, carbon disks and EMA braking system in order to have low cost and weight. The ECS has a bleed-less CAU sub-freezing bootstrap with a dedicated compressor. The Anti-ice system is all-electric while having a pneumatic system for the engines. The Fuel is stoked in the wing. The propulsion system work with two open-rotor engines which has an higher speed than Turboprop and a lower consumption that turbofan. The electric system consists in two electric generator at 230 VAC ad a 28 VDC battery; the electric power s provided to the user at 230 VDC or, using transformers, at 28 VDC, 270 VDC and 115 VAC@400 Hz. The flight control system uses 230 VAC Electro-Hydrostatic-Actuators for the primary flight control end the spoilers while the flaps and slats are actuated by 270 VDC Electro-Magnetic-Actuators; with this architecture the system is lighter and more maintainable. The configuration and design of the aircraft tail allow o reduce the engines noise.

The aircraft will costs 52 M$, has a failure rate of 30,16 failure per 1000hours and a MMH/FH of 5,41.
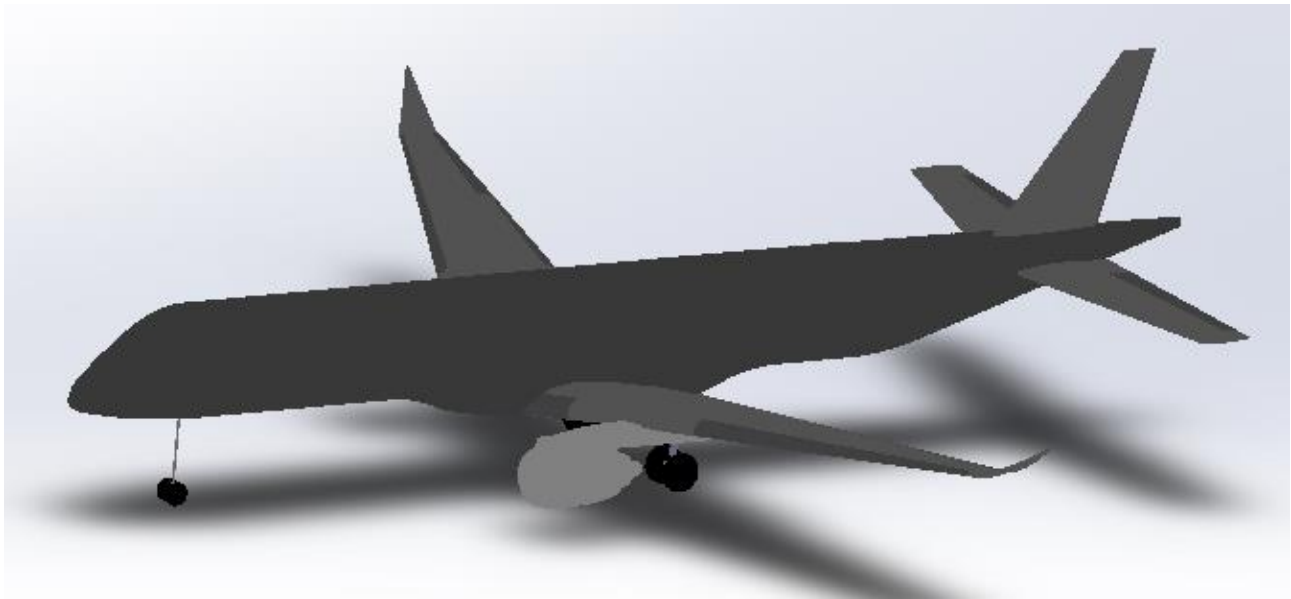
17.5.   REGIONAL TURBOFAN

Figure 17.5: Regional Turbofan

The aim of this project is to realize a classical turbofan aircraft with the typical configuration of this class of aircraft. The requirements are: 90 passengers, 3200+200 km range, take-off and landing distance less than 1500m, cruse speed M=0.9 at 11000m. The design of the engines led to properly defined engines that can provide the correct thrust in all mission phases reducing the fuel consumption.

The avionic system, located in the nose, in the tail and in the base of the fuselage, sees the classical equipment powered at 115 VAC. The FCS has the classical primary and secondary control surface. The landing gear has the classical tricycle configuration; the landing gear brakes are oversized in order to satisfy the requirements on the landing distance. The Anti-Ice system has a bleed system that carries the hot and pressurized air from the engines to the leading edge of the wing. The ECS has a sub-freezing CAU for the regulation of the cabin temperature. The fuel system has four wing-integrated tank with a cross-feed valve and the supply lines to the APU positioned in the tail. The aircraft has two refuel filler for each wing in order to can refuel both with pressurized pump and gravity-fall pump. The hydraulic system works at 3000psi and has two operative lines, right and left, and one back-up line, central; at the central line al linked the fundamental users so that the aircraft could work properly also in case of emergency. The electric system generates power at 115 VAC @ 400Hz; for the users at 28 VDC, the system include the TRU that convert the current. The starter for the engines is pneumatic.

The costs of this aircraft is about 54 M$.

17.6. HYBRID GA AIRGRAFT

Figure 17.6: hybrid GA aircraft

This project must realize a general aviation aircraft with parallel hybrid propulsion. The two-seat aircraft has a thermal engine and a electrical engine that provide the over-boost power in critical phases, while it works as electric power generator in the other phases. The requirements are: two passengers and the hybrid propulsion system. Furthermore, there are some additional requirement like lowing, fixed landing gear, Aluminum structure and traditional systems.

During the take-off and climb phase, the electric engine provide the surplus of power to the thermal ones. The cruise phase, which use only the thermal engines, provides the design reference for the thermal engine; doing so, the thermal engines has been designed with minimum consumption and pollution. The peculiarity of this project is the full autonomous management of the function of thermal and electric engines. Furthermore, in order to reduce noise pollution and to save fuel, in the taxi phase, the electric engine powers the aircraft.

The avionic system has all the classical equipment and function. The hybrid control system consists in a clutch installed on the engine shaft and managed by the avionic system that aims to manage properly thermal engine and electric engine work. For the FCS, in case of emergency, the aircraft endowed of some equipment that works also in case of avionic failure. The propulsion system has a four-cylinders reciprocating engine and it is supplied by AVGAS. The tank are integrated in the two wing and they are linked with the engine via two electric booster pump. The ECS has a non-subfreezing CAU that take the put side air, pressurize it and heats or cools the flow before it goes into the cabin. The anti-ice system has high power consumption so it is shouted-off in take-off and climb phases.

The study of reliability of this aircraft are not simple because it present both validated elements and innovative ones. The cost of the aircraft is about 350.400 €.